Several Multi-Port SAW MEMS Resonator Designs Analysis

Ahmed Mamdouh El-Baroudy 201305036

Ahmed Mohamed Shahin 201300129

Mohamed Hesham Mohamed Kamel 201303931

Mohamed Hassan Zidan 201303650

Nader Mohamed Hozayin 201301218

Sherif Mohamed Atef Soliman 201304406

Senior Design Project Submitted to Fulfill the Degree of Engineering

in

Nanotechnology Engineering

Zewail City University of Science and Technology

Supervisor

Dr. Hassan Mostafa

2018

I-Abstract

Surface Acoustic Wave resonators are considered to be very crucial elements in RF technology since they are CMOS compatible. They emerged strongly in the market for many wireless and sensing applications. SAW devices' theory of operation includes propagation of surface waves generated by transducers on a piezoelectric substrate with the capability of reflecting these waves back and forth at a certain frequency to be used as a filter, oscillator, resonator etc. However, SAW design and implementation demands controlling a lot of variables and has some major challenges. Some of these challenges include frequency shift due to temperature and high insertion loss. This work models and simulates multiport SAW resonators operating at 320 MHz on COMSOL Multiphysics with proposing novel ideas for further advancements.

Several designs of multiport SAW resonators are compared regarding their specs in aim to find a trend between the number of ports and the simulated specs like quality factor, insertion loss, phase depth, temperature coefficient of frequency (TCF) and resonant frequency. Various designs of buried and semi-buried transducers are also analyzed to find the lower TCF value according to the application needed. The resonance frequency is obtained from COMSOL Multiphysics frequency domain analysis along with the (TCF). The rest of the specs are calculated from the BVD circuit model on Cadence Virtuoso. The TCF was calculated by considering the Bleustein-Gulyaev wave approximation to obtain the relation between the velocity and temperature. The relation is then imported in COMSOL to obtain the frequency shift in $ppm/^0C$. The fabrication steps of the various designs are reported for future considerations and the needed masks are designed according to CleWin layout editor software.

II-Acknowledgement

First of all, our gratefulness to Allah for helping us through dark times, difficult situations, help us reach our goal and be with us all along our journey.

Our most gratitude to our thesis supervisor Dr. Hassan Mostafa for his assistance, guidance and dedication to make this work comes to light. His help, follow up, and instructions made this result possible to achieve. Thank you for your constant guidance and extensive care and effort you gave to us.

We would like to thank Dr. Sherif Sedky and Si-Ware Systems administration for the general supervising on the project and to highlight main schemes of the projects. Our path in work and

Main guidelines were instructed by them and helped to shape the way to proceed with our project. Also, their comments on our preliminary approach helped us to correct many confusions and put us back on the right track to points related to electrical model simulations and coupling effects between substrate and IDTs. Without there guidance many results could have been missed and we would be proceeding on a totally wrong direction.

We would like also to thank Zewail City for providing needed legal copies of software programs needed in our simulations and providing access to workstation and labs all along our work.

We would like also to thank Dr. Amr Bayoumi for providing all ways of help and support in providing technical support for simulation programs and lab access, and for his advice in our first term presentation which was very helpful to us.

Getting through our thesis can't be with academic support alone, as friendship was the corner stone to help us get us through tough days and to provide psychological help and relieving stress and to have good company and help through our work. We are grateful to our friendship and bond to overcome differences between us and the different ideas of proceeding in the project. Putting our differences aside and to unite on one decision help us to overcome any problems.

We would like to thank our friends and colleagues in the department of Nanotechnology. They were always there to provide any assistance on any technical problems we might face and for sharing their expertise in any problem we might face during our work.

The most important of all is not to forget that this could not have accomplished without their love, support and their constant prayers. Our mothers call every night to check on our progress, their ways of making us comfort at home and to welcome all of us to work at each other's homes. To our mothers, fathers, brothers, and sisters, thank you for being so kind and patient and to support us in our weakest days. This work is a clear evidence of your unconditional love and support all along from the start, thank you.

III-Gant Chart

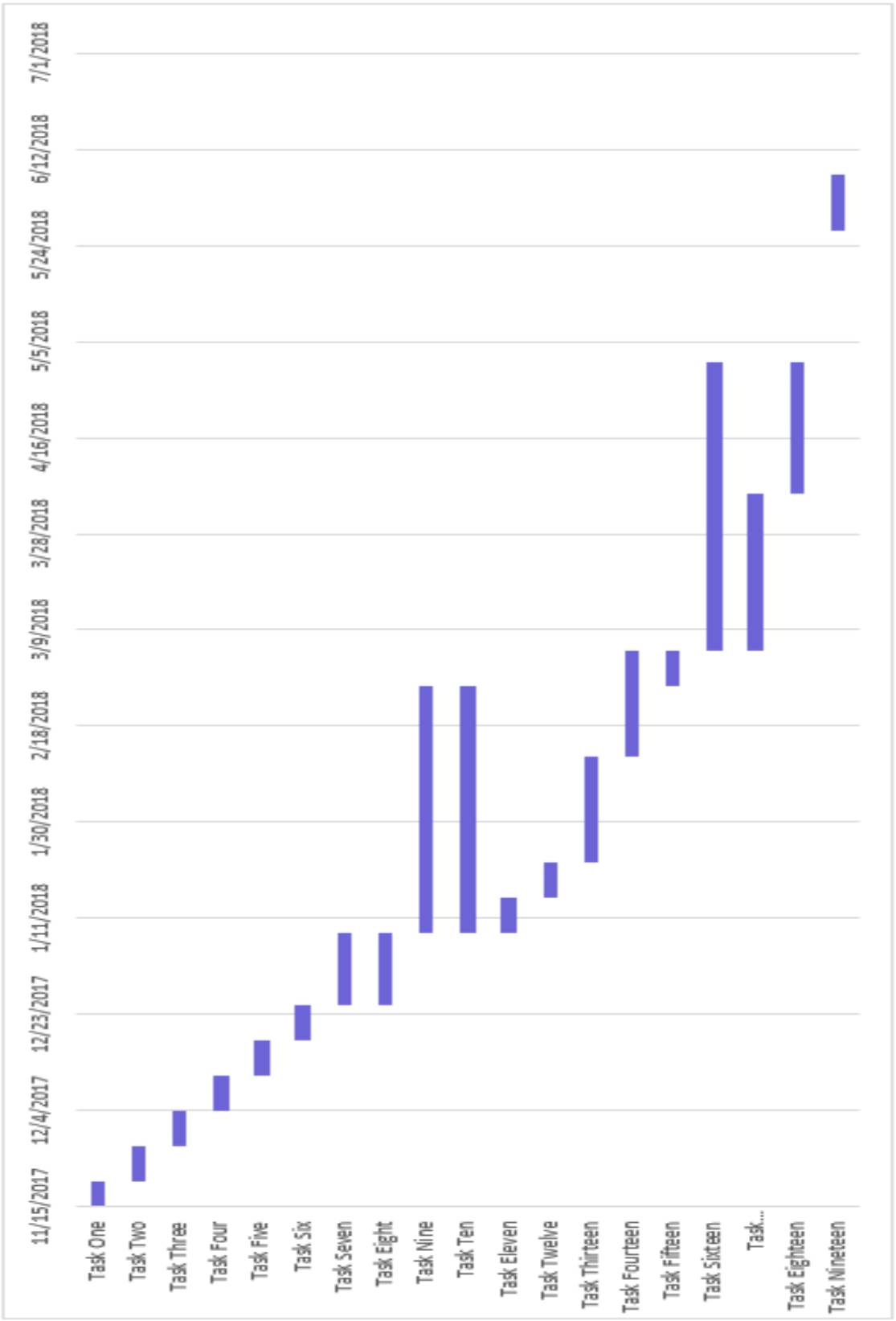

Task One: Understanding quartz resonators theory of operation.

Task Two: Understanding the SAW resonators theory of operation.

Task Three: Gaining knowledge of previous designs aspects.

Task Four: comparison between Quartz and SAW MEMZ OSC.

Task Five: Understanding methodology of extracting properties from simulation.

Task Six: COMSOL simulation for fixed-fixed beam resonator.

Task Seven: COMSOL simulation for 3D SAW MEMS resonator.

Task Eight: Verilog A Op-Amp Circuit simulation on Cadence.

Task Nine: COMSOL simulation for 2D SAW MEMS resonator.

Task Ten: COMSOL Simulation for 2D buried SAW MEMS resonator.

Task Eleven: Cross coupled Circuit simulation Cadence.

Task Twelve: Colpitts Circuit on Cadence.

Task Thirteen. Single stage Pierce OSC on Cadence.

Task Fourteen: Four stage Pierce OSC on Cadence.

Task Fifteen: COMSOL Simulation for 2D Semi- buried SAW MEMS resonator.

Task Sixteen: Applying admittance from COMSOL in Cadence simulation and extracting results for all designs.

Task Seventeen: Calculating TCF of the proposed designs.

Task Eighteen: Concluding and collecting all results of the proposed designs.

Task Nineteen: Writing the thesis and Finishing the presentation.

Task	Start date	End date	Duration
Task One	11/13/2017	11/20/2017	7.00
Task Two	11/20/2017	11/27/2017	7.00
Task Three	11/27/2017	12/4/2017	7.00
Task Four	12/4/2017	12/11/2017	7.00
Task Five	12/11/2017	12/18/2017	7.00
Task Six	12/18/2017	12/25/2017	7.00
Task Seven	12/25/2017	1/8/2018	14.00
Task Eight	12/25/2017	1/8/2018	14.00
Task Nine	1/8/2018	2/26/2018	49.00
Task Ten	1/8/2018	2/26/2018	49.00
Task Eleven	1/8/2018	1/15/2018	7.00
Task Twelve	1/15/2018	1/22/2018	7.00
Task Thirteen	1/22/2018	2/12/2018	21.00
Task Fourteen	2/12/2018	3/5/2018	21.00
Task Fifteen	2/26/2018	3/5/2018	7.00
Task Sixteen	3/5/2018	5/1/2018	57.00
Task Seventeen	3/5/2018	4/5/2018	31.00
Task Eighteen	4/5/2018	5/1/2018	26.00
Task Nineteen	5/27/2018	6/7/2018	11.00

IV-Table of Figures

Figure 1-Oscillator Feedback Loop[1] 16
Figure 2-Signal Progress in Oscillator[2] 17
Figure 3-Colpitts Oscillator with SAW Resonator Configuration[2] 17
Figure 4-The electrical circuit model for an electrostatic resonator with the addition of two transformers as the transducers, [3]. 20
Figure 5-The constructive interference between the transmitted and the reflected waves illustrating the acoustic cavity of the resonator, [4]. 21
Figure 6-: Different types of SAWs 22
Figure 7-Propagation mechanism of surface waves [15] 23
Figure 8-Representation of the stresses causing the wave propagation [16] 23
Figure 9-View of the deformations in the piezoelectric layer[16] 25
Figure 10-Schematic view of the SAW resonator IDTs 25
Figure 11-Schematic view of the SAW resonator with reflectors 26
Figure 12-Equivalent circuit BVD model for the SAW resonator [20] 28
Figure 13-Frequency with Phase relation 29
Figure 14-Frequency with admittance relation 29
Figure 15-Quartz Resonator [23] 31
Figure 16-The Three Modes of Resonation of Quartz [25] 32
Figure 17-The circuit model of the quarts resonator [25] 32
Figure 18-Power Consumption of crystal and MEMS resonator [28] 34
Figure 19-Start up characteristics of 40MHz MEMS oscillator and 40 MHz crystal oscillator [28] 34
Figure 20-Phase Noise of Crystal and MEMS oscillators [29] 35
Figure 21-Frequency temperature characteristics of MEMS and Quartz OSC [28] 36
Figure 22-frequency stability of both MEMS and quartz OSC at 3.3 V, Temperature 25℃ for 50 ms [29]. 36
Figure 23-Golledge SAW Resonator [30] 38
Figure 24-Qualcomm SAW Resonator [31] 39
Figure 25-Qualcomm SAW filter & resonator kit [32] 39
Figure 26-Rayleigh Surface Waves [14] 41
Figure 27-Basic SAW device[14] 41
Figure 28-A plan view of the basic design 43
Figure 29- a- Cross section for the 1st and 2nd designs of the CMOS SAW resonator. 43
Figure 30-Implementation of a two-port SAW resonator structure in CMOS. 43
Figure 31--Two Port RF SAW Resonator[33] 45
Figure 32-Proposed Circuitry[33] 45
Figure 33-Plan view of the design and the parameters[33] 46
Figure 34-Results of the 3 designs[33] 47
Figure 35-3D model of the 2 Port SAW resonator [34] 48
Figure 36-Top View of the proposed design, 2 Port SAW resonator [34] 49
Figure 37-Zno SAW resonator Design resonance frequency and quality factor. [34] 50
Figure 38-AlN SAW resonator Design resonance frequency and quality factor. [34]] 50

Figure 39-AlN SAW resonator resonant and anti-resonant frequencies [34] 51
Figure 40-ZnO SAW resonator resonant and anti-resonant frequencies [34] 51
Figure 41-Thin film SAW Device Configuration [37] 52
Figure 42-SEM view of the thin film SAW Device Configuration[37] 53
Figure 43--Design of two ports delay line [37] 53
Figure 44-S21 magnitude with frequency for three IDTs thicknesses [37] 53
Figure 45-One port IDT schematic and electrical equivalent[39]. 54
Figure 46-Two dimensional representation of the one port device[39] 55
Figure 47-Results of the frequency domain study. (a) Plot of admittance versus frequency to obtain the resonant and anti-resonant frequencies. (b) Plot of the Quality factor.[39] 56
Figure 48-Final circuit model of the one port device.[39] 57
Figure 49- geometry of the device and the materials used in simulation 59
Figure 50- dimensions of the basic device 59
Figure 51- estimated resonance frequency of the device 60
Figure 52- modes shape 60
Figure 53- Admittance graph extracted from COMSOL 5.3. 61
Figure 54- the geometry of the device and the materials used in simulation 62
Figure 55- dimensions of the basic device 62
Figure 56- modes shape 63
Figure 57- Admittance graph extracted from COMSOL 5.3 63
Figure 58- geometry of the device and the materials used in simulation 64
Figure 59- the dimensions of the basic device 64
Figure 60 - modes shape 65
Figure 61- Admittance graph extracted from COMSOL 5.3 65
Figure 62- 2 and 7 pairs devices of the Basic design 66
Figure 63- Admittance graph of all devices extracted from COMSOL 5.3 66
Figure 64- 2 and 7 pairs devices of the Buried electrodes design 67
Figure 65- Admittance graph of all devices extracted from COMSOL 5.3 67
Figure 66- 2 and 7 pairs devices of the Semi-Buried electrodes 68
Figure 67- Admittance graph of all devices extracted from COMSOL 5.3 68
Figure 68- BVD equivalent circuit model 69
Figure 69- Admittance vs frequency COMSOL result 70
Figure 70- Pierce oscillator schematic 72
Figure 71- SAW resonator equivalent circuit schematic 73
Figure 72- SAW transient response for 10 and 100 nm stop time for Pierce oscillator 74
Figure 73- PSS simulation results 75
Figure 74 - admittance for 1 port basic SAW resonator 76
Figure 75- S21 dB for 1 port basic SAW resonator 77
Figure 76- S21 phase for 1 port basic SAW resonator 78
Figure 77- Quality factor with bandwidth at – 3dB for 1 port basic SAW resonator 79
Figure 78 - quality factor vs IDT pairs for basic design SAW resonator 80
Figure 79- S21 dB for 1 port buried SAW resonator 81
Figure 80- S21 phase for 1 port buried SAW resonator 81
Figure 81 - Quality factor with bandwidth at – 3dB for 1 port buried SAW resonator 82

Figure 82 - quality factor vs ID pairs for buried design SAW resonator 83
Figure 83- a) s21 dB for 1 port semi buried design, b) s21 phase for 1 port semi buried design 84
Figure 84 - Plan view of the parameters[17] 86
Figure 85- c_ij values and first order dependence in AlN. [44] 89
Figure 86- (a) the complete elasticity matrix notation for a material, (b) the shortened matrix 91
Figure 87- the elasticity matrix notation for a material in COMSOL 91
Figure 88- the admittance curve with temperature sweeping, and the effect of geometry and density change with temperature on the resonance frequency shift. 92
Figure 89- resonance frequency of the basic design at each temperature taking into account the geometry and material parameters 93
Figure 90-TCF of the three designs 94
Figure 91-Quality factor of the three designs 95
Figure 92- Insertion loss of the three designs 95
Figure 93-One Pair two-ports SAW MEMS resonator fabrication mask 99
Figure 94-Two Pairs two-ports SAW MEMS resonator fabrication mask 99
Figure 95-Three Pairs two-ports SAW MEMS resonator fabrication mask 99
Figure 96-Six Pairs two-ports SAW MEMS resonator fabrication mask 100
Figure 97-Seven Pairs two-ports SAW MEMS resonator fabrication mask 100
Figure 98-Four Pairs two-ports SAW MEMS resonator fabrication mask 100
Figure 99-Five Pairs two-ports SAW MEMS resonator fabrication mask 100
Figure 100 -MCM-based approach (a, b, c, d), and commercial wire bonding (e, f, g) Hybrid integration modes. [47] 105
Figure 101-Heterogenous integration 107
Figure 102-The electrical characterization setup for the resonator[4] 108
Figure 103-The two-port circuit representation to define the S-parameters, [4] 109
Figure 104-The quality factor calculation based on the phase response in the open-loop[4] 111
Figure 105-Simple SAW delay line device,[6] 113
Figure 106 SAW oscillator using the SAW resonator as a feedback element [11] 114
Figure 107-SAW biosensor implementation and analyte detection [10] 115
Figure 108-(a) the configuration of one-port SAW resonator, (b) the modeled circuit for the resonator,[11] 116
Figure 109-The Fabry-Perot model of the one-port SAW resonator,[11] 116
Figure 110-An example of the device realization of the SAW resonator, [4] 117
Figure 111-a) the configuration of two-port SAW resonator, (b) the modeled circuit for the resonator, [11] 117
Figure 112-The Fabry-Perot model of the two-port SAW resonator,[11] 118
Figure 113-An example of the device realization of the two-port SAW resonator,[4] 118

V-List of Tables

Table 1 - Results of the Phase Jitter for Both MEMS & Crystal OSC ……35

Table 2 - Comparison between the three designs ……44

Table 3 - Simulation results for both designs…… 52

Table 4 - comparison between multi ports basic design SAW resonator…… 79

Table 5 - comparison between multi ports buried design SAW resonator…… 82

Table 6 - comparison between multi ports semi buried design SAW resonator ……85

Table 7-Simulation results for both designs. ……74

Table 8 - comparison between multi ports basic design SAW resonator……74

Table 9 - comparison between multi ports buried design SAW resonator……77

Table 10 - comparison between multi ports semi buried design SAW resonator……80

Table 11- Basic Design……91

Table 12-Buried Design……91

Table 13-Semi-Buried Design……92

Table 14-Footprint of the delay-line of multi-ports SAW MEMS resonators……95

VI-Nomenclature

f_f : Resonant frequency

λ: wavelength

v: Acoustic wave velocity

W : Width of aperture

N : Number of reflectors

N_t: Number of transducers pairs

L_g: Distance between reflector and transducer

L_c: Distance between input and output transducers

L: Distance between reflectors

L_P: Penetration depth of the wave

Q_r: Quality Factor

k^2: electromechanical coupling coefficient

v: Velocity

f_r: Resonance frequency

T: Stress Tensor

C^E: elasticity matrix

S: Stain Tensor

e: Piezoelectric Coupling Constants

E_k: Electric Field

D_i: Electric Displacement

ε_{ik}^S: dielectric Permittivity Matrix

w_s: series resonance (resonance)

w_p: parallel resonance (anti-resonance)

X: Displacement.

M: Mass.

ξ: Damping.

$\dot{x}$: Velocity.

F: Force.

1/k: Compliance.

q: Charge.

L: Inductance.

R: Resistance.

I: Current.

V: Voltage.

C: Capacitance.

$\emptyset_a$: amplifier phase shift.

$\emptyset_c$: phase shift around the loop.

P : integer number.

f_A : operating frequency

m: mass loaded on the surface

σ : conductivity

c : constant for the mechanical properties

ε : dielectric constant

ρ : density

S_r: sensor sensitivity

$C0$: parallel capacitance

L_m: motional inductance

R_m: motional resistance

C_m: motional capacitance

$[e]$: piezoelectric matrix of the material

$[S]$: strain matrix

$[c]$: stiffness matrix.

Contents

Abstract 2

Chapter One- Introduction: 15

Oscillators 16

Resonators 19

Transduction Mechanisms 19

Capacitive transduction 19

General Resonators Modeling 20

Acoustic Micro-resonators 20

Surface Acoustic Waves (SAW) 22

Theory of Operation 25

Modeling 27

Equivalent circuit model 28

Chapter Two- Problem Definition 30

Power consumption 34

Oscillator start up characteristics 34

Phase noise and phase jitter 35

Frequency temperature characteristics 35

Frequency stability 36

Chapter Three- Market Research 37

Chapter Four -Literature Review 40

Chapter Five- Simulation 58

COMSOL Simulation 59

Cadence Simulation 69

Parameter extraction 69

Design & Simulation 72

Results and Discussion 74

Temperature Coefficient of resonant Frequency (TCF) 86

Delay line effect on temperature 86

Velocity effect on temperature 87

Bleustein-Gulyaev Wave 87

Temperature Coefficient Compensation 89

TCF Simulation 90

Thermal expansion 90
Elasticity Matrix 90
Density 91
Chapter Six- Fabrication & Characterization 98
Fabrication Masks 99
Fabrication Steps 102
MEMS & CMOS Integration 105
Hybrid integration 105
Mono-lithic Integration 106
Heterogenous integration 106
SAW Lab Characterization Techniques 108
Low & High Frequency Electrical Characterization 108
Low-Frequency Characterization and Open-Short DC measurements: 108
Scattering-Parameters Representation and Network Theory 109
SAW Quality Factor Measurement 110
Chapter Seven- Applications of SAW Devices 112
SAW Devices 113
SAW Delay Lines 113
SAW Oscillators: 113
SAW Sensors: 114
SAW Port Configurations: 115
One-Port SAW Resonator: 115
Two-Port SAW Resonator: 117
Chapter Eight- Conclusions & Recommendations 119
Appendix 125

Chapter One
Introduction

Oscillators

Oscillators are an essential part of any electronic circuit. Their applications are widely used in telecommunications in carrier synthesis and as clock generators in CMOS ICs. Oscillator circuits are made basically of two parts, the amplifier circuit, and a damping frequency-selective RLC circuit, forming a negative feedback system. Oscillators circuit usually produce a periodic output voltage indefinitely. Oscillator circuits has no input, it only has an output and the input can be considered as a noise trigger to the closed loop circuit which initializes the loop[1].

Theory of operation:

A negative feedback system is shown in the graph below. oscillators can be considered as bad negative feedback amplifier, as the aim to is get is a periodic signal with the same gain.

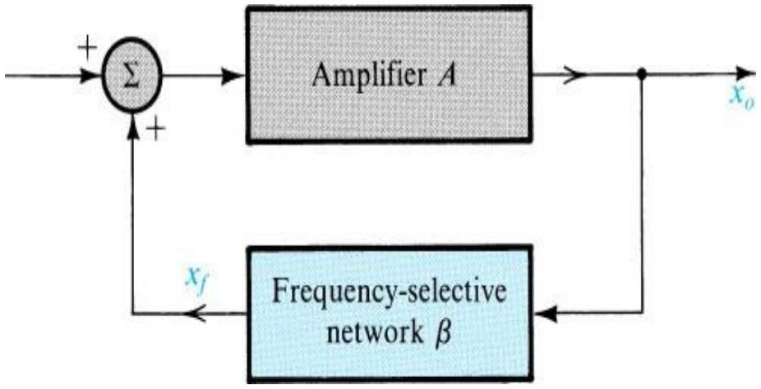

Figure 1-Oscillator Feedback Loop[1]

The concept is that a signal enters to the amplifier, this signal is amplified with a gain A of the amplifier. The negative feedback network, β, is a damping RLC circuit. The amplified signal should be damped by a factor of $\beta = \frac{1}{A}$ as to regain the original signal amplitude and shape. Assuming the transfer function is of the form:

$$A_f(s) = \frac{A(s)}{1 - A(s)\beta(s)} \quad (1)$$
$$where\ s = j\omega$$

A(s) is the amplifier gain, $\beta(s)$ is the feedback gain. If the amplifier suffers from a great phase shift it may become a positive feedback, at which the oscillation occurs. At this case, the closed-loop gain gets to infinity. In this case the oscillator starts to amplify its noise.

For the transfer function above, the oscillation criteria become:

$$|L(j\omega_0)| = |A(j\omega_0)\beta(j\omega_0)| = 1 \quad (2)$$
$$\langle L(j\omega_0) = \langle A(j\omega_0)\beta(j\omega_0) = 0 \quad (3)$$

Where $A(s)\beta(s)$ is the open loop gain, This is called the Barkhausen criteria. Of course, in reality this doesn't happen due to many variations, so the open loop gain is made greater than 1 to maintain the oscillation. For the phase criteria, a negative feedback system usually suffers a

180◦ phase shift. The overall shift has to be zero as to restore the original signal. The progress of the signal is shown below[2].

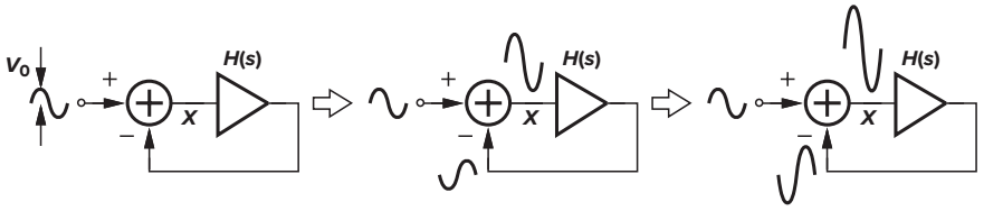

Figure 2-Signal Progress in Oscillator[2]

–It has to be mentioned that the RLC feedback circuit (RLC resonator) is frequency selective, it only works with its resonant frequency, which is the needed frequency of operation, and eliminates the rest. The RLC model of MEMS oscillator is derived from the topology and features of the design to account for the same resonant frequency of the mems resonator.

The Colpitts is shown in the following figure[2]:

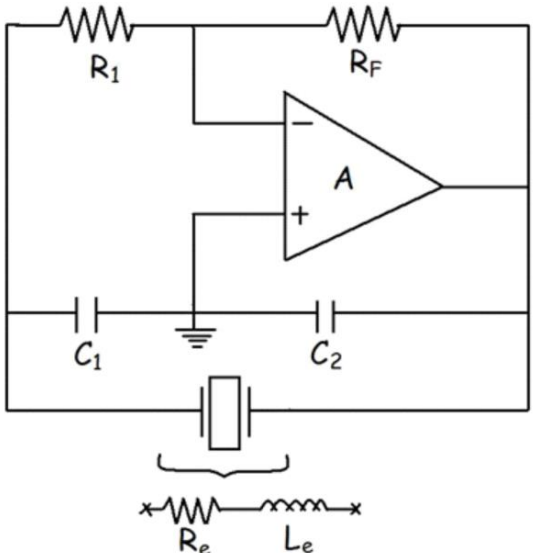

Figure 3-Colpitts Oscillator with SAW Resonator Configuration[2]

Applying the oscillation condition, this results in:

$$\frac{R_2}{R_1} = \frac{C_1}{C_2} \quad (4)$$

The block below the capacitors in the figure represents the MEMS resonator equivalent RLC circuit.

MEMS SAW resonators resonates at it's natural frequency. For a closed feedback loop oscillator, the oscillation starts with a sine wave, and the amplitude starts to build up until in reaches its maximum. The maximum is determined by the oscillator circuit so the sine wave become clipped and transform to a square wave. In most cases, the output signal of SAW oscillator is a sine wave[2].

For SAW resonator to be work with an oscillator circuit, the gain of the oscillator must be maximum at the natural frequency of the resonator and to be minimum at every other frequency. This can be done by connecting the resonator in series with the oscillator circuit.

Resonators

The concept of using MEMS as mechanically resonating structures was introduced in early sixties and has gained a significant interest both commercial-wise and research-wise. These resonating microstructures offered many advantages and applications for the MEMS market and have captured a large portion of this market due to their impactful solutions and crucial applications such as filters, high quality clock signal generators, or sensors[3].

These MEMS structures can be electrically brought into resonance. In this vibrating mechanical system, there is the continuous conversion between the potential and electrical energies. Each MEMS structure has frequency dependent responses, known as the resonance frequencies, in which this energy conversion is at its optimum point (minimum losses) [3]. For each of these resonance frequencies, there is a unique shape or pattern of motion for the mechanical system, it is called the mode shape of the structure. In order to achieve resonance, the structure must have the capacity to store the potential and kinetic energies similar to the idea of a mass-spring system. In the real systems, there are always loss mechanisms in the energy that reduce the vibration and resonance of the system,[3].

Transduction Mechanisms

For the proper operation of the resonator, transduction mechanisms are used to interface between the mechanical domain of the structure and the electric domain of the external circuits. So an electrical signal (voltage) should excite the mechanical vibrations in the structure and the output is sensed by the change in the electric current signal. Choosing the proper transduction mechanism is crucial for the overall performance and efficiency of the system. The different parameters to compare between the different mechanisms are the implementation complexity, coupling coefficient (determining the energy conversion efficiency), and the power consumption. Capacitive, piezoelectric, and thermal/piezoresistive are the common transduction mechanisms for the resonators, [3]. In this project, the main interest is the capacitive and piezoelectric mechanisms, so they are explained in the following paragraphs.

Capacitive transduction

If there is a voltage applied on two conducting surfaces with an insulating medium separating them, this results in a force that moves the two surfaces apart. The reverse can happen, if a force is applied on one of the two plates and the separating distance changed, the capacitance will change leading to a change in the current (if a constant voltage is applied between the two plates). They can be used in both the input (actuation) and output (sensing) mechanisms. It is easy to implement as it only requires the electrode plates material to be of high electric conductivity. Capacitive resonators have some of the highest ($f.Q$) figure of merit. Due to this simplicity and high efficiency, it was the mechanism used for the first MEMS resonators published and many commercial products, [3].

Piezoelectric transduction

The direct conversion between the external mechanical stress and the internal electric polarization inside a specific group of crystalline materials (piezoelectric materials) is the basis of the piezoelectric transduction. The reverse mechanism is allowed as if a voltage is applied, a mechanical stress is achieved. These materials can be fabricated as films or be used in their crystal structure such as aluminum nitride (AlN) and Quartz respectively. The key feature here is that the transduction mechanism is self-generating, i.e., no excess power consumption, [3]. It also has large coupling coefficient so the transduction efficiency is high. Similar to the capacitive transduction, the piezoelectric one can be used for the actuation and the sensing parts in the input and output of the resonator,[3].

General Resonators Modeling

The MEMS structure operates in the mechanical domain and interferes with the electronics and electric circuits necessary for operation. The mechanical simulations for such complex structures are computationally expensive while the electric counterpart simulations are much easier to perform the simulation. So, the resonating structures in general are represented and modeled in the electrical domain. A proper mapping between the two domains is needed and it allows the co-simulation for the whole system. So the quantities mapping should be as follows,[3].

Table 0-Electromechanical Mapping

Mechanical Domain	Electrical Domain
Displacement, x	Charge, q
Mass, M	Inductance, L
Damping, ξ	Resistance, R
Velocity, $\dot{x}$	Current, I
Force, F	Voltage, V
Compliance, $1/k$	Capacitance, C

The common modeling for a MEMS resonant system is an RLC circuit, series resistance, inductance and capacitance. The energy transductions between the electrical and mechanical domains are electrically represented as transformers in the simulating circuit. The figure below is an example of an electrical circuit representation of an electrostatic resonator, [3]:

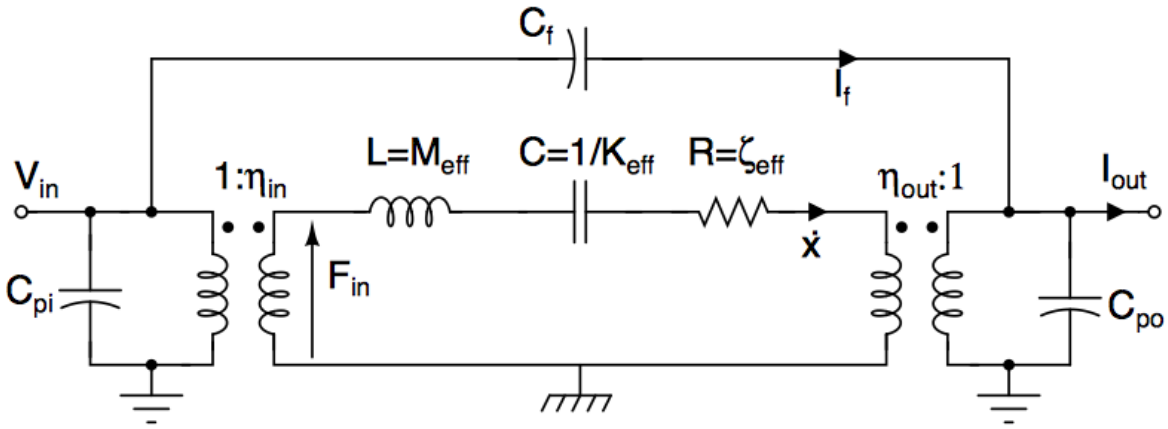

Figure 4-The electrical circuit model for an electrostatic resonator with the addition of two transformers as the transducers, [3].

As it is seen that the $R, L,$ and C are the mechanically modeled parameters of the resonator and the transformers model the transduction mechanisms and interfaces with the outer "real" circuits. So the first input transformer converts the voltage to a force which is applied to the structure, and the output transformer converts the structure velocity into current for the output circuit, [3].

Acoustic Micro-resonators

This project is concerned with using SAW MEMS resonators. SAW-based MEMS resonators are a subclass of the acoustic microresonators. The acoustic microresonators are devices having an acoustic wave propagation leading to vibration at one of the resonance frequencies. These resonance frequencies

are determined by the device dimensions and the material mechanical properties. Here the resonator structure operates as an acoustic cavity which traps the wave propagating in the medium. For this trapping, both the wave reflection and transmission are controlled by the proper electrodes design and the layer the acoustic wave propagates through at this chosen frequency, [4]. The constructive interference between the transmitted and reflected waves concentrates the energy in this cavity. To achieve this constructive interference, the transmitted and the reflected waves need to be aligned in-phase so they have to be $\lambda, \frac{\lambda}{2}$ or $\frac{\lambda}{4}$ phase-shifted (valid for any shift of $\frac{\lambda}{n}$, where n is an integer number). If both of waves are out of phase, a destructive interference leads to suppressing both of them. The following figure shows this principle of propagation, [4].

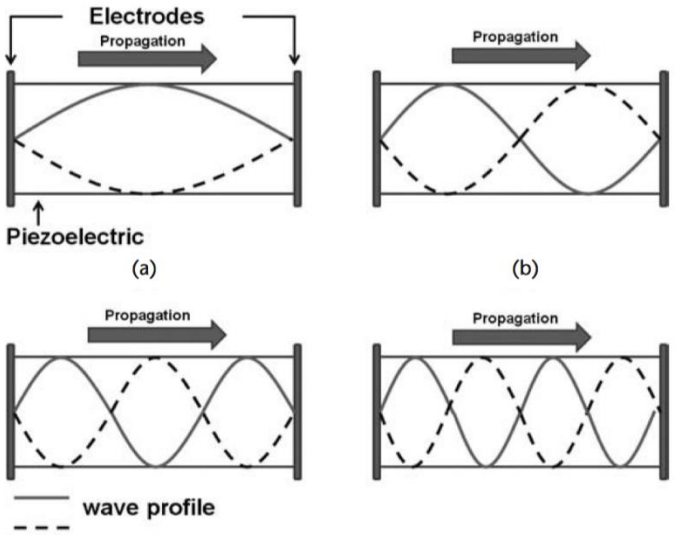

Figure 5-The constructive interference between the transmitted and the reflected waves illustrating the acoustic cavity of the resonator, [4].

Surface Acoustic Wave (SAW) Resonators

SAW resonators are the core of this project. They are based on SAW propagation and using one of the electromechanical transduction mechanisms explained above. Accompanied with the appropriate electronic circuit, they can be used as sensors, oscillators or filters. The transduction is done using metallic capacitive electrodes (or piezoelectric electrodes) and a piezoelectric layer for the wave to propagate through, [4]. Similar to the acoustic resonators, the SAW resonator works as a resonant cavity with the input transducer electrode uses the electric signal to generate the mechanical SAW (vibrations) which propagates through the piezoelectric layer to transmit to the second transducer electrode at the output which converts this mechanical wave to the electrical domain. The SAW bounces back and forth between the two electrodes and the transductions are repeated. A SAW resonator consists of these components: transducers, a piezoelectric substrate or a piezoelectric deposited layer, and reflection gratings or grooves, [4]. The input and output transducers transform between the electrical and acoustic energies. Input transducers can easily excite this wave by introducing compression and tensile stress in the piezoelectric substrate forming this wave. The output IDT is used to sense the change in phase or frequency of SAW in the form of current. And the reflectors are used to produce reflections of waves to minimize insertion losses and any wave losses through the substrate, [4].

Surface Acoustic Waves (SAW)

A glimpse on surface acoustic waves would facilitate the theory of operation and proposed ideas later. Surface acoustic waves are mechanical waves composed of transverse and longitudinal waves that propagate on the surface of a piezoelectric and elastic material. The amplitude of the surface wave suffers from an exponential decay into the material in the direction normal to the material. Different kinds of surface waves can be utilized for the SAW resonator, namely: Rayleigh, Shear-Horizontal, Love and Sezawa-SAW [12, 13]. Firstly, in Rayleigh SAW, the energy confinement during the wave propagation occurs very near to the surface. They are very sensitive to the surface perturbations. Secondly, in the Shear-Horizontal SAW (SH-SAW), the wave propagation direction is in the same surface plane and perpendicular to the particles displacements. Specific crystal orientations only allow such propagation. Thirdly, Love SAW is a special kind of the SH-SAW in which an additional elastic layer has to overlay the medium guiding the SH-SAW. During wave propagation, the energy is confined in this overlayer [12]. This waveguide action requires specific conditions and optimizations over the overlayer thickness and acoustic properties.

The following figure compares those three types [12, 13]:

Rayleigh-SAW (MHz-GHz)	**Shear-Horizontal SAW (MHz)**	**Love-SAW (MHz)**
The energy confinement is very near to the surface. Displacement is perpendicular to the propagation direction.	The wave propagation direction is in the same surface plane and perpendicular to the particles displacements.	The energy is confined in this overlayer.
41 YX cut $LiNbO_3$, ST-cut Quartz, 128 Y-cut $LiNbO_3$	36 YX-cut $LiTaO_3$, or 64 YX-cut $LiNbO_3$	An additional elastic layer is added to the SH-SAW (SU-8, ZnO, TiO_2 to SiO_2)
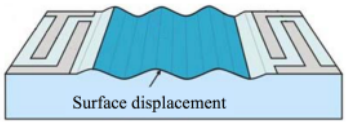	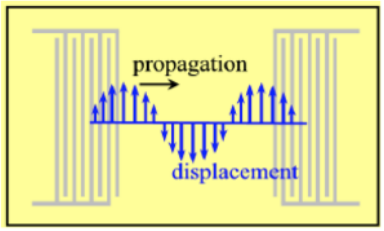	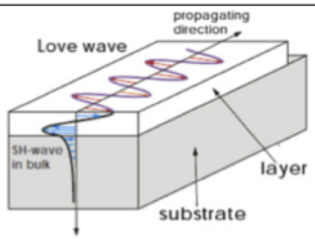

Figure 6-: Different types of SAWs

Accordingly, SAW devices operate by engendering these waves that are able to be used as sensors if a change in the amplitude or phase of the wave is detected. Moreover, it can be used as a clock generator if it is stable in terms of frequency. Acoustic wave velocity ranges from 2 to 5 km/s and operates in the frequencies of 30 MHz to 17 GHz in theory. This range of velocity is much slower than that of electromagnetic waves, which makes SAW more promising in the scope of lowering the sizes of the components or antennas.

The propagation of surface acoustic waves on a piezoelectric material is described by an elliptical path taken by the particles on the surface. This elliptical path can be broken down into two components: one in the same direction of propagation and the other normal to it and to the

surface of the material, which is responsible for the deformation carried out by the wave on the piezoelectric material. By having these two components, the wave propagates by causing a deformation in the material along with a forward motion to the other side of the material, which will be discussed later in the theory of operation[12].

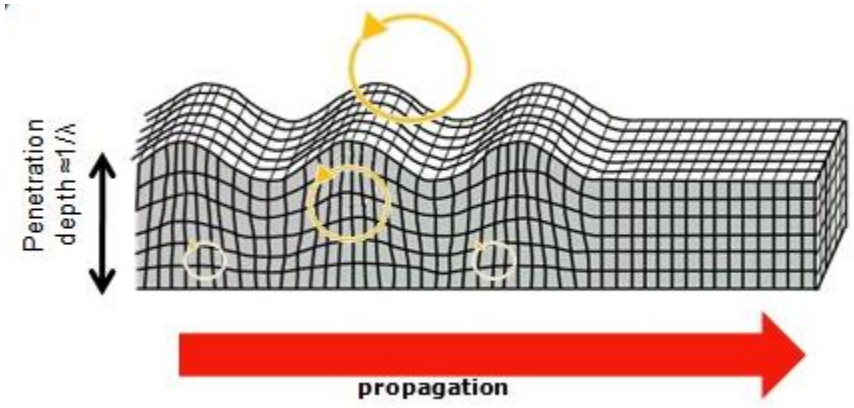

Figure 7-Propagation mechanism of surface waves [15]

These two components of propagation cause longitudinal and transverse stresses on the material that are useful in considering the coupling between the electrical and mechanical components that are discussed later.

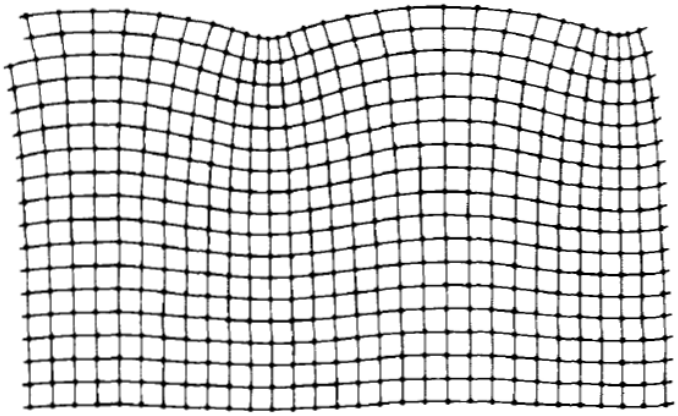

Figure 8-Representation of the stresses causing the wave propagation [16]

The designs present in this thesis involve electric to mechanical coupling as the mechanical wave is electrically initiated. Moreover, the surface material used is a piezoelectric material to allow the Rayleigh waves to travel on the surface of the material for the applications to be discussed. So basically dielectric, stiffness, and piezoelectric coupling effects are considered. The equations governing the motion of the surface acoustic are both Maxwell's and continuum motion equations.

Recall from basic electromagnetic that the electric displacement field $D = \epsilon_0 \epsilon_r E$, where D accounts for the displacement of the free and bound charges by an applied electric field. However, if we have a piezoelectric surface material, we have to consider the displacement field

that are present due to the stresses in the piezoelectric material. Piezoelectricity is the accumulation of electric charges engendered by a mechanical stress and vice versa[17]. Piezoelectricity explains how the applied electric field could cause a mechanical deformation, which is the reason behind the initiation of the surface mechanical waves.

Theory of Operation

The 2-port SAW resonator is basically constructed out of two interdigital transducers (IDTs), a piezoelectric layer either thin or thick, and reflectors. The IDT looks like a comb-drive and it is used to form a mechanical stress on the piezoelectric material successively to initiate the surface acoustic wave as shown in Fig-9. The input IDT could be triggered by any form of noise and it starts to oscillate till it reaches the designed resonance frequency. As the input could be thought of an AC signal, the polarity of the charges on the IDT fingers starts alternating from positive to negative and vice versa, creating the stress and forming the deformation in the piezoelectric material to create a wave and transfer it to the output IDT. Fig-10.

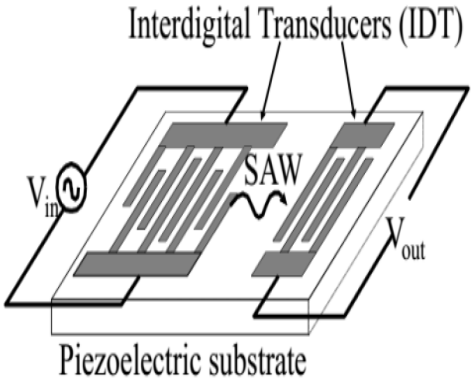

Figure 10-Schematic view of the SAW resonator IDTs

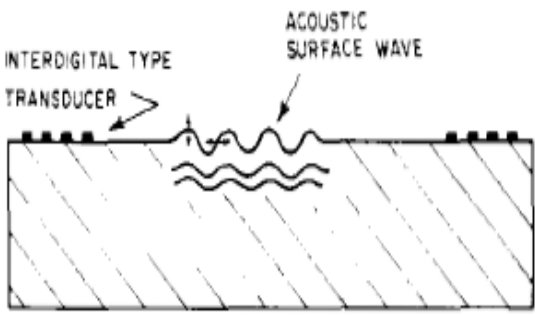

Figure 9-View of the deformations in the piezoelectric layer[16]

The wave is then coupled to the output IDT by the same mechanism for detection or sensing. To control the frequency of the wave, the IDTs have to be designed with specific dimensions to get the resonance frequency needed. The spacing between two successive fingers is equal to $\lambda/2$ where λ is the wavelength of the travelling surface acoustic waves and is given by

$$\lambda = \frac{v}{f_r} \qquad (5)$$

Where v represents velocity of the surface acoustic waves propagating in the piezoelectric material and f_r represents the resonance frequency. Since the interspacing in one period of fingers is in the range of micrometers, SAW MEMS resonators are used in RF applications.

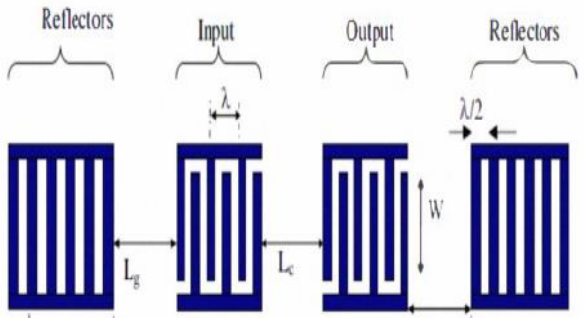

Figure 11-Schematic view of the SAW resonator with reflectors

The reflectors are gratings placed on the sides of the device, as shown in Fig-11, to reflect the wave back to the delay line to minimize substrate losses and obtain a better oscillation condition. In other words, the reflectors make the device act like a resonance cavity.

Acoustic waves propagating through a piezoelectric material are governed by the piezoelectricity equations of state[16]:

$$\boldsymbol{T_{ij} = C^{E}_{ijkl} S_{kl} - e_{ijk} E_k} \quad (6)$$

$$\boldsymbol{D_i = e_{ikl} S_{kl} + \varepsilon^{S}_{ik} E_k} \quad (7)$$

Where:

$T: Stress\ Tensor$
$C^E: elasticity\ matrix$
$S: Stain\ Tensor$
$e: Piezoelectric\ Coupling\ Constants$
$E_k: Electric\ Field$
$D_i: Electric\ Displacement$
$\varepsilon^S_{ik}: dielectric\ Permittivity\ Matrix$

From these equations, one can deduce that the elastic waves are accompanied by an electric field. Moreover, the velocity of the wave inside the piezoelectric material depends mainly on dielectric, elastic and piezoelectric properties. The coupling results in excess potential energy in the medium, as a result, the stiffness increases by a factor of $1 + k^2$where $k^2$is the electromechanical coupling coefficient, the effective stiffness is given by:

$$c_{effective} = c_{before}(1 + k^2) \quad (8)$$

And

$$k^2 = \frac{e^2}{c\varepsilon} \quad (9)$$

Where e, c and ε depend on the direction of propagation, the electromechanical coupling coefficient k is an indication of the electromechanical coupling inside the piezoelectric material and its maximum is *unity*.

To obtain the best results, the electromechanical coupling coefficient k of the piezoelectric material is to be as large as possible, as well as a large velocity of waves in the piezoelectric layer, moreover, the piezoelectric material has to eliminate other unwanted bulk waves.

Modeling

The development and evolution of present day SAW devices has been possible only due to simultaneous efforts to simulate these devices. The theoretical modeling and physical development of devices go together, contributing to each other. Various models have been used since the introduction of SAW devices in the late 1960's to the present date and it has been a constantly evolving process. In this chapter, the underlying assumptions, abilities, pitfalls, and potentials of various models are discussed, eventually leading into finite element modeling for SAW resonators.

Modeling SAW devices has been an important requirement since they were firstly introduced in the late 1960's because they are to be fabricated in cleanrooms and require specific designs and materials. This fabrication process is not cheap and needs time, in addition the design of the device has become complicated [18, 19]. So the accurate model for the device is not a choice and is significantly important as it can predict the response before the fabrication step which leads to overcome the different errors in the design and the production and consequently reduce the costs needed for the whole process.

To achieve the required specifications, Different design parameters are to be accurately calculated and optimized. These parameters include: 1-materials (substrate, over-layers, if any, and different metals used), 2- geometry (IDTs, device thicknesses and the piezoelectric layer thickness) [19].

There are various models proposed to simulate the SAW devices. Those models which describes the SAW resonator behavior are divided into two categories: ***phenomenological models*** and ***physics based models***. For the first category, the model starts with physics governing the generation of the waves in the piezoelectric domain and then solve those differential equations describing these physics. In the latter model, previously obtained set of parameters is used to predict the output response. This set of parameters can be obtained from experimental data of physics-based models simulations [19]. So, it can be seen that both complement each other. Four common models exist under those two categories: ***delta function model***, ***equivalent circuit***

model, ***coupling of modes model***, and ***P-matrix model***. In this project, the ***equivalent circuit model*** will be utilized because it can be easily incorporated for subsequent electrical circuits simulation using Cadence Virtuoso software.

Equivalent circuit model

The physics used in modeling the SAW devices is complex as it requires to couple the theory of acoustic wave propagation, electric field approximations, piezoelectric material physics, geometric dimensions and other mechanical properties of the materials [20]. The basic importance of the equivalent circuit model is that it doesn't need to delve in those complex physics to solve for the device parameters. It is based on mapping the physics parameters and equations into electrical lumped elements which are configured in certain circuit that produces the same response. Here there are two conversions used: 1- the acoustic forces to the equivalent electrical voltages, and 2- the surface waves to electrical currents [18].

In order to extract the equivalent electrical circuit model, the ***Butterworth Van-Dyke model*** (BVD) is applied in the analysis conducted in this report. This is a commonly used model for different filters, oscillators and sensors SAW devices [20, 21, 22]. The model utilizes a circuit with two parallel branches: The R-L-C branch and C-branch. The first branch maps the series resonance, it occurs when the value of the impedance has a minimum of (R). At this value, the inductive part cancels the capacitive part in that resonance frequency. The latter branch determines the parallel resonance or the so called antiresonance which occurs at higher frequencies where the value of the reactance along the loop becomes zero and the current primarily goes in the loop and doesn't pass it. The following Fig.12 illustrates the circuit 20:
To derive the formulas for those electrical elements, the transfer function is directly expressed

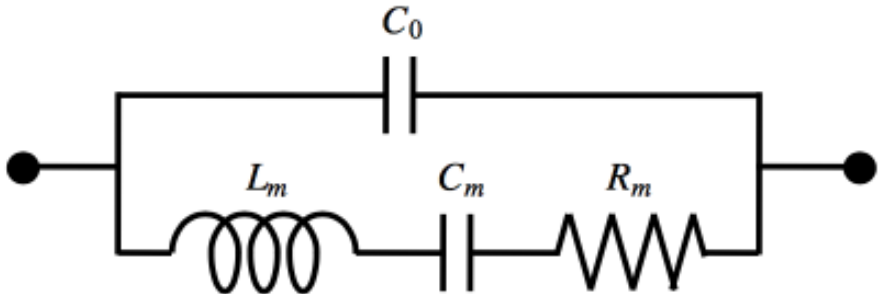

Figure 12-Equivalent circuit BVD model for the SAW resonator [20]

using the resonator figure of merit parameters (resonance, anti-resonance and quality factor) and is represented as [20]:

$$Z_{BVD} = \frac{1}{sC_0} \frac{s^2LC + sRC + 1}{s^2LC + sRC + 1 + \frac{C}{C_0}} \quad (10)$$

and, the series resonance (resonance) w_s, the parallel resonance (anti-resonance) w_p, and quality factor Q are given by [20]:

$$w_s = \sqrt{\frac{1}{LC}} \qquad (11)$$

$$w_p = w_s \sqrt{1 + \frac{C}{C_0}} \qquad (12)$$

$$Q = \frac{1}{w_s RC} = \frac{w_s L}{R} \qquad (13)$$

so, by substituting these parameters in the Z_{BVD} equation, we get:

$$Z_{BVD} = \frac{1}{sC_0} \frac{s^2 + s\frac{w_s}{Q} + w_s^2}{s^2 + s\frac{w_s}{Q} + w_p^2} = \frac{1}{sC_0} \frac{s^2 + s\beta + w_s^2}{s^2 + s\beta + w_p^2} \qquad (14)$$

and this impedance function can be plotted in Fig-13 & Fig-14 showing the relation of the frequency with both admittance and phase[20].

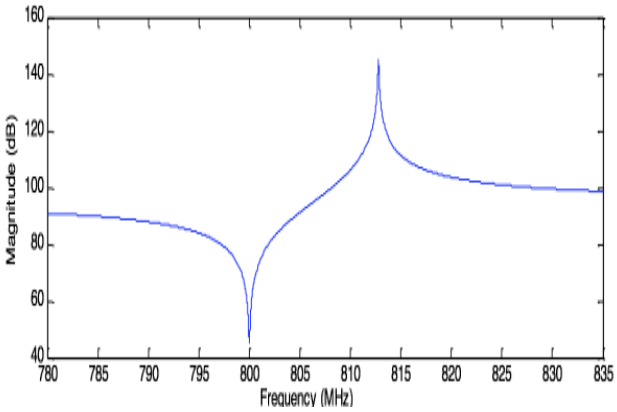

Figure 14-Frequency with admittance relation

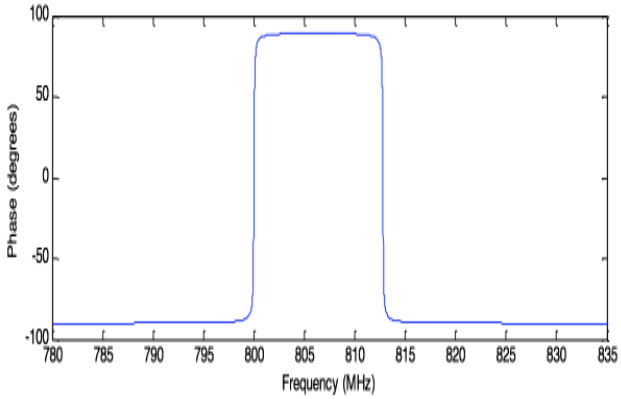

Figure 13-Frequency with Phase relation

Chapter Two
Problem Definition

In this section, both quartz crystal resonator and SAW MEMS resonator are compared. First, a glimpse over the theory of operation of quartz crystal resonator and its properties is needed.

Simply quartz crystals are made in the form of a piece of quartz between two electrodes as shown in Fig-15 [23], quartz is well known with its high quality factor and its piezoelectric properties. The piezoelectric material is simply a material that is affected by any electric charge, which means that any applied electric charge will cause the material to mechanically deform not only this, but also any mechanical deformation will cause the production of electric charges in the material. Quartz has some advantages and disadvantages which are listed below [24]:

- **Advantages [24]:**

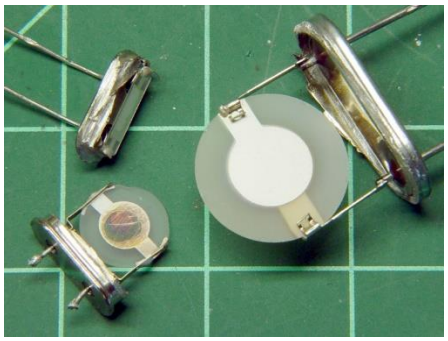

Figure 15-Quartz Resonator [23]

  - Very high quality factor, which implies great stability and low phase noise as an oscillator, and high selectivity when used as filter
  - Low cost
  - Very stable with respect to temperature and time.
- **Disadvantages [24]:**
  - Size: the frequency produced is directly proportional to the dimensions of the piece of quartz but there is limiting size or dimension, so it needs to be taken care of, also the thinner the higher the frequency that's why this is limited to certain range of frequencies.
  - Fixed frequency: one of the advantages of the quartz crystal is that it can be very accurately cut to get the exact accurate needed frequency with very tiny error and that can be one of the disadvantage since it only has one frequency and if another frequency needed it must be replaced with another resonator.
  - Quartz is CMOS not compatible, so it is not applicable to make it on chip, but it is off chip that's why the MEMS resonators are introduced to help make it on chip.

Quartz crystal can resonate in three different ways; Longitudinal mode, low frequency face-shear mode and high frequency shear mode as shown in Fig-16. The mode is controlled by the method and directing of cutting the piece of quartz from the source. There are several ways of cutting

that are discussed later but the most important way that is widely used in radio frequency applications is called AT cut [25].

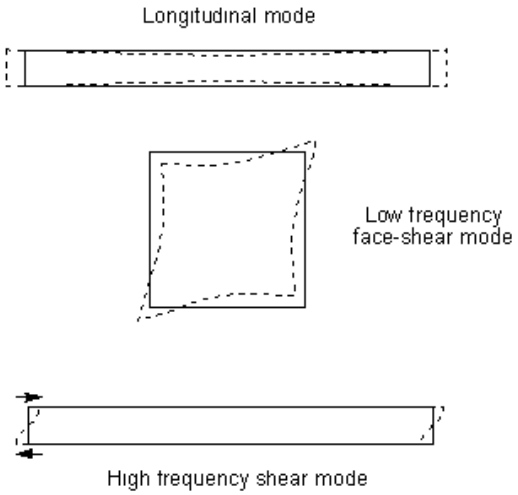

Figure 16-The Three Modes of Resonation of Quartz [25]

Quartz crystal resonator can be modeled into an electric circuit model that is needed to help matching it to the feedback circuit that will form an oscillator at the end, and the circuit model

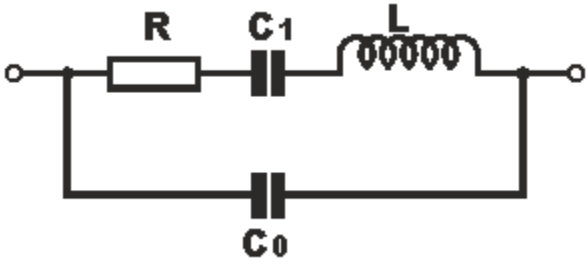

Figure 17-The circuit model of the quarts resonator [25]

shown in Fig-17 is the same for most resonators [25].

C_1: capacitance because of the compliance of the crystal
R: this resistance is mainly a result of the losses in the system and here the main loss is because of the friction during mechanical stress.
L: inductance because of mass of the material
C_0: Capacitance because of the capacitance of the two electrodes surrounding the quartz crystal.

As stated before quality factor of the crystal is very high and this is the most important advantage of the quartz crystal besides giving an accurate resonating frequency. The quality factor can be easily calculated by using the following equation:

$$Q = \frac{1}{2\pi F_s R C_1} \qquad (15)$$

Where F_s is the series frequency of the resonator [25].

There are several quartz crystal cuts that are used to get the needed dimensions exactly with the exactly needed orientation and plan of the cut, since this is a very important aspect that controls the quality factor, temperature dependence and many other properties of the resonator, some of the cuts are introduced below with the range of frequencies of each cut [26].

- AT cut: 0.5 - 300 MHz
- SC cut: 0.5 – 200 MHz
- BT cut: 0.5 – 200 MHz
- XY cut: 5 -100 KHz
- GT cut: 0.1 – 2.5 MHz
- IT cut: 0.5 – 200 MHz

Manufacturing of the crystal passes by many steps since as stated before the dimensions of the crystal is the only thing that affects the frequency and determines it, also as stated before the thinner the higher frequency so the first step is to start by growing the quartz itself, then crystal cutting and lapping according to the exact dimensions calculated that can determine the frequency then final dimensioning, etching and polishing. Then the electrodes material is chosen to give the best performance then the electrodes are cut and then everything is packed together either in a class pack or other materials and it is evacuated and filled with nitrogen as an inert gas to prevent any reaction between parts [27].

The main reason of this part is to compare the quartz crystal resonator and SAW MEMS resonator, so the comparison will be based on some important points according to [28] & [29]:

- Power consumption
- Oscillator start up characteristics
- Phase noise and phase jitter
- Frequency temperature characteristics
- Frequency stability

Power consumption

Power consumption is calculating how much current that resonator consume, as stated in [28], power consumption of 40MHz MEMS resonator and 40 MHz crystal resonator was calculated and shown in Fig-18.

As appears from the graph, the MEMS oscillator consumes around five times more power than the crystal one, this is due to the increased circuitry in MEMS oscillator since it uses increased current, PLL and LC VCO to reduce the jitter.

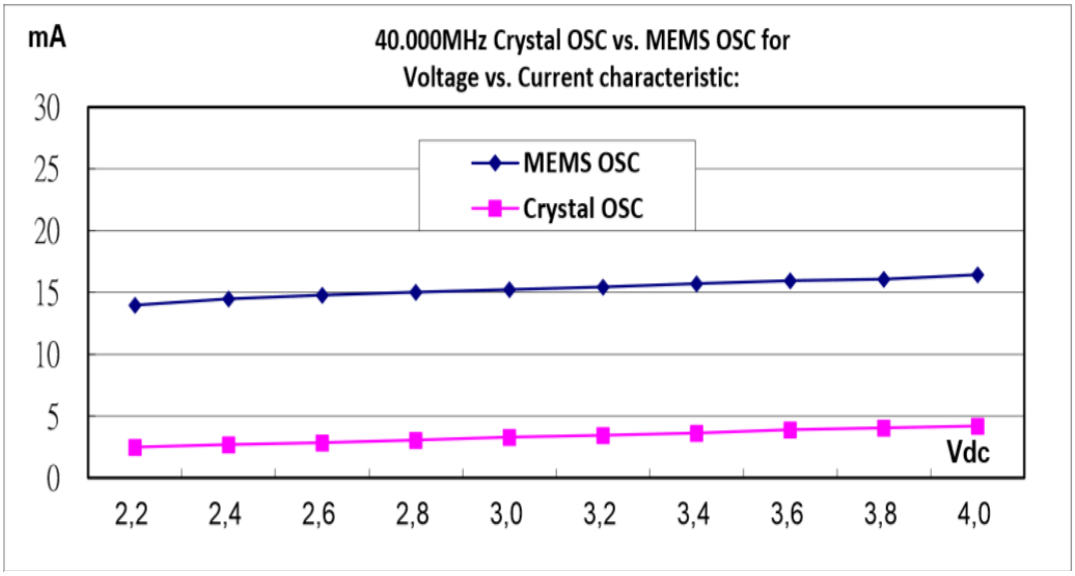

Figure 18-Power Consumption of crystal and MEMS resonator [28]

Oscillator start up characteristics

This property studies how fast do the resonator starts resonating after the power is on, and how stable is it, this has a great influence on the battery life especially in those equipment that are switched on and off quickly to save the battery power. The characteristics of 40MHz MEMS oscillator and 40 MHz crystal oscillator are shown in Fig-19 [28]

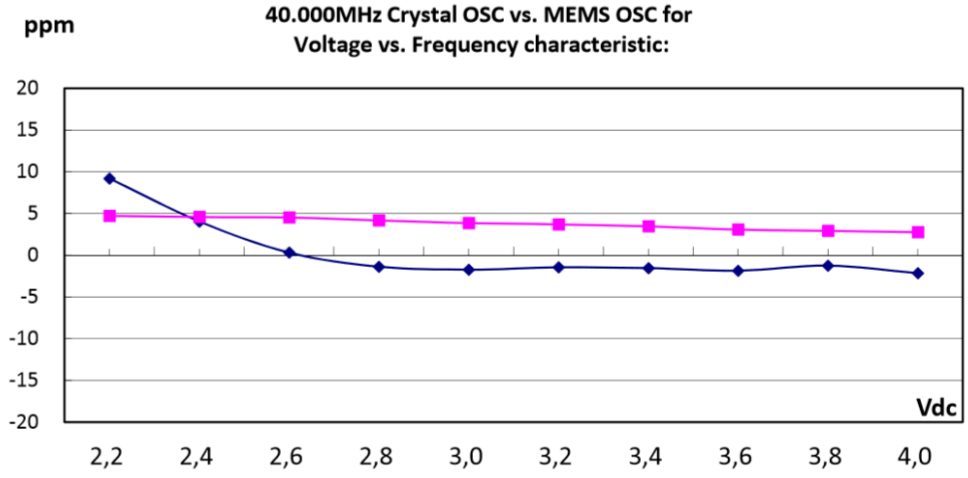

Figure 19-Start up characteristics of 40MHz MEMS oscillator and 40 MHz crystal oscillator [28]

From the above graph appears that crystal oscillator has faster start up and are more stable than MEMS oscillator.

Phase noise and phase jitter

This property measures the noise performance, [29] held an experiment that compared Epson SG-210S*B crystal oscillator to two silicon MEMS oscillators and the result is shown in Fig-20, but [28] held another experiment with three different frequencies (40MHz, 100MHz and 156.25 MHz) and compared both oscillators. The results of [28] are in Table-1.

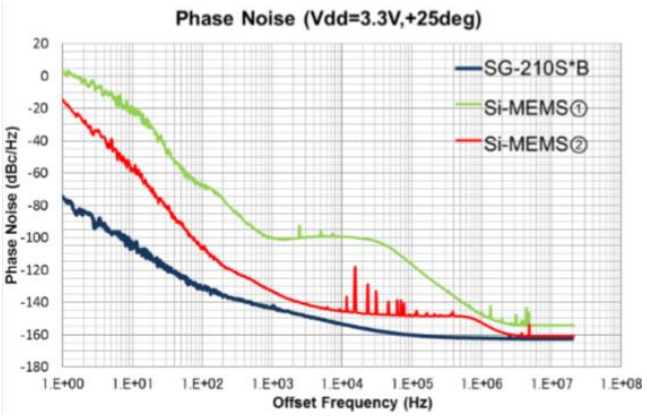

Figure 20-Phase Noise of Crystal and MEMS oscillators [29]

Frequency (MHz)	Phase jitter MEMS OSC	Phase jitter Crystal OSC
40	5.67 ps	0.19 ps
100	2.61 ps	0.07 ps
156.25	1.87 ps	0.03 ps

Table 1-Results of the Phase Jitter for Both MEMS & Crystal OSC [28]

From the above results, it appears that crystal OSC has much better phase noise than the MEMS OSC.

Frequency temperature characteristics

Frequency temperature characteristics were measured firstly be reaching a stable temperature -40 ℃ and then keep increasing temperature by 2 $℃/min$ until reaching 85 ℃ [28], [29]. The results are shown in Fig-21.

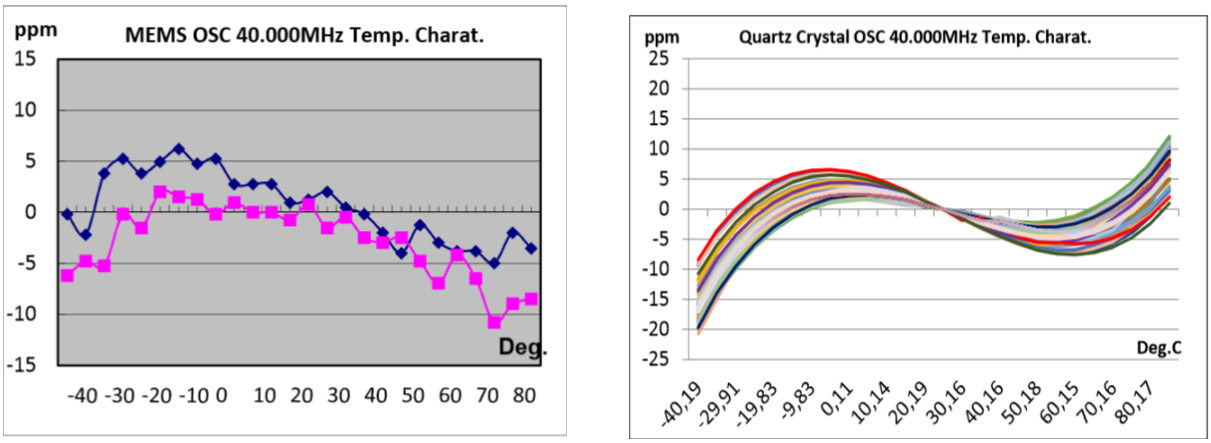

Figure 21-Frequency temperature characteristics of MEMS and Quartz OSC [28]

Quartz crystal OSC has analog compensation system, so it doesn't suffer from any frequency jumps and they are available, so even if the frequency temperature characteristics of the quartz are higher than MEMS, it is still affordable since the temperature compensation are available [28].

Frequency stability

From graph in Fig-22, appears that the quartz OSC is far more stable than MEMS OSC[29].

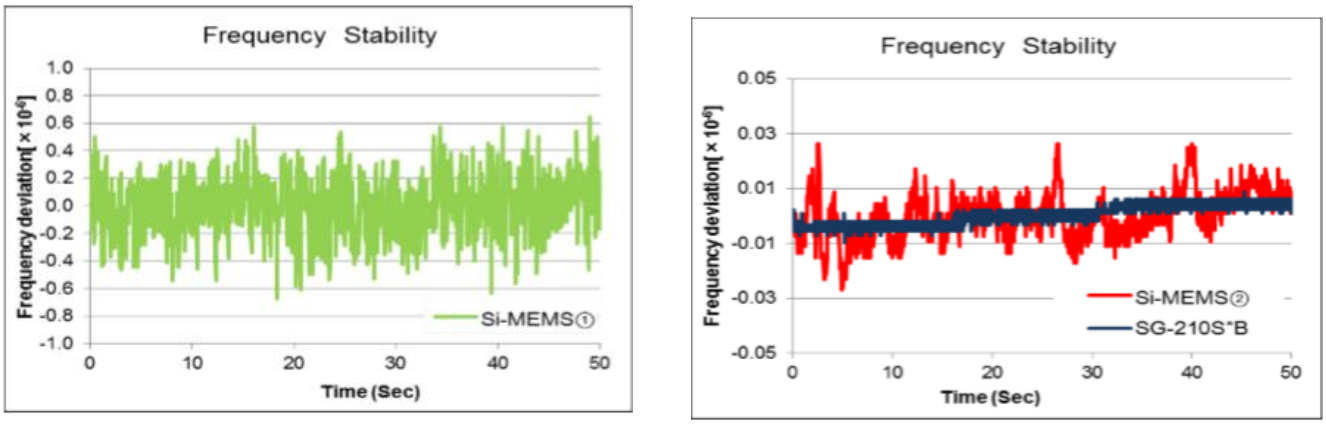

Figure 22-frequency stability of both MEMS and quartz OSC at 3.3 V, Temperature 25 ℃ for 50 ms [29].

From the above experiments, it appears that quartz OSC are much better than MEMS OSC but as it was stated above the size, fixed frequency and CMOS compatibility are the things that can help MEMS OSC dominate in some specific applications.

Chapter Three
Market Research

SAW resonators are not that widely used since they are still under research and have a lot of developments to be done to it in order to replace resonators in quartz crystal oscillators and be on chip instead of being of chip.
That's why there is limited number of companies that produce commercial SAW resonators or oscillators, and they are listed below with the specs of each product.

1-Golledge SAW resonator Fig-23 [30]:

It is produced by Golledge Company, the frequency of operation ranges from 100MHz ~ 1.1GHz, mostly one port SAW resonator.

Applications: Wireless communications Wi-Fi & Remote control.

Figure 23-Golledge SAW Resonator [30]

2-Qualcomm SAW resonator Fig-24 [31]:

It is produced by Qualcomm company, the frequency of operation ranges from 315MHz ~ 1.1GHz, insertion loss ranges from 1.1dB to 1.5dB, Temperature ranges from -40 ℃ to 125 ℃.

Figure 24-Qualcomm SAW Resonator [31]

3-Qualcomm SAW filter & resonator kit Fig.25 [32]:

It is a kit that has both SAW filter and resonator, it has two types:

- Wideband product ranges from 1MHz to 97 MHz
- Narrow band product ranges from 0.1MHz to 0.36MHz

Its center frequency ranges from 25KHz to 150 KHz. The price ranges from 37$ to 46$ per kit.

Figure 25-Qualcomm SAW filter & resonator kit [32]

Chapter Four
Literature Review

SAW and SAW devices are reported in the early literature but they became more valuable in the 70s in the work of Richard White [14]. The main idea of the work presented in this paper is discussing the new applications of surface elastic waves in electronic systems.

Surface elastic waves are basically waves that have longitudinal and transverse components to allow the deformation to occur on the normal direction to the material and to propagate in the direction of motion, making a wave that travels on the surface of the material with a confinement of few wavelengths.

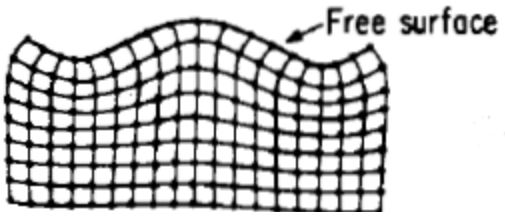

Figure 26-Rayleigh Surface Waves [14]

It briefly mentions that the idea that surface elastic wave devices are devices that work with the principle of generated surface acoustic waves from electric signals by a transducer and that this wave propagates on piezoelectric crystals. Then these electric waves are converted back to an electric signal on the second transducer, which demonstrates the reversible mechanism underwent by the mechanical and electrical coupling.

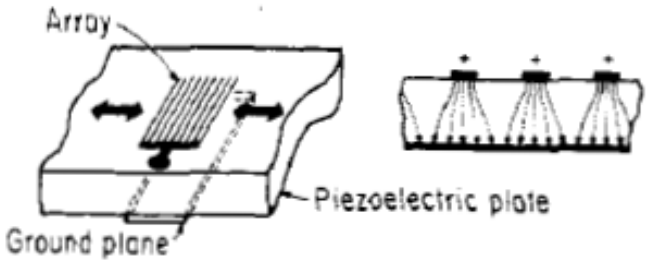

Figure 27-Basic SAW device[14]

Such mechanism is handled because according to Maxwell's equations and continuum equations, the presence of such successive alteration of electric field on the surface, a wave must be present.

Significance of elastic waves reside in the fact that their propagation velocity is low with respect to electromagnetic waves, around 10^5 times smaller than electromagnetic waves. So elastic wave resonators are 100,000 times smaller than electromagnetic wave resonator for the same frequency. Previously, fabrication limitations suppressed the frequency under 100 MHz. It all started from discovering Rayleigh Waves and how the travel on surfaces and then SAW devices emerged. Surface waves are more accessible than bulk waves, which is more favored.

As mentioned earlier in the discussion of SAW, the electrical and mechanical coupling are governed by the following equations

$$D = [e][S] + [\epsilon]E \quad (16)$$

$$T = [c][S] - [e]E \quad (17)$$

The transducer is reversible, it can initiate waves and detect them as well. Although only two fingers are sufficient for generating a surface wave, more fingers are better for better efficiency, without mentioning the negative side of parasitic capacitance, and it accounts for less band width. In the Interdigital Electrode array, the field components change sign from one gap to another, creating stress in the piezoelectric material.

The work also discusses that surface acoustic waves velocities depend solely on the material properties $e_{15},\ \epsilon_{11},\ \&\ c_{44}$ according to earlier models of surface acoustic waves. The velocity of the surface wave on an electrode surface is

$$v_s^2 = \left(\frac{\bar{c_{44}}}{\rho}\right)(1 - K^4) \quad (18)$$

Where

$$\bar{c_{44}} = c_{44}(K + 1) \text{ and } K^2 = \left(\frac{e_{15}^2}{c_{44}\epsilon_{11}}\right) \quad (19).$$

Applications:

- Surface Studies: Studies by geologists regarding cracks and voids near the surface. So surface waves attenuation and speed could give information
- Signal Generation and Processing: Electronic amplifiers or oscillators
- Surface scanning optical sensors.

A. N. Nordin and M. E. Zaghloul reported in a two port SAW resonator integrated using the 0.6 µm CMOS technology. The main trend in this work is to study three designs of CMOS SAW MEMS resonator figuring out their characteristics at different frequencies and compare between their results using the fabricated resonators to obtain the S_{21} as well as S_{11} parameters for each of them.

The basic design of the CMOS SAW MEMS resonators presented in this work consists basically of two ports for output and input interdigital transducers(IDT), and on each side there are reflectors to eliminate the losses of the waves is shown in Fig-29, then three designs with different parameters and different operating frequencies are obtained by making differences in number of transducers, the distance between input and output IDTs, reflectors heights, etc. Fig-30.

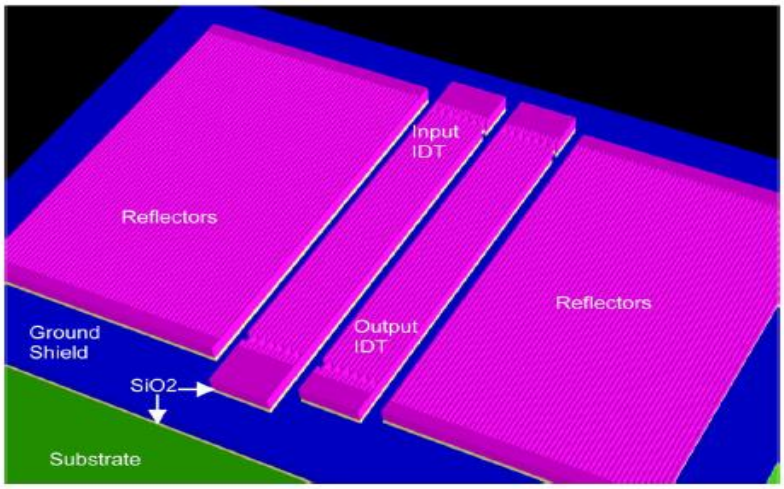

Figure 30-Implementation of a two-port SAW resonator structure in CMOS.

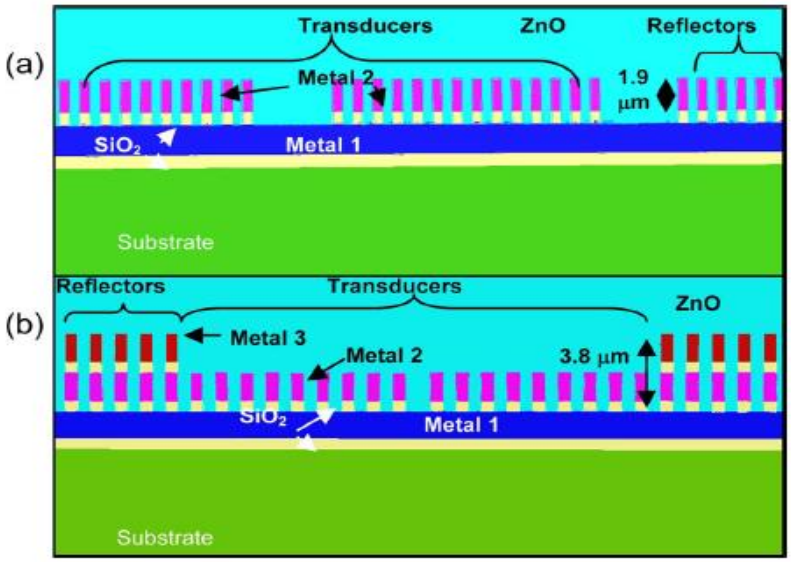

Figure 29- a- Cross section for the 1st and 2nd designs of the CMOS SAW resonator.

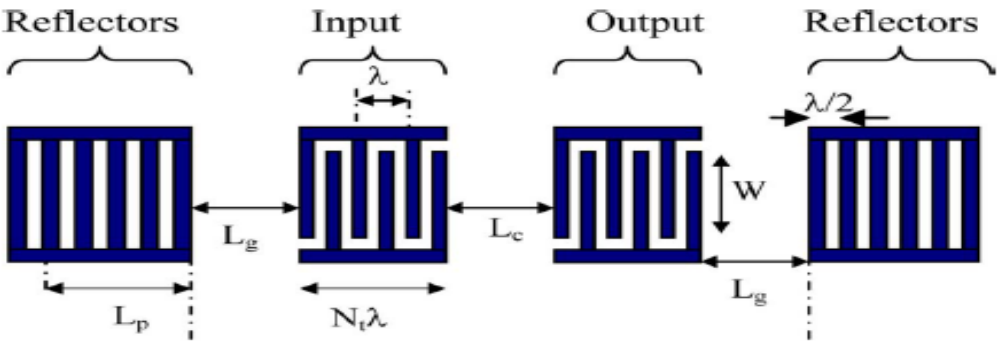

Figure 28-A plan view of the basic design

A plan view of the basic design is shown in Fig-28, where:

f_f: $Resonant\ frequency$
λ: $wavelenght$
v: $Acoustic\ wave\ velocity = \lambda * f_r$
W: $Width\ of\ aperature$
N: $Number\ of\ reflectors$
N_t: $Number\ of\ transducers\ pairs$
L_g: $Distance\ between\ reflector\ and\ transducer$
L_c: $Distance\ between\ input\ and\ output\ transducers$
L: $Distance\ between\ reflectors$
L_P: $Penetration\ depth\ of\ the\ wave$

The three designs are obtained by using different values of these parameters for them as shown in Table-2

Table 2-Comparison between the three designs

Design	$\boldsymbol{\lambda}$ (μ**m**)	$\boldsymbol{f_f}$ GHz	$\boldsymbol{W}$ (μ**m**)	$\boldsymbol{N}$	$\boldsymbol{L_g}$ (μ**m**)	$\boldsymbol{L_c}$ (μ**m**)	Q
1	3.6	1	144	39	7.2	7.2	44
2	4.2	0.857	168	100	1.05	2.1	86
3	6	0.6	160	33	1.5	3	285

.

At first an AC signal is directed to the input IDTs, as a result, surface acoustic waves propagates into the piezoelectric material towards the output IDTs, these waves are detected at the output IDTs and then translated again to electrical signals. The reflectors are used to confine the surface acoustic waves inside the piezoelectric material and eliminate the losses which in turn improves the quality factor of the resonator. And it can be concluded ,from Table-3, that increasing the reflectors height increases the quality factor.

These designs are fabricated using only three processes of micromachining, firstly, reactive-ion etching to release the electrodes of the SAW from the SiO_2 insulating layer. Secondly Zinc-Oxide is deposited, and it was chosen as it provides outstanding performance compared to other piezoelectric materials that can be used. Finally, the Zinc-Oxide is etched to release the structure and to provide connection pads used for probing.

More specification of applications are considered in the last decade, and this can be seen in the work of F.Sidek ,A.N. Nordin, M. E. Zaghloul [33].

The paper presents RF-CMOS circuit model designed for SAW resonators used in RF electronics and transceivers. As SAW technology progressed to the range of GHz, it became an important component in RF communication systems. Some applications include signal processing systems, receivers, control units, keyless entry systems, etc. CMOS compatibility is a privilege as well.

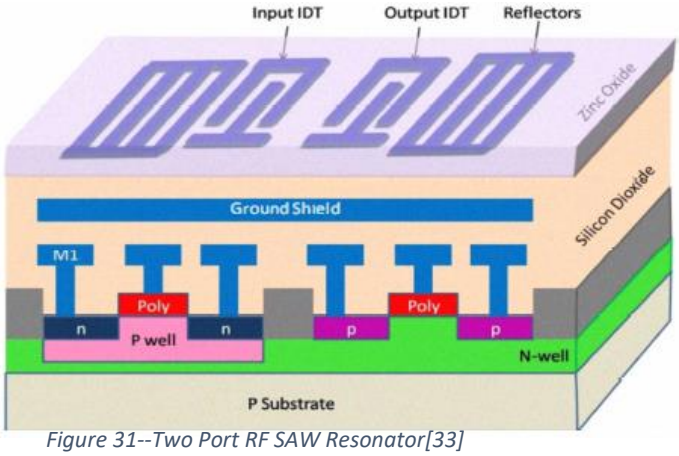

Figure 31--Two Port RF SAW Resonator[33]

This paper proposes a novel integration of RF-CMOS resonator on top of CMOS circuitry.

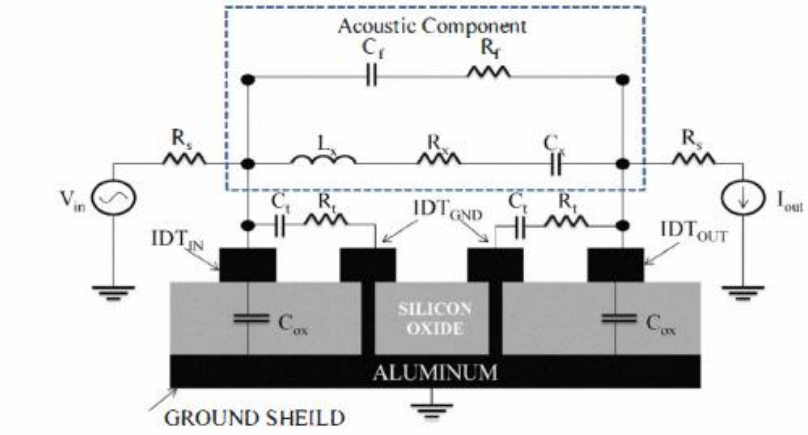

Figure 32-Proposed Circuitry[33]

The circuit is divided into two parts: Acoustic and Parasitic components. The acoustic components describe the wave propagation by RLC where R_x , C_x , $and\ L_x$ produce the series resonance frequency and C_f produce the parallel resonance frequency. R_s , C_{ox}, $and\ C_t$ are the parasitic components and they exist to account for the presence of structures and layers.
Based on the design parameters in Table-3.

Table 0-Design Parameters

Design	$\lambda(\mu m)$	f_r(GHz)	W(μm)	N	Lg(μm)	$L_c(\mu m)$	L(μm)	$L_p(\mu m)$
1	4.20	0.90	126.0	90	1.05	2.10	56.7	69.342
2	2.16	1.80	108.0	100	2.70	1.08	37.8	35.661
3	2.08	1.90	124.8	100	2.60	1.04	44.72	34.341

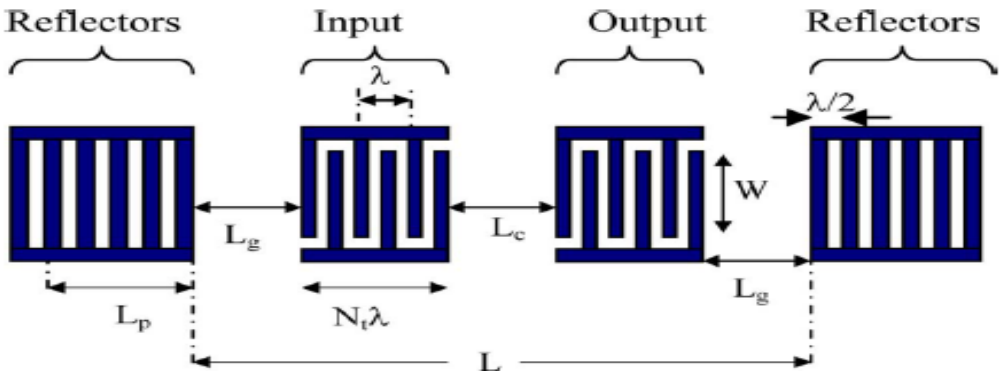

Figure 33-Plan view of the design and the parameters[33]

the devices' performances are measured after they are fabricated experimentally with IBM 0.18 μm technology and by simulation tools to get the following results.

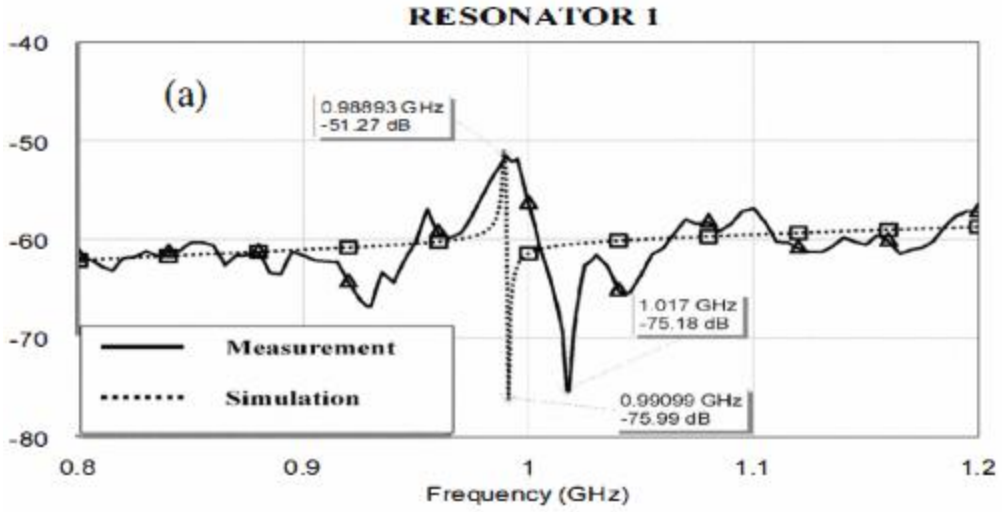

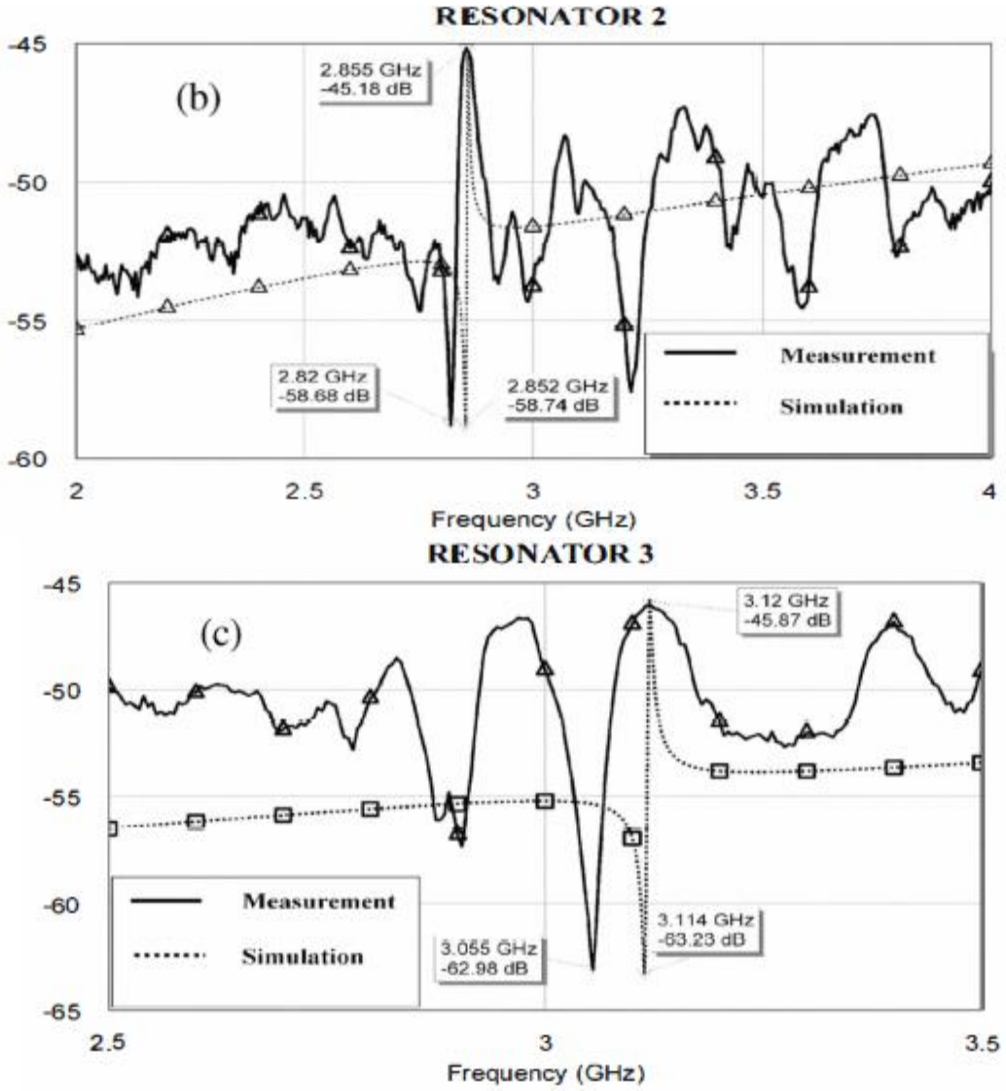

Figure 34-Results of the 3 designs[33]

The modeling of the parameters is based on the following equations:

$$C_t = W\epsilon_{ZnO}N_t \quad (20)$$

$$C_{ox} = W\epsilon_{ox}N_t \quad (21)$$

The resonant impedance:

$$Z_{res} = \frac{R_x + \frac{1}{sC_x} + sL_x}{sC_f\left(R_x + \frac{1}{sC_x} + sL_x\right) + 1} \quad (22)$$

The Parasitic Parallel impedance:

$$Z_p = \frac{R_s}{s(C_t + C_{ox})R_s + 1} \quad (23)$$

According to the given parameters and designs, the extracted circuit parameters are summarized in Table-4.

Table 4-Extracted circuit parameters

Design	$R_x(k\Omega)$	C_x(aF)	L_x(mH)	C_f(fF)	$R_f(k\Omega)$	$C_{ox} + C_t$(pF)	$R_t(k\Omega)$
1	14.8	5.02	5.155	1.87	1.00	2.998	0.50
2	21.4	-3.96	-0.786	1.51	0.50	0.336	0.70
3	19.7	-3.27	-0.796	1.108	0.25	0.434	0.80

Accordingly, the results obtained are:

Table 0-Measured Parameters

Design	f_s	f_p	Series Quality Factor	Parallel Quality Factor
1	0.9889 GHz	1.017 GHz	61.36	317.8
2	2.855 GHz	2.82 GHz	71.37	201.42
3	3.12 GHz	3.055 GHz	38	235

A comparison between ZnO and AlN as IDTs for the SAW resonator is reported in, also introduced the benefits behind the 2 ports design as input output instead of only one port design. The paper used in simulations $0.35\mu m$ CMOS process.
he 3D model of the stated design appears in Fig-35, but the paper depended on the 2D simulation of the design on COMSOL, a top view for the design is in Fig-36.

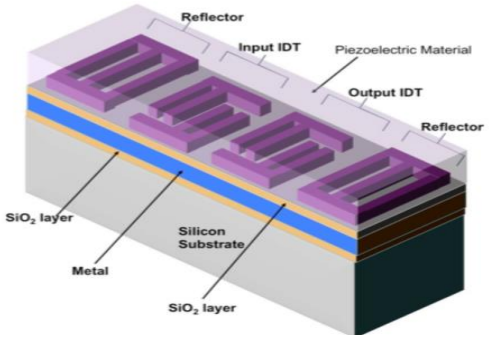

Figure 35-3D model of the 2 Port SAW resonator [34]

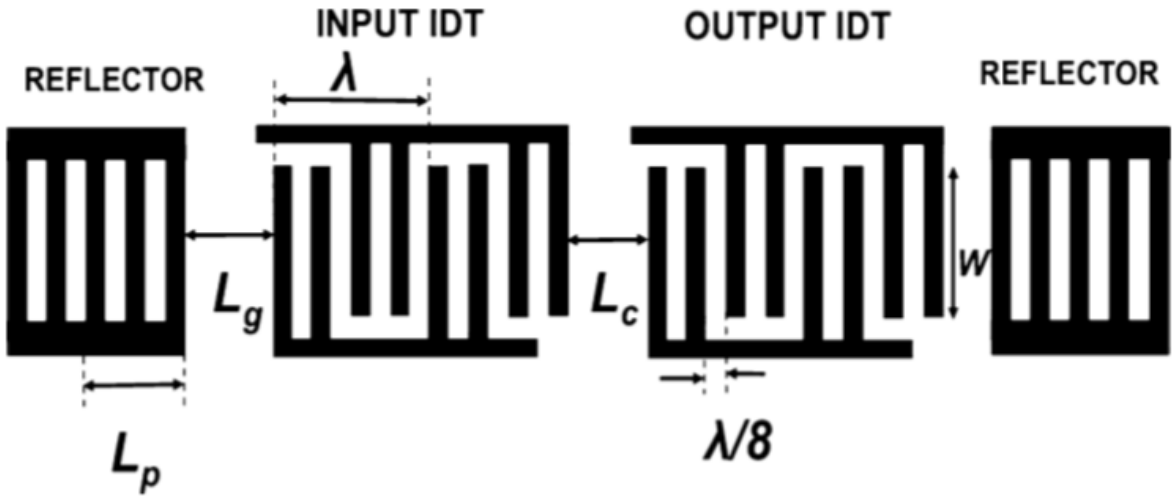

Figure 36-Top View of the proposed design, 2 Port SAW resonator [34]

W: $Width\ of\ aperature$
L_g: $Distance\ between\ reflector\ and\ transducer$
L_c: $Distance\ between\ input\ and\ output\ transducers$
L: $Distance\ between\ reflectors$
L_P: $Penetration\ depth\ of\ the\ wave$

In the comparison between the 1 port Design and the 2 port design, the 1 port didn't need reflectors on the sides, but it suffered from internal reflections that are weak on it's own although it would cause great deviation if it was constructively interfered, this is totally avoided in the 2 port design that the electrodes have 180 degrees phase and those weak reflections are canceled, that's why the 2 port are used when the frequency accuracy is needed since it can accurately get the needed frequency without being deviated by any small reflections. But of course, it has a disadvantage since it limits the maximum resonance frequency since divides the pitch by two.
The material used is to be chosen according to[35]:

- CMOS compatibility and ease of deposition.
- The piezoelectric properties of the material.

One of the main properties that must be taken into consideration is k^2 which is the electromechanical coupling coefficient, the higher it is the more suitable the material is for SAW resonator, previously the quartz was used since it has a very high k^2 but it is not CMOS compatible that's why research is looking for CMOS compatible material with high k^2, ZnO and AlN, has high k^2 and they are CMOS compatible, that's why they are a very good candidate for being used in SAW resonators[35].
The design parameters are stated in Table-6.

Table6-Design Parameters for both AlN and ZnO SAW resonators.

Parameters	ZnO SAW resonator	AiN SAW resonator
Wavelength (μm)	3.48	3.48
Width of aperture, W (μm)	150	150
Metal 2 width ($\lambda/8$) (μm)	0.435	0.435
Distance between input and output IDT, Lc (μm)	1.74	1.74
Distance between reflector and transducer, Lg (μm)	3.48	3.48
Piezoelectric thickness (μm)	2.0	2.0

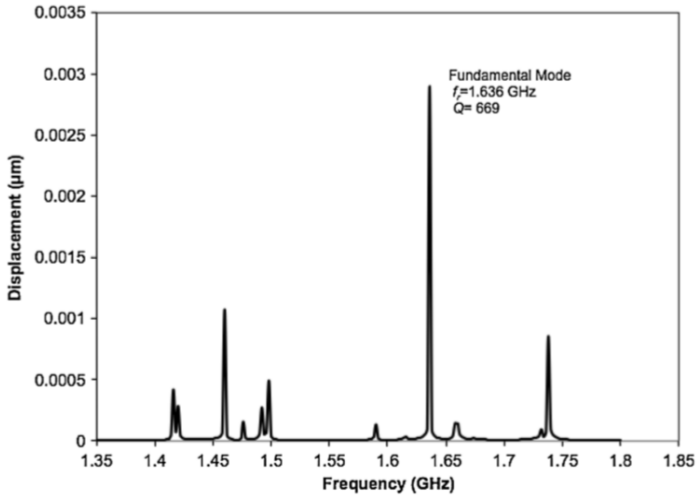

Figure 38-AlN SAW resonator Design resonance frequency and quality factor. [34]]

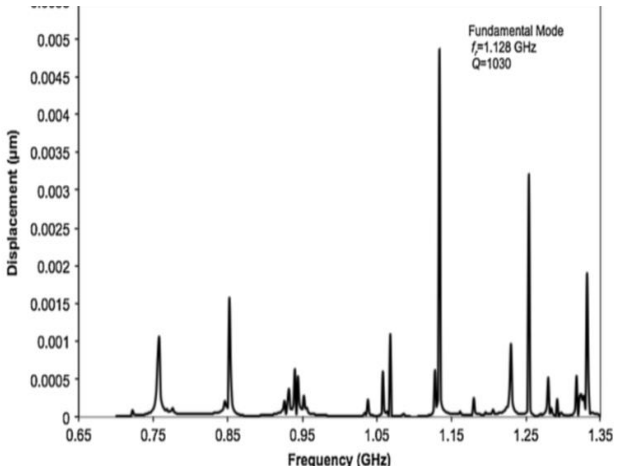

Figure 37-Zno SAW resonator Design resonance frequency and quality factor. [34]

The susceptance versus frequency graph for both designs is in Fig-39 and Fig-40, it is used to get the resonant and anti-resonant frequency used to get the values of the electrical model of the resonator to help matching it to the oscillator circuit.

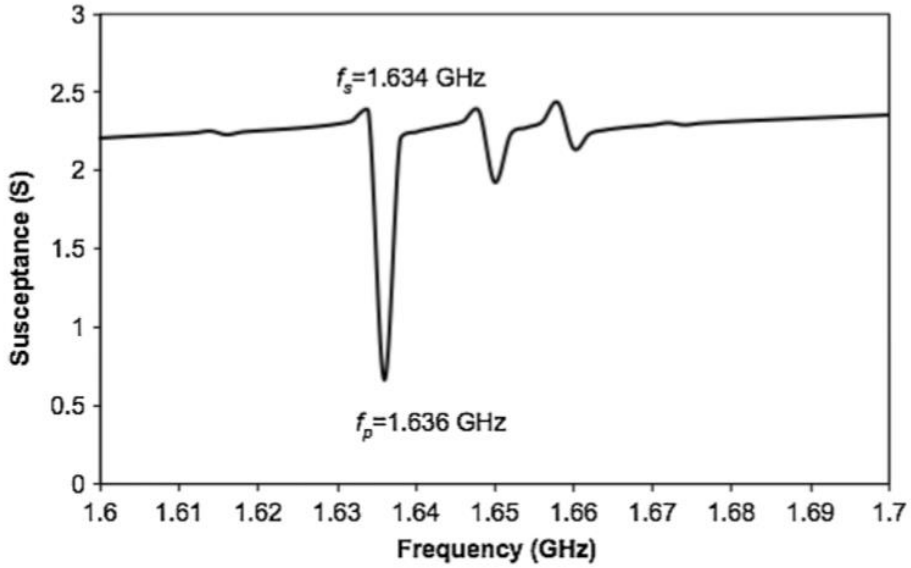

Figure 39-AlN SAW resonator resonant and anti-resonant frequencies [34]

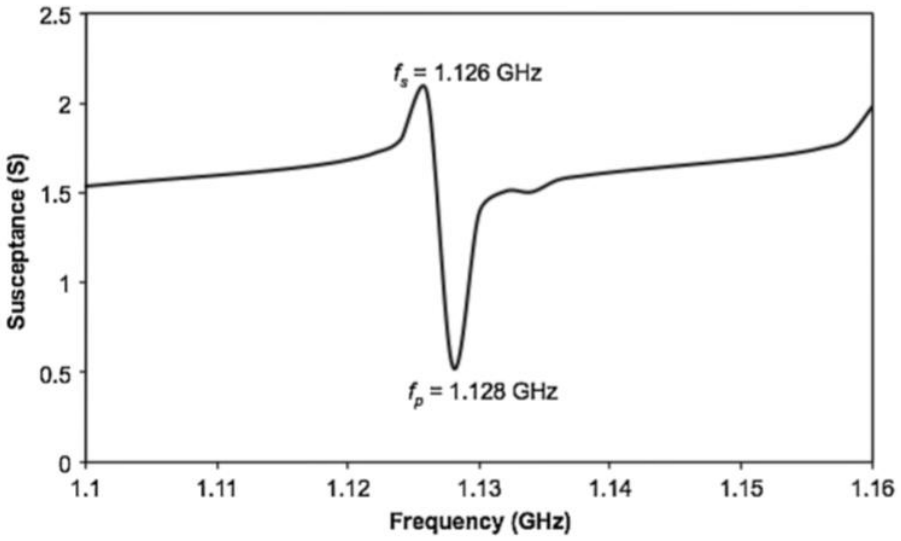

Figure 40-ZnO SAW resonator resonant and anti-resonant frequencies [34]

The results of the simulation is shown in Table-7.

Table 7-Simulation results for both designs. [34]

Parameters	ZnO SAW resonator design	AlN SAW resonator design
Acoustic velocity, v (m/s)	3,925	5,953
Wavelength, λ (μm)	3.48	3.48
Fundamental Resonant Frequency, fr (GHz)	1.128	1.636
Max displacement (nm)	4.86	2.90
Quality factor, Q	1,030	669
Coupling coefficient, k^2	0.43748	0.30164

Finally, as a conclusion form the above results, ZnO material is better than AlN material for the same design parameters, since it produced higher k^2 and Q_s, also the 2-port design is better than one port design since it decreases the undesirable reflections.

M. S. Pandian et, al. reported in 37 a new way for designing the interdigital transducers (IDTs) different from the conventional ways of designing them. The conventional ways depend mainly on a thick film of the piezoelectric material and the transducers are think metal layers, on the contrary, they reported a new way by using a thin film piezoelectric material typically AlN, and it is isolated from the substrate using a dielectric thin film as shown in Fig-41.

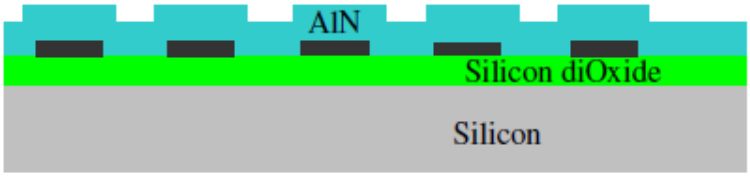

Figure 41-Thin film SAW Device Configuration [37]

Aluminum Nitride, which is a CMOS compatible material, is deposited using Physical Vapor Deposition (PVD) which forms non-planar films. Fig-42 shows a scanning electron microscope for the proposed design and the non-planarity is clear.

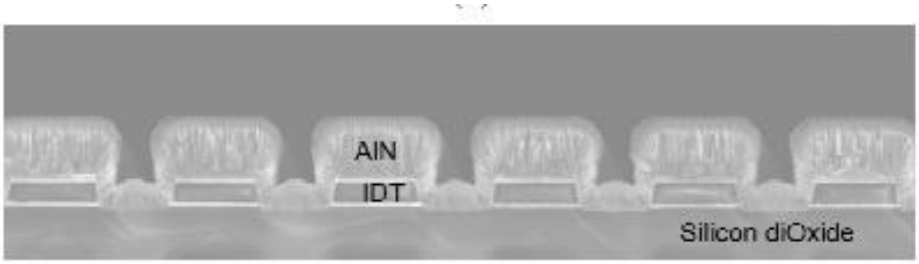

Figure 42-SEM view of the thin film SAW Device Configuration[37]

The schematic of the proposed design is shown in Fig-43 the device is designed to operate at 1.4 GHz, as the velocity of the surface acoustic waves is assumed to be $5600\ m/s$ and λ is chosen to be 4 µm, number of fingers per transducers is chosen to be 72, the width of aperture W = 260 µm, and the input and output IDTs has a distance difference of L= 5600 µm.

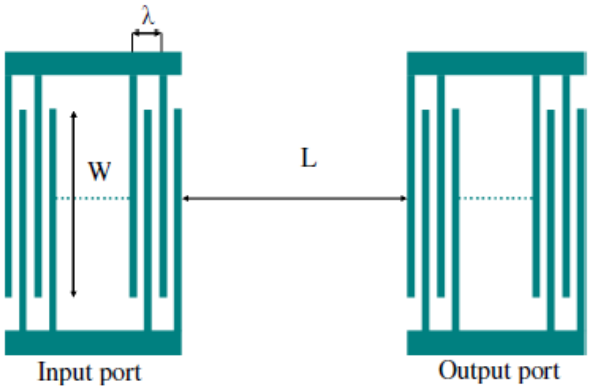

Figure 43--Design of two ports delay line [37]

This device is fabricated using the SAW MEMS on CMOS platform of the SilTerra Malaysia Sdn Bhd [38]. Firstly, the Aluminum transducers are deposited by PVD on a silicon-on-insulator SOI wafer, three different thicknesses are deposited in this work to figure out the variations in results resulted from the change of the transducer thickness ($t_1 > t_2 > t_3$) where first and second thicknesses are considered high non-conformal structure while the third one is considered the best one in conformity , secondly, the Aluminum Nitride thin film is deposited by PVD and patterned to provide padding.

Once the devices are fabricated, they are employed to a network analyzer characterizing them to

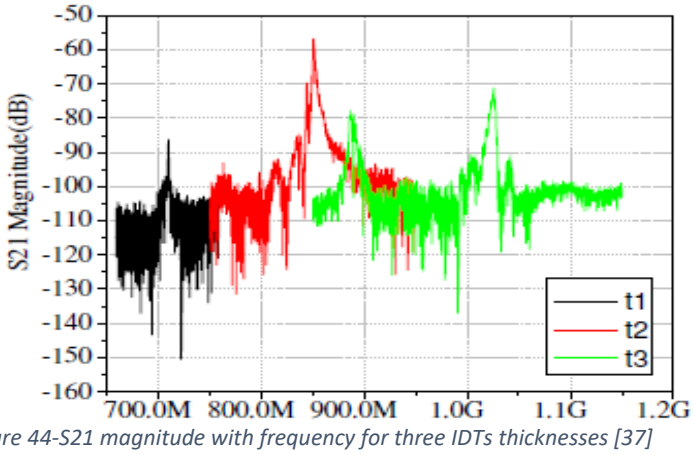

Figure 44-S21 magnitude with frequency for three IDTs thicknesses [37]

obtain the S_{21} magnitude graph with frequency as shown in Fig-44, it's shown that the closest achieved frequency to the theoretical value(1.4GHz) is of the design of $t_3$which proves the point that the more conformal the transducers are, the closer the measured frequency to the theoretical one.

This design has the advantages of eliminating the electrical feed-through that may happened thus only first mode of the surface acoustic waves is detected at the output transducer, as well as the device implements no reflectors avoiding the interference of any undesired signals in the electrical response at the output transducer.

As we have seen previously that there was not a clear method of extracting the electrical circuit model, many efforts were spent in this scope to find a direct way to extract the electrical circuit parameters. This can be seen [39]

Present a method to extract circuit parameters from a one port SAW device.

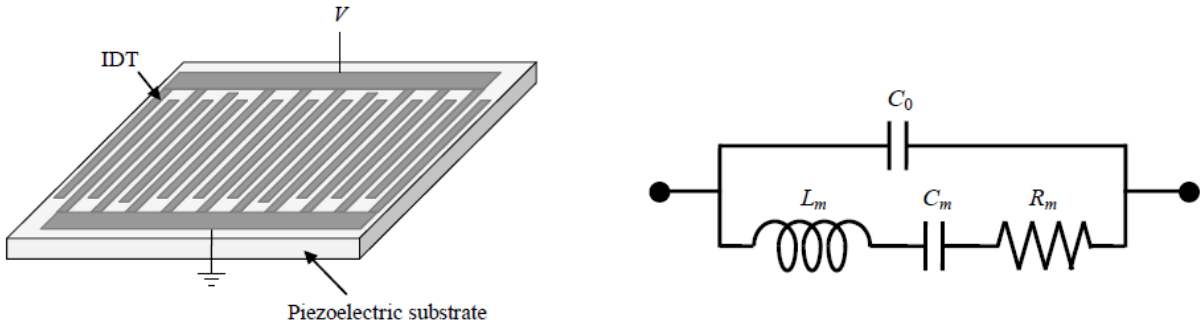

Figure 45-One port IDT schematic and electrical equivalent[39].

L_m *and* C_m are the motional inductance and capacitance that account for inertia and elasticity while R_m accounts for the damping of the propagating wave. While C_0 is the static capacitance of the comb-like structure responsible for generating the surface waves. It is inferred logically that the motional capacitance and inductance are related to the material properties like stiffness, piezoresistivity, and dielectric constants. Which is true as these properties also control the resonant and anti-resonant frequencies, f_r and f_{ar} respectively, along with the quality factor Q that are used in return to calculate the circuit model parameters. Capacitance and inductance are known to account for energy storage while resistance account for the speed of the wave and the stiffness of the material. Accordingly the following parameters are governed by the following equations:

$$R_m = G_r = G|_{f=f_r}$$

$$C_m = \frac{1}{\omega_r Q_r G_r}$$

$$C_0 = \frac{C_m}{\left(\frac{\omega_{ar}}{\omega_r}\right)^2 - 1}$$

$$L_m = \frac{G_r Q_r}{\omega_r}$$

$$Q_r = \frac{f_r}{\Delta f}$$

Where Δf is calculated from the resonance graph by marking the peak of the resonance and subtracting 3 dB from the peak and measuring the bandwidth, which constitutes 50% of the peak value. To calculate the circuit elements, Q_r, f_r, and f_{ar} are calculated and plotted by COMSOL Multiphysics of the given design.

The COMSOL simulation of the one port SAW device uses the periodic nature of the device and considers only one periodic part of IDTs and periodic boundary conditions are applied on the boundaries as follows:

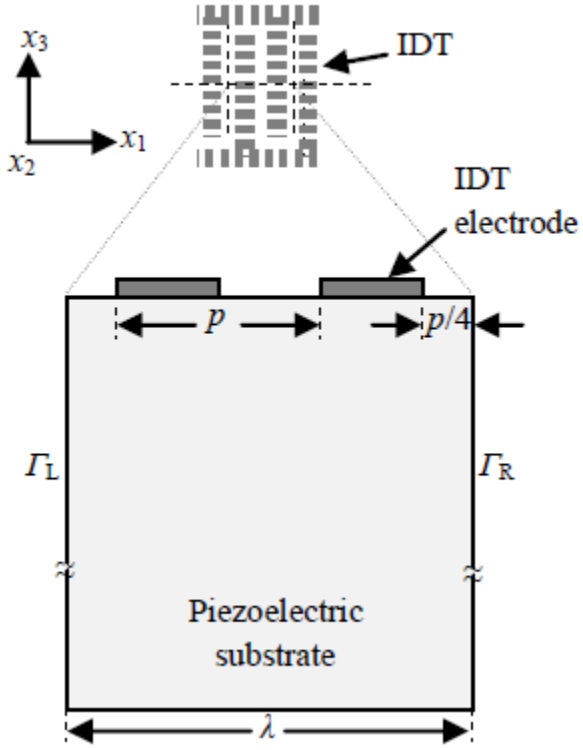

Figure 46-Two dimensional representation of the one port device[39]

The design parameters are presented in following table:

Width of Substrate (x_1)	Thickness of Substrate ($-x_3$)	Period (p)	Thickness of the IDT (x_3)
16 μm = 1 λ	160 μm = 10 λ	8 μm	0.2 μm

The piezoelectric material is lithium niobate and the IDTs material is aluminum. The bottom of the substrate is considered to be fixed because the thickness was used large enough in order to prevent any wave reflection, so considering the bottom to be a fixed constraint is plausible and feasible in this case. The frequency domain analysis is carried on and the following graphs are obtained:

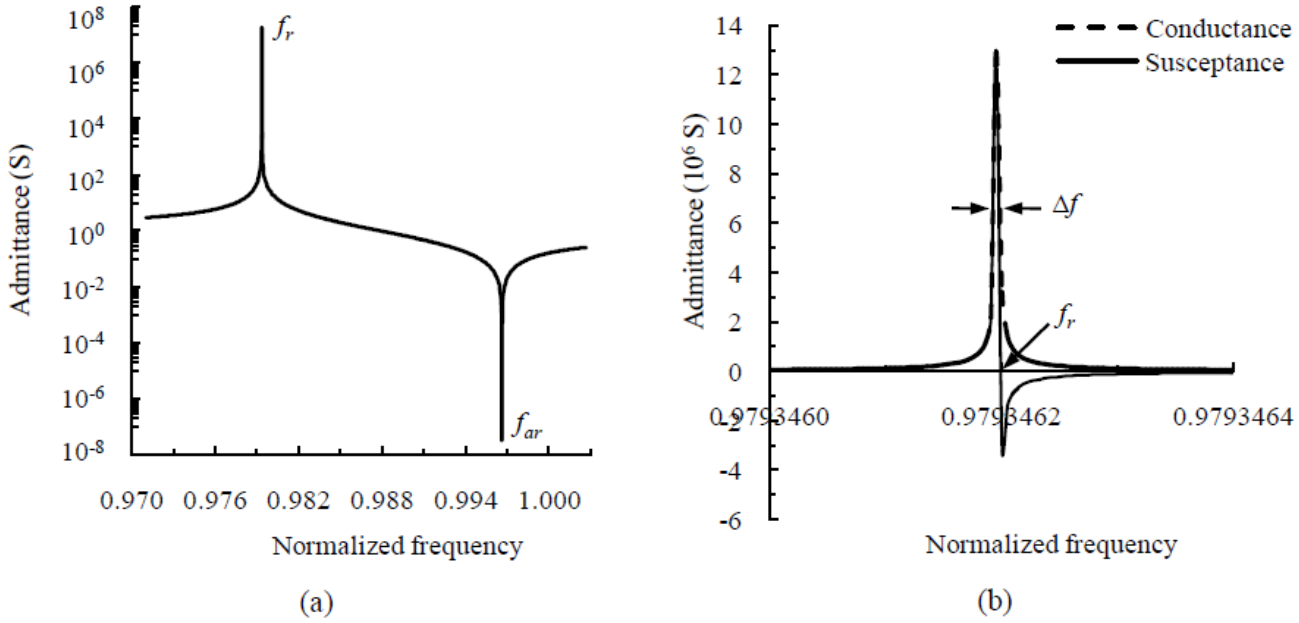

Figure 47-Results of the frequency domain study. (a) Plot of admittance versus frequency to obtain the resonant and anti-resonant frequencies. (b) Plot of the Quality factor.[39]

According to these values of f_r , f_{ar} , and Q_r , the parameter extraction equations are used to obtain the following values:

Parameter	Value
R_m	77.29 nΩ
C_m	16.16 pF
L_m	9.72 nH
C_0	16.16 pF

So the final circuit model is:

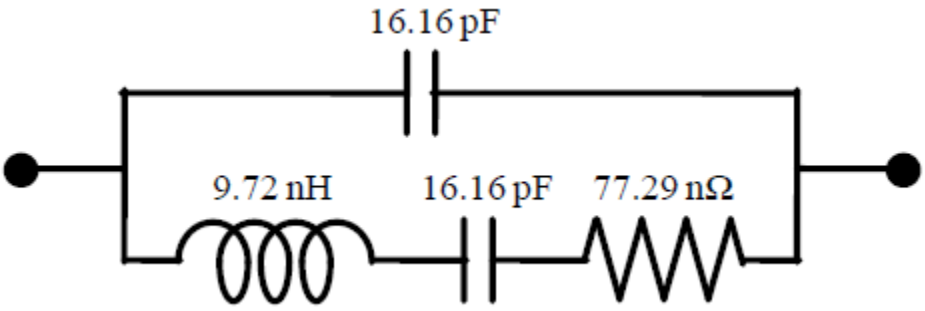

Figure 48-Final circuit model of the one port device.[39]

Chapter Five
Simulation

COMSOL Simulation

Usually, the 3-D FEM with COMSOL for SAW devices is implemented on some assumptions which can give the displacement of the acoustic waves on the surface and showing the modes shape on the device but the 3-D FEM model cannot show the admittance graph which has the resonance frequency that are required, to calculate the features of our devices like Series resonance frequency, Quality factor Insertion Loss, phase depth, Temperature Coefficient Factor (TCF), ….etc. Therefore, the 2-D FEM model was adopted instead. The 2-D FEM models in our study was prepared in COMSOL 5.3. The geometry of our design that was simulated is shown in Fig-49 this was simulated (the input interdigital transducers IDTs).

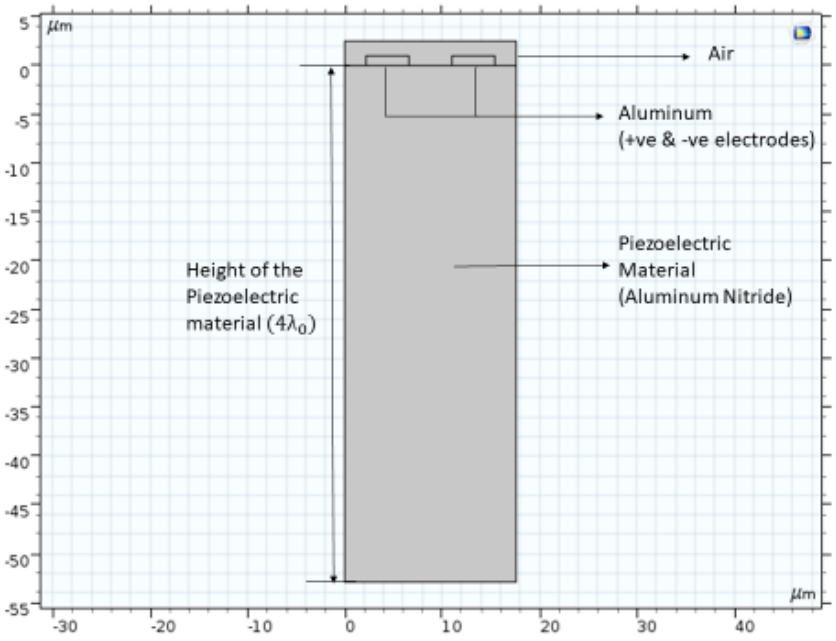

Figure 49- geometry of the device and the materials used in simulation

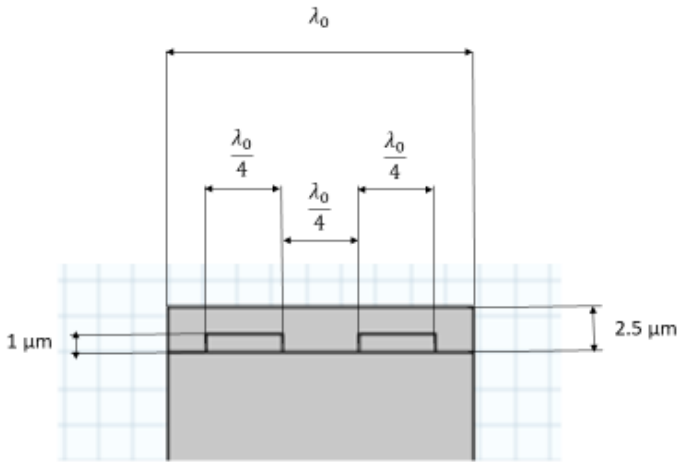

Figure 50- dimensions of the basic device

The resonance frequency of the SAW device depends on the width (λ_0) and the Rayleigh wave velocity of the piezoelectric material which is Aluminum Nitride in our case. Fig-51 shows the wave velocity, width and estimated SAW frequency from COMSOL parameters. The width was calculated by trial and error to get a resonance frequency at exactly 320 MHz which was required.

vR	5760[m/s]	5760 m/s	Rayleigh wave velocity
width	17.63[um]	1.763E-5 m	Width of unit cell
f0	vR/width	3.2672E8 1/s	Estimated SAW frequency

Figure 51- estimated resonance frequency of the device

The voltage applied on one of the electrodes and the other electrode is connected to ground, this applied voltage is 1 volt. This volt represents a disturbance to the device to resonate it and chose the resonance frequency to allow it to flow through the device reaching the output IDTs. The width of the device must be equal to one wavelength (λ_0), the width of each electrode is ($\frac{\lambda_0}{4}$), the spacing between the two electrodes is ($\frac{\lambda_0}{4}$), the thickness of the electrodes is 1 μm and the thickness of the surrounding insulator medium (Air is our case) is 2.5 μm. These dimensions constraints are to allow the resonance of the device to take place which is as required by the SAW devices. [40]

The boundary conditions of our designs are:

- Periodic boundary condition at the two sides of the device.
- Fixed constraint at the bottom of the piezoelectric material.
- The thickness of piezoelectric material is ($4\lambda_0$) or more to avoid the leakage of the waves to the substrate. [40]

The modes shape of the basic design at the resonance and anti-resonance frequencies are shown in Fig-52.

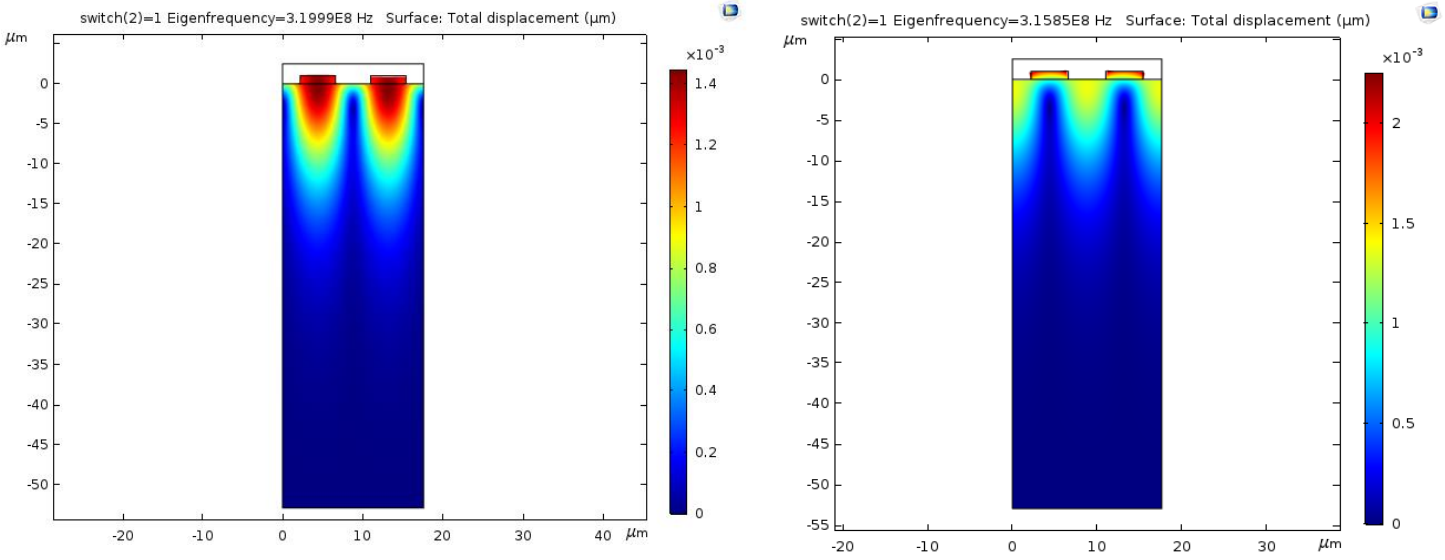

Figure 52- modes shape

The admittance versus frequency graph is shown in Fig-53. It shows the resonance and anti-resonance frequencies which are the basic parameters of the SAW device. The resonance frequency means the frequency at which the response amplitude is relatively maximum.

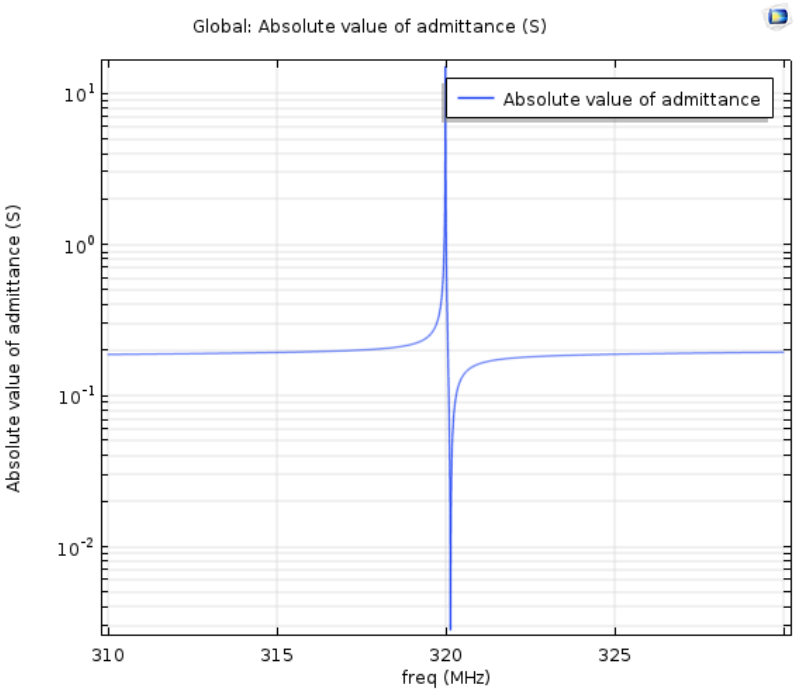

Figure 53- Admittance graph extracted from COMSOL 5.3.

After getting the admittance graph and extracting the data from COMSOL, other parameters are calculated from cadence simulation it is explained in cadence simulation section.

The designs simulated didn't stop at this basic design of SAW resonator, another ideas are implemented to see if they give us better device performance. There is a study done by Silterra Company in Malaysia which is one of the leaders in CMOS and MEMS technologies [41]. They changed the position of IDTs in the SAW device, they made them buried in the piezoelectric material instead of being on the surface. A design is prepared having their idea to see if it will acquire better parameters or not. The design is shown in Fig-54& Fig-55, it is exactly the same as the basic design but the only difference is that the IDTs are buried in the piezoelectric material.

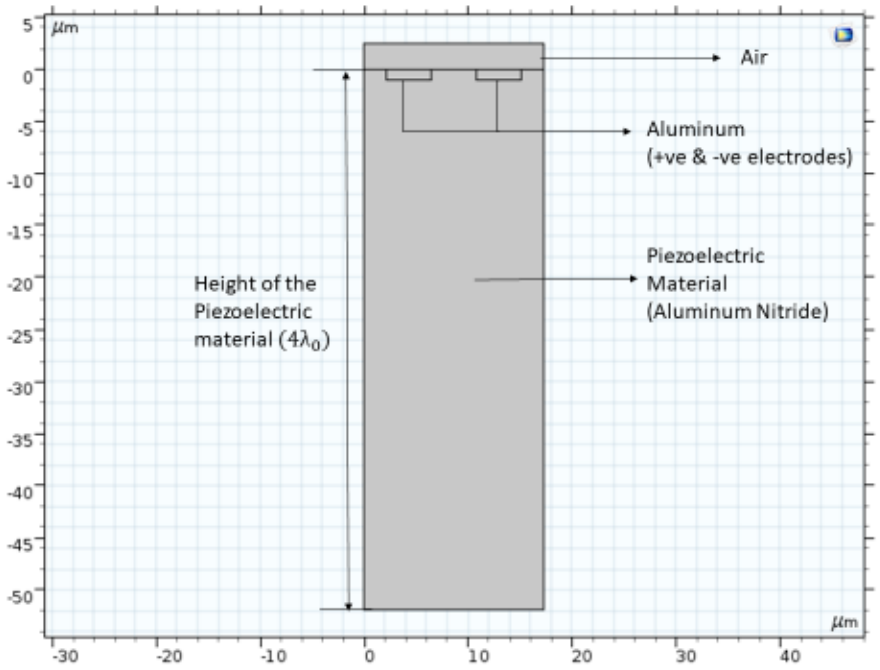

Figure 54- the geometry of the device and the materials used in simulation

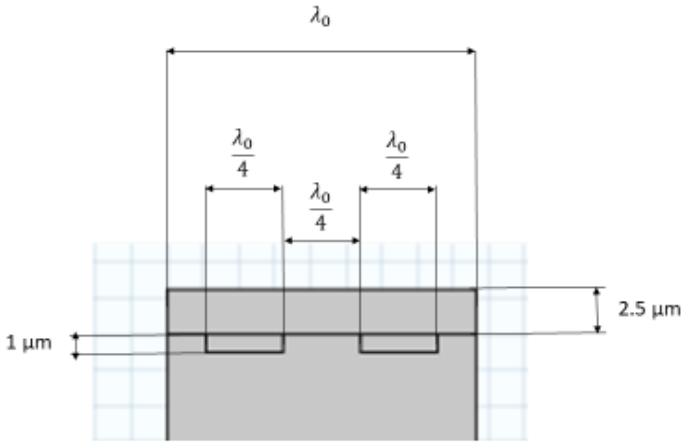

Figure 55- dimensions of the basic device

The materials used, boundary conditions and dimensions constraints are the same as the basic design but the width of the device (wavelength) is different as said before each design has its own wavelength to give the resonance frequency required which is 320 MHz.

The modes shape of this design is shown in Fig-56.

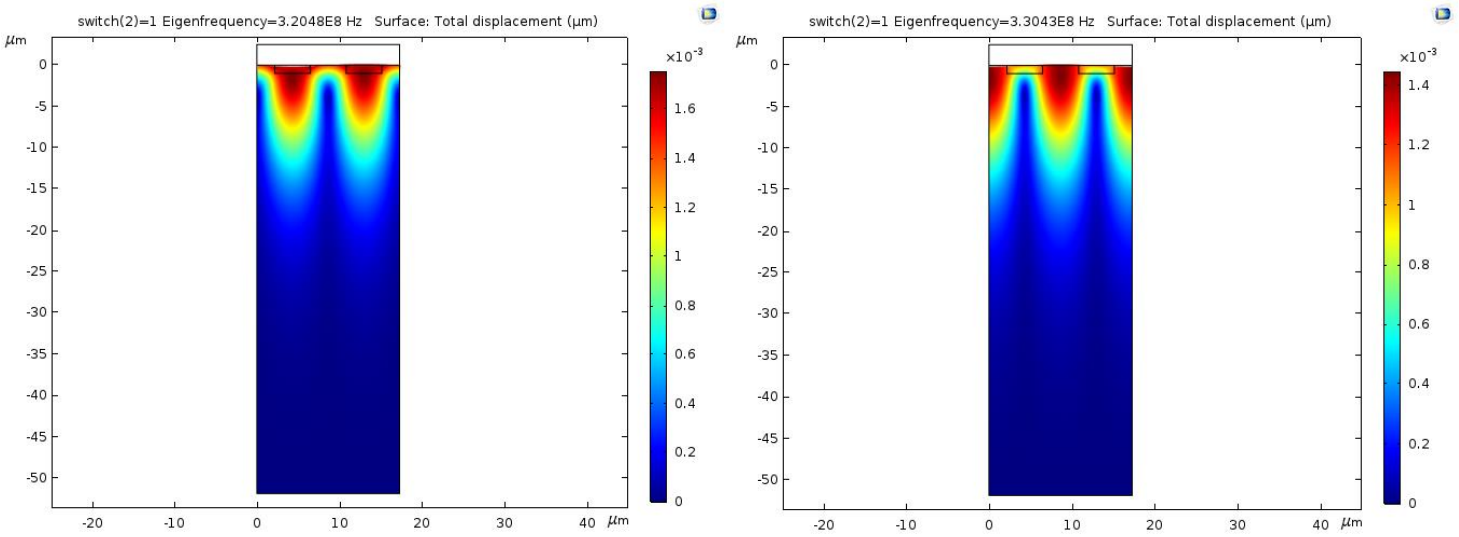

Figure 56- modes shape

The admittance graph for this design is shown in Fig-57.

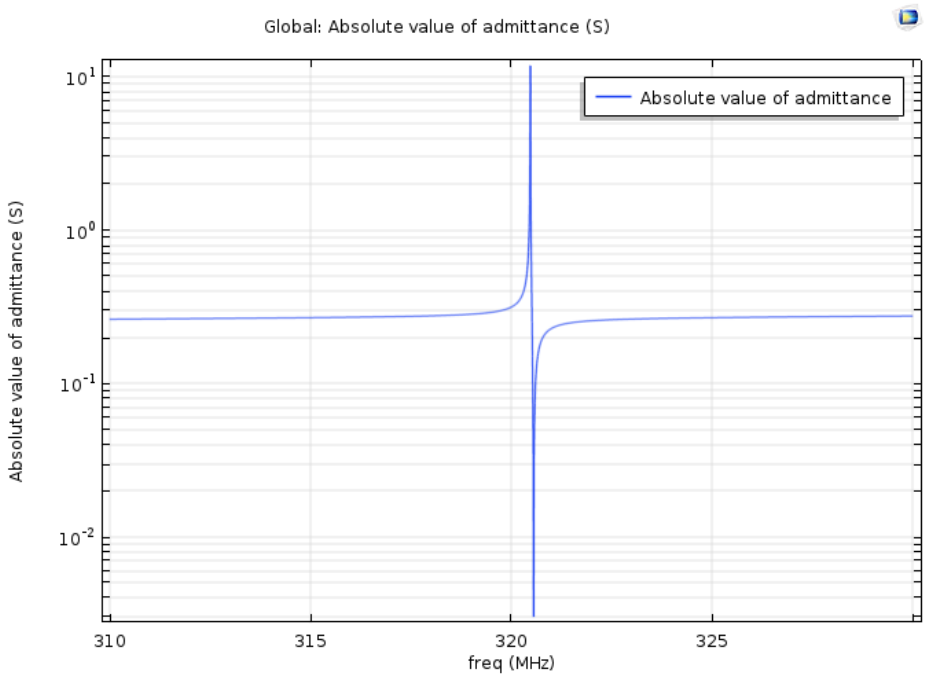

Figure 57- Admittance graph extracted from COMSOL 5.3

The proposed idea in our study is the Semi-Buried IDTs SAW device, in this design the electrodes are semi-buried in the piezoelectric material which means that half of the electrode is at the surface and the other half is buried in the piezoelectric material. The aim from this design is to get a better performance than the other two designs which have the electrodes at the surface or the electrodes are totally buried in the piezoelectric material. The geometry of this design is shown in figures 58 & 59.

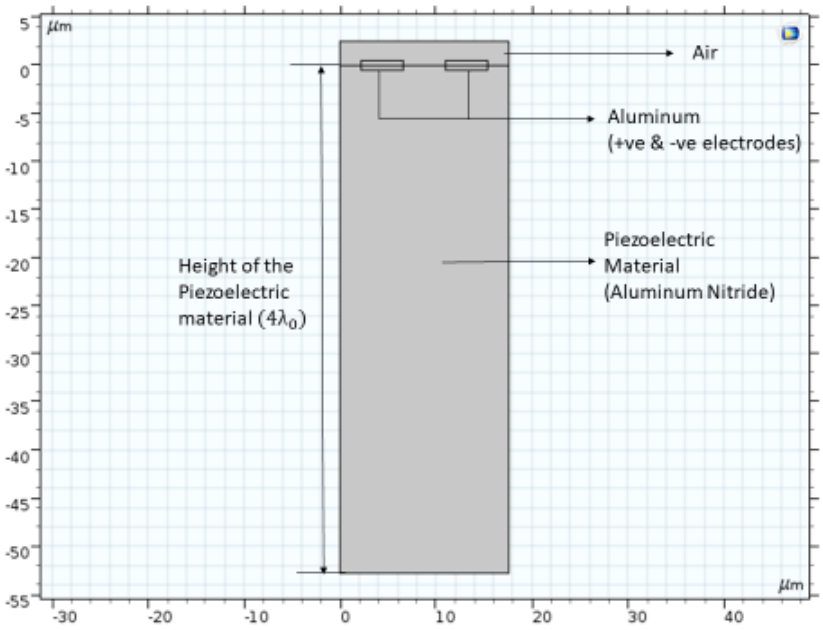

Figure 58- geometry of the device and the materials used in simulation

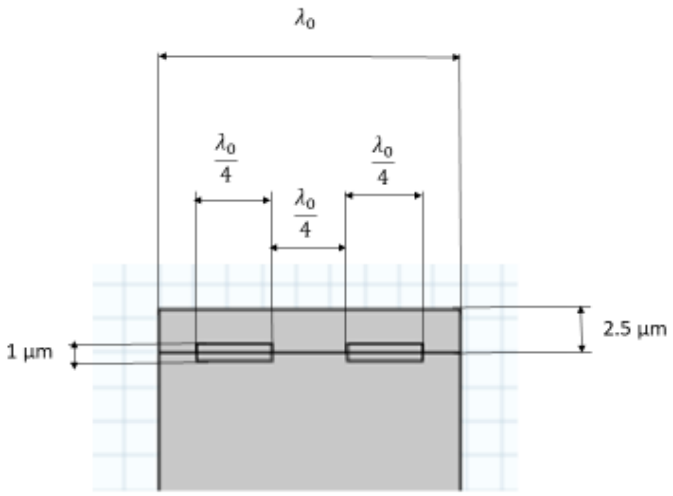

Figure 59- the dimensions of the basic device

The modes shape of this design is shown in Fig-60.

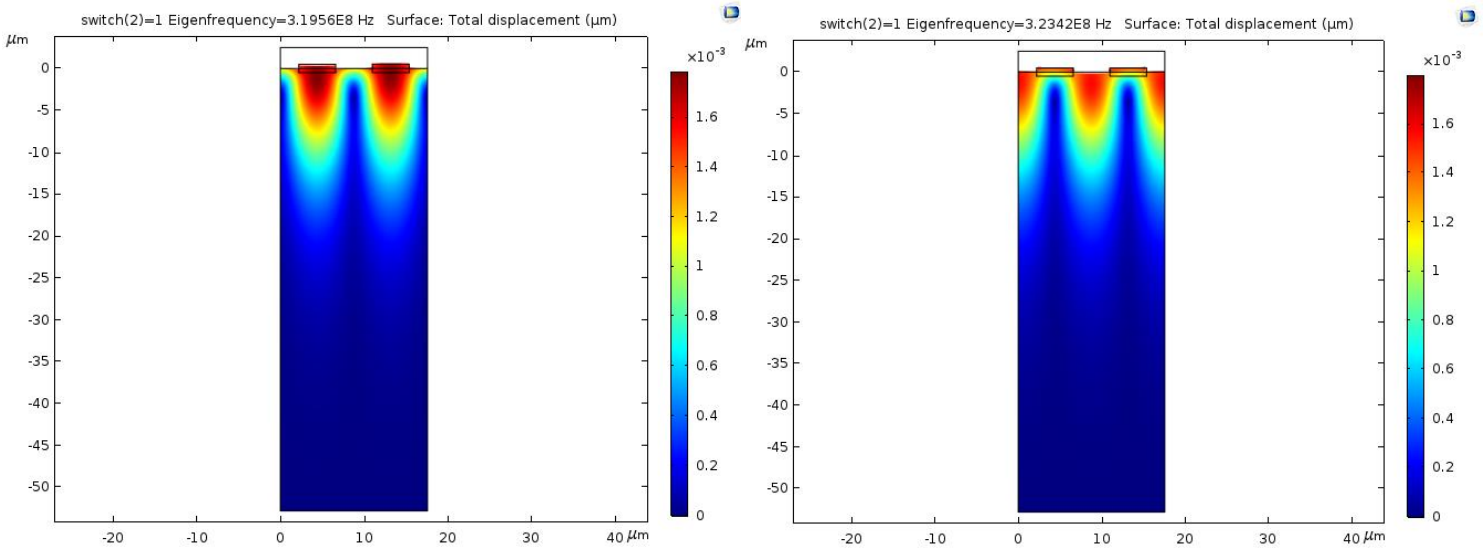

Figure 60 - modes shape

The admittance graph for this design is shown in Fig-61.

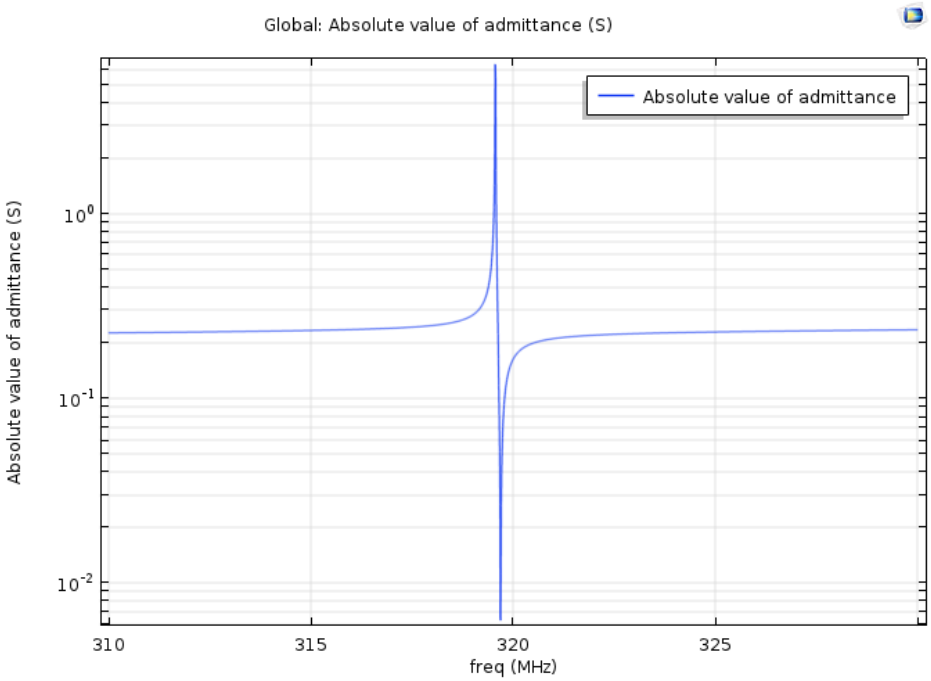

Figure 61- Admittance graph extracted from COMSOL 5.3

The aim of the project is to find the optimum number of IDTs that will acquire the best performance. The multiple ports devices are simulated for each design, started at 1 IDT pair (+ve & -ve electrodes) to 7 IDT pairs. So the total number of designs simulated are 21 model. Figure 14 has some designs of 2 pairs and 7 pairs of the basic design (which has the electrodes at the surface).

Fig-62 shows 2 and 7 pairs of the devices simulated only, the other designs just have different number of pairs of electrodes.

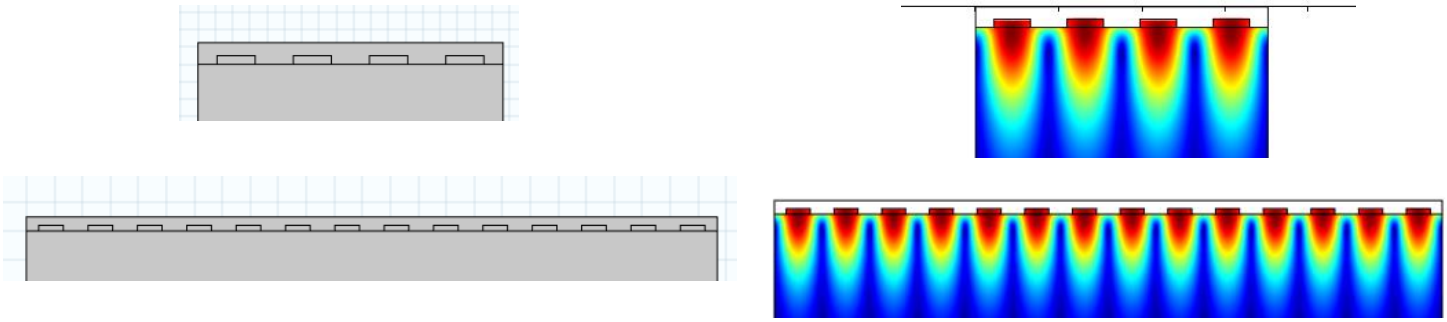

Figure 62- 2 and 7 pairs devices of the Basic design

The admittance curves of all the designs are shown in Fig-63

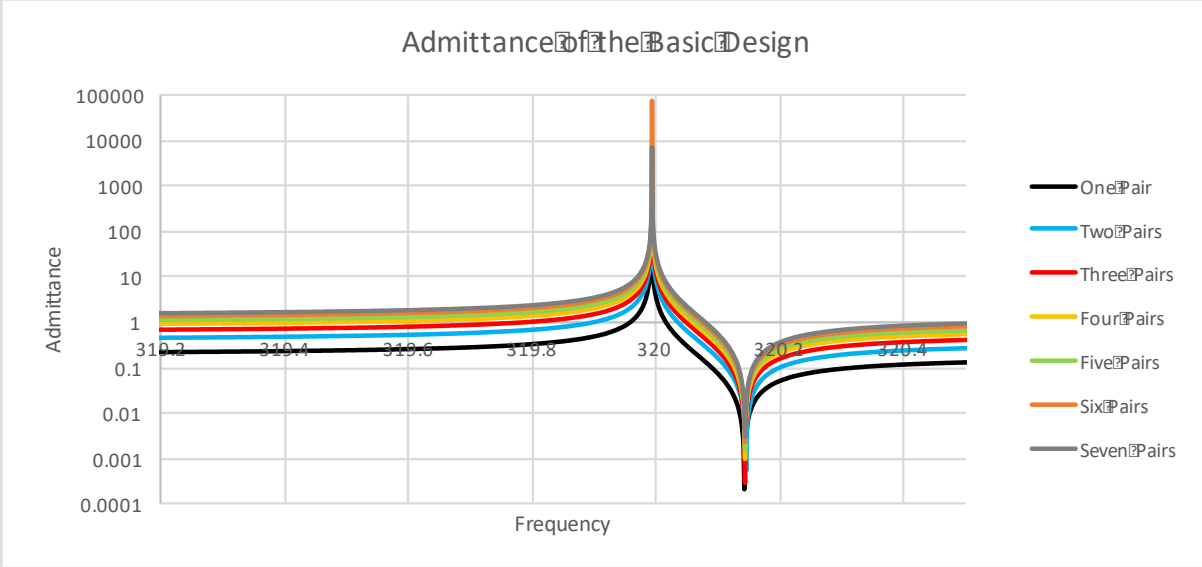

Figure 63- Admittance graph of all devices extracted from COMSOL 5.3

The buried designs are shown in Fig-64.

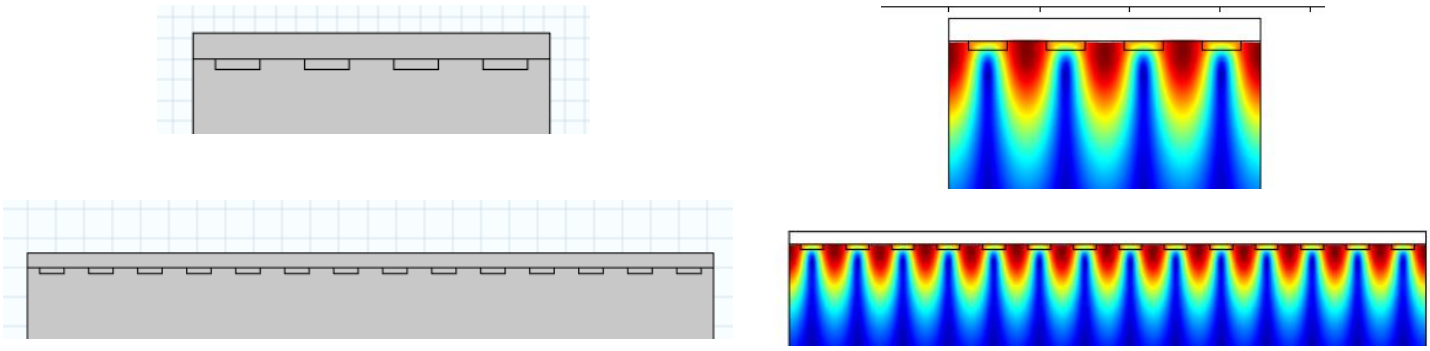

Figure 64- 2 and 7 pairs devices of the Buried electrodes design

The admittance curves of all the designs of Buried SAW devices are shown in Fig-65.

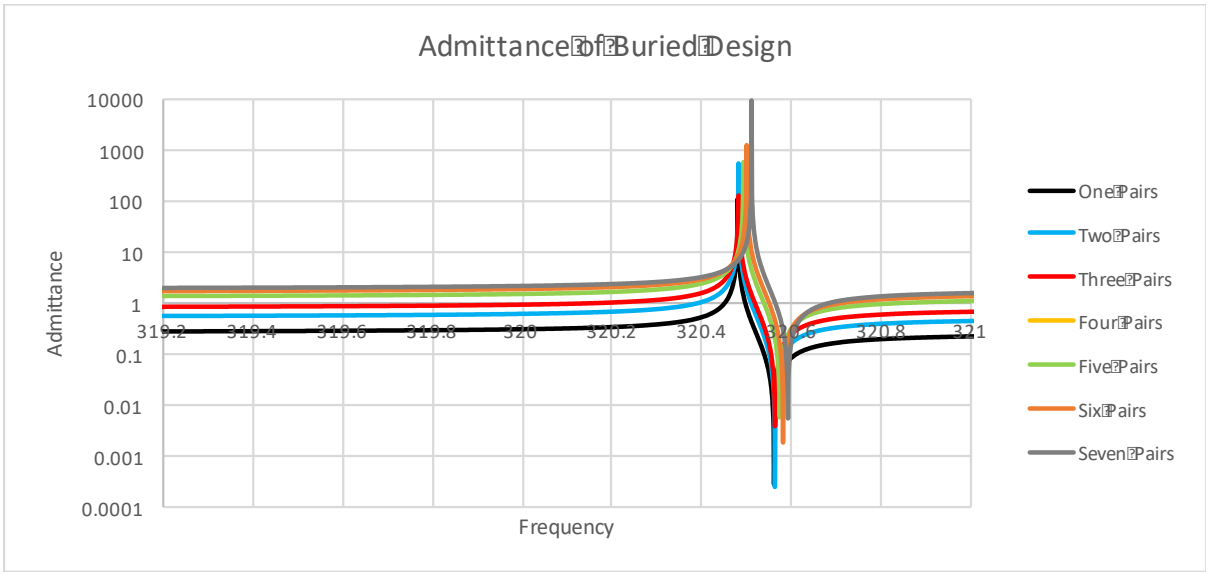

Figure 65- Admittance graph of all devices extracted from COMSOL 5.3

The Semi-buried designs are shown in Fig-66.

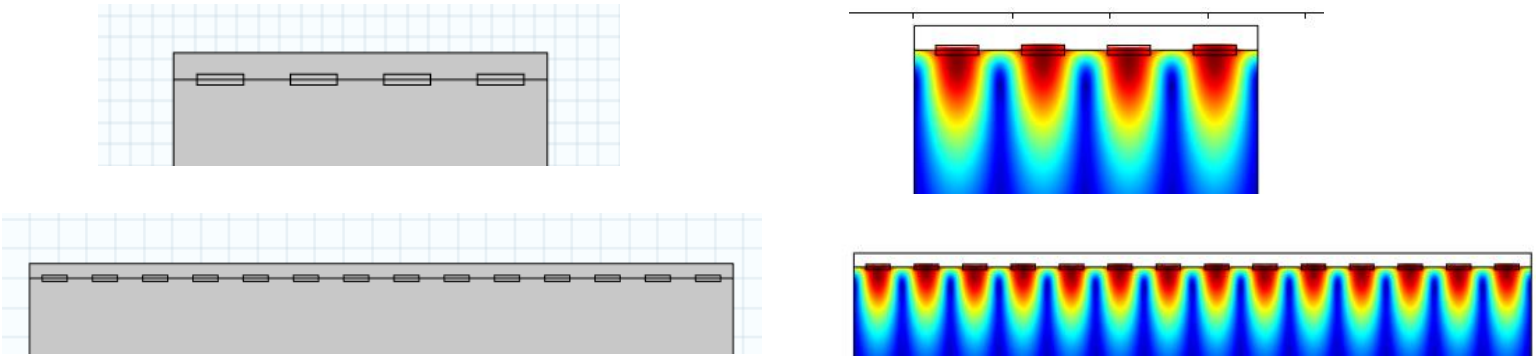

Figure 66- 2 and 7 pairs devices of the Semi-Buried electrodes

The admittance curves of all the designs of the Semi-Buried SAW device are shown in Fig-67.

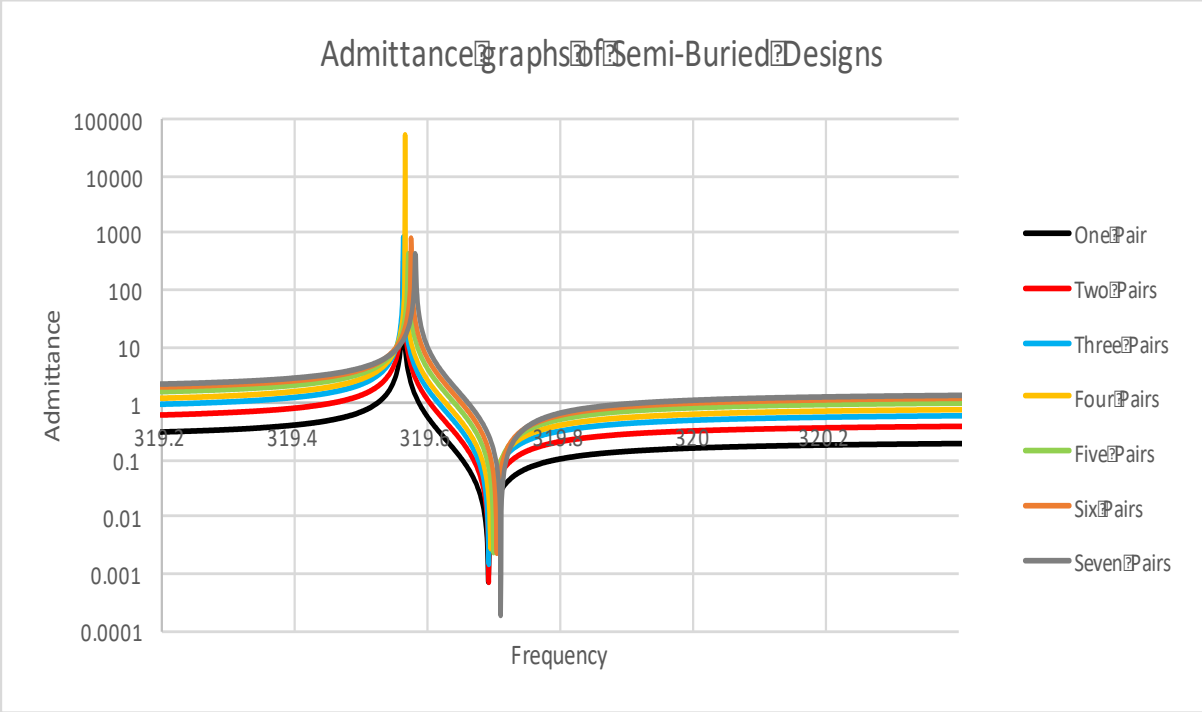

Figure 67- Admittance graph of all devices extracted from COMSOL 5.3

Cadence Simulation

Parameter extraction

As discussed before, the equivalent circuit model for a SAW resonator consists of two parallel branches: the first branch is the static capacitance C_0, which is related to the capacitance between the electrodes due to the piezoelectric material between them, and the other branch is the motional branch, which consists of L_m, C_m, and R_m. The motional branch model the physical properties of the resonator. Although themselves they don't have any physical meaning, motional impedance parameters are related to the dimensions, material-related constants and process-dependent variables. The model is shown:

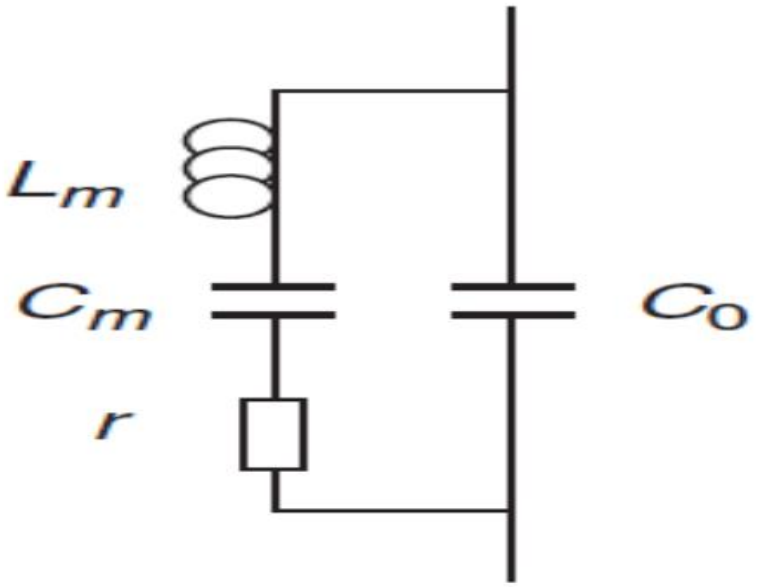

Figure 68- BVD equivalent circuit model

The series and parallel resonant frequencies are f_s and f_p, respectively, which represent the emotional and static branches of the equivalent circuit. Since the admittance is maximized (minimum impedance) at the series resonant frequency, it is the most used and the dominant part in natural vibration. The impedance is maximum at the parallel resonant frequency.

In SAW resonators, parallel resonance is merely used in calculations as most of them operate near the series resonant frequency, and only represent the situation where the resonator has a high impedance.

The quality factor at resonance frequency is also an important value to measure. Quality factor represents the ratio between the energy stored in the system and the dissipated energy per cycle.

A high-quality factor usually means a low energy loss. It also represents the resonator bandwidth at half power compared to the resonance frequency, and represented as: $\frac{f0}{\delta f}$

Quality factor is usually related to the motional impedance of the resonator. Since the bandwidth at half power is related to the electrical parameters via $\frac{R}{L_m}$, to equal $f_0 \frac{L_m}{R_m}$. For the resonant frequency being equal to $\frac{1}{2\pi\sqrt{L_m C_m}}$, the quality factor usually is represented as the imaginary component of the impedance over the real component. It is worthy to mention that this value is related to the motional (series) part of the resonator.

but how are those parameters extracted from COMSOL simulation admittance graph? COMSOL produces admittance graph of each design showing the maximum admittance (Y11) value and the resonant and anti-resonant (parallel) frequencies. The graph of one design is shown

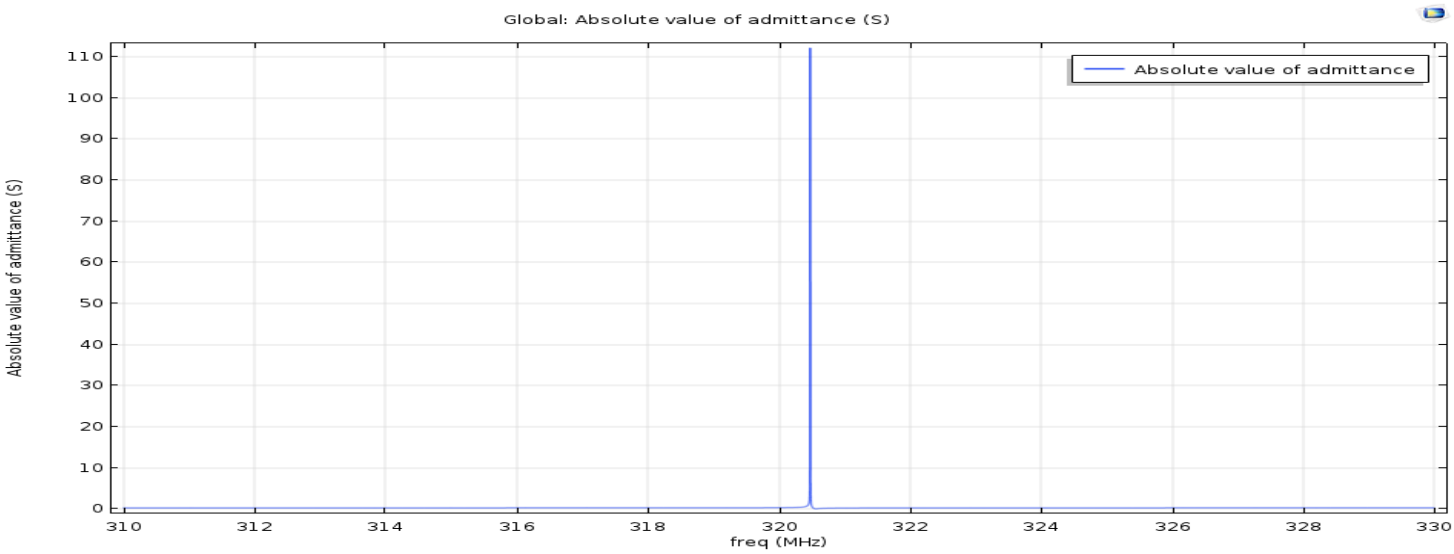

Figure 69- Admittance vs frequency COMSOL result

the admittance function of the BVD model can be written as:

$$Y = j\omega C_0 + \frac{1}{R + j\left(\omega L_m - \frac{1}{\omega C_0}\right)} \quad (24)$$

and parallel and series resonance frequencies equal:

$$f_r = \frac{1}{2\pi\sqrt{L_m\, C_m}}\ , f_a = f_r\left(1 + \frac{C_m}{2C_0}\right) \quad (25)$$

For a dominating series resonance, the BW at half admittance value (half power bandwidth) of series RLC is given by:

$$BW = \frac{1}{2\pi}\frac{R}{L_m} \quad (26)$$

The maximum admittance occurs at resonance frequency. at this point admittance is purely real and its value is equal to $\frac{1}{R}$ and it the minimum occurs at anti-resonance frequency.

the procedure to extract R, L, C, and C_0 parameters from COMSOL admittance graph is as follows:

1. Get series & parallel resonant frequencies at maximum and minimum Y
2. At maximum, all Y is real and the maximum value equals $\frac{1}{R}$
3. Get the bandwidth, δf at half the maximum value of admittance (half power, 3 dB value)
4. Calculate L_m from BW relation
5. Calculate C_m, C_0 from resonant and anti-resonant frequency relation.

COMSOL results are extracted as a text file to get the exact values of maximum and minimum admittance. A MATLAB code is used to determine the values of the RLC resonator parameters using the text file values from COMSOL.

In the next section, Cadence simulation and results are discussed for both resonator and proposed oscillator.

Design & Simulation

Cadence virtuoso tool is used to simulate the electrical model of the resonator along with designing a new pierce oscillator circuit to drive the resonator.

pierce oscillator design is modified from a proposal from [42]. it consists of four stages of common-source amplifier. The oscillator and the resonator are shown:

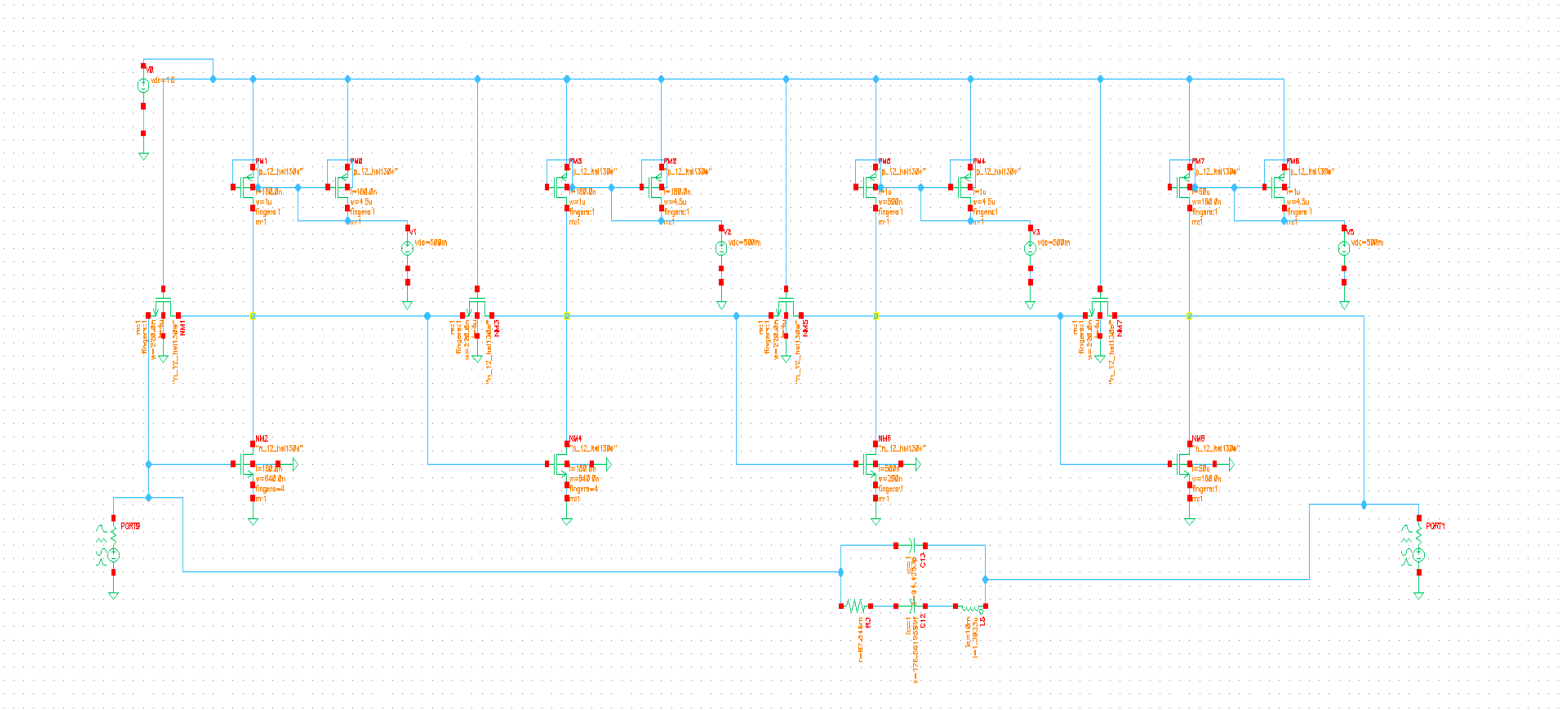

Figure 70- Pierce oscillator schematic

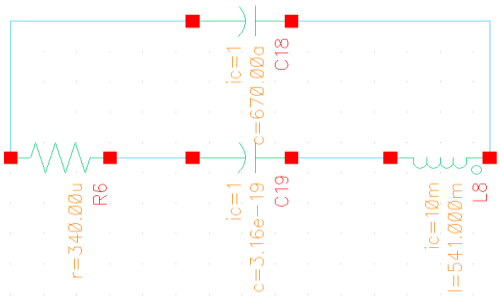

Figure 71- SAW resonator equivalent circuit schematic

The transistor in the lower level are the main transistor, which provides needed transconductance for the amplifier gain to be high. Each stage has a transistor which provides the bias current and another to perform as the large bias resistor for the gate. The resonator circuit is connected in series with the pierce oscillator as is expected from it to be looking at minimum impedance circuit.

This circuit is biased in weak inversion region. Which results large gate area, weak BW and the resulting gate capacitance is large. This last problem affects the phase shift condition in the operation of the oscillator. On the other hand of these disadvantages, the design has a very large gain which is needed for the operation, low voltage needed to drive the circuit, high transconductance and low power consumption. Gain of the of the circuit is designed to be high as for the oscillation to start and maintain. The phase is designed to be near 360 degrees to meet the oscillation condition.

Results and Discussion

Transient analysis is performed to see the oscillation output signal. The transient stop time is varied to make sure the oscillation is continuous and maintained. Transient response at 10and 100nm stop times are shown in the following figure:

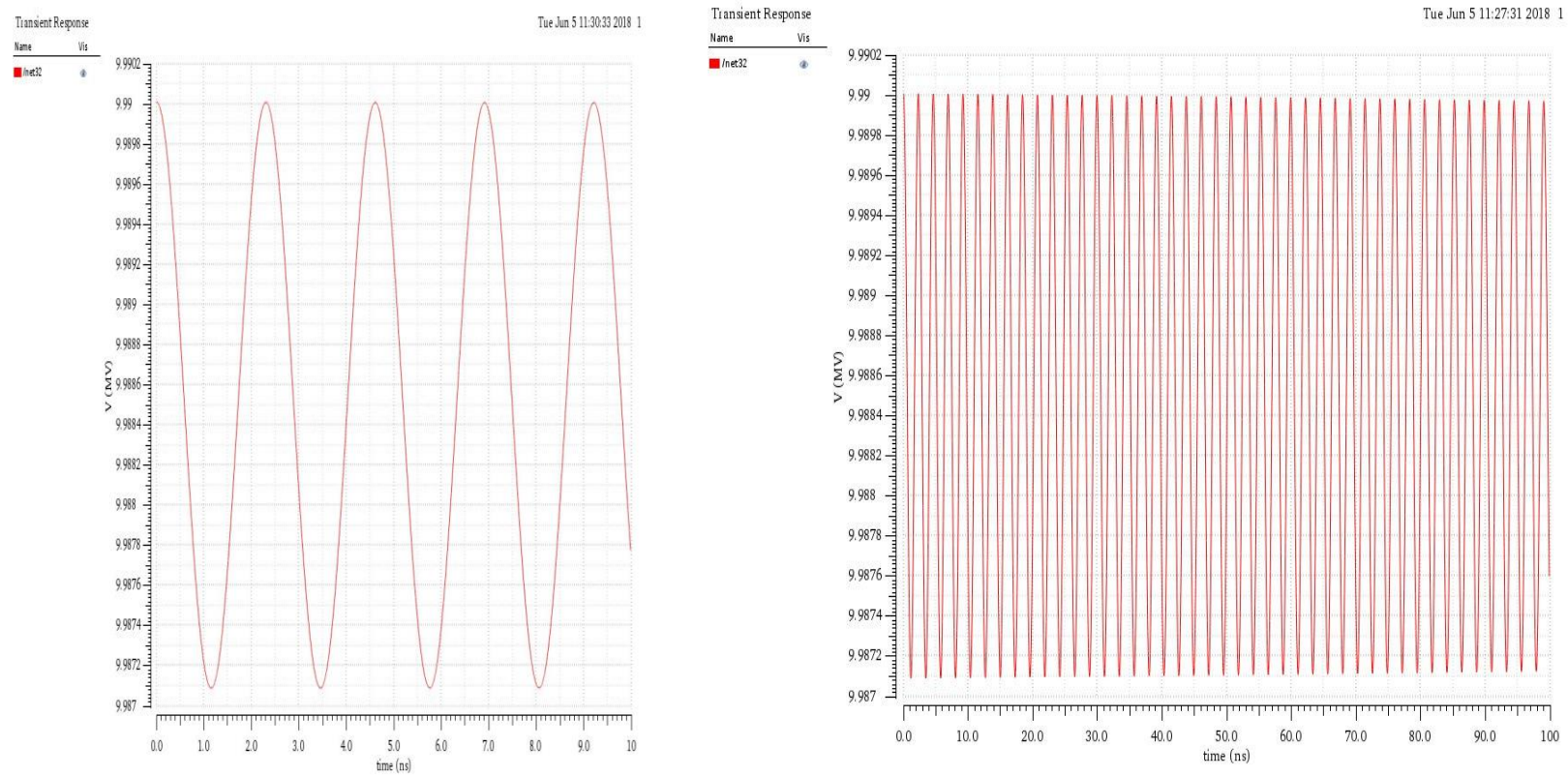

Figure 72- SAW transient response for 10 and 100 nm stop time for Pierce oscillator

PSS analysis is an essential parameter for oscillator simulation as it describes the behavior of the oscillator at the steady state after long oscillation time. PSS analysis using harmonic balance method is used. Results are shown in the next figure:

Figure 73- PSS simulation results

Transient and PSS results differs sometime due to initial conditions and large capacitors in the circuit and transient time need to be run for a longer time to reach the same values as PSS.

Next, Reproducing the Same graph as COMSOL is needed to verify the results.

In order to get the admittance graph vs frequency, S parameters simulation is required. SP simulations used input and output ports for multi-port SAW devices, to measure Y and S parameters. The ports of SP should be matched with the real impedance of the resonator circuit in order to right parameters, which is translated to the maximum power transfer to the load port, so matching the ports is needed.

Next, results for different multi-port SAW resonators are shown. Simulation for 1 to 7 pairs of ports are shown. A compare between insertion loss, phase depth, Quality factor is presented for different configuration: Basic, Buried, Semi buried IDT ports.

1. **Basic ports**

The produced admittance graph for 1 port SAW resonator is Shown:

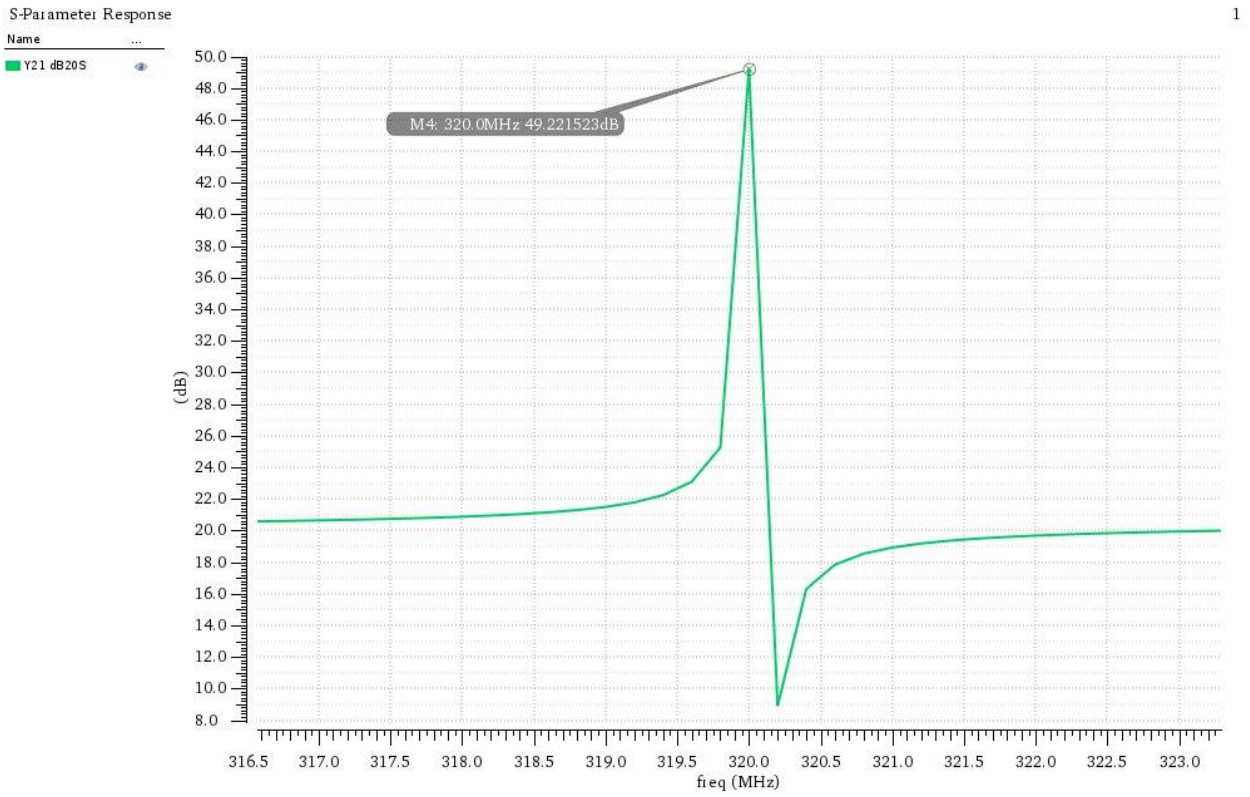

Figure 74 - admittance for 1 port basic SAW resonator

As shown, series resonance is much more dominant and in accordance with the same resonant frequency value as COMSOL results.

Insertion loss of a resonator is defined as the value of S21 in dB (- 20 log S21). Insertion loss represents the power loss that results from inserting the device in a system. It is defined as the ratio between the power transmitted before insertion to the power received by the load after insertion. The simulation is shown in the following figure:

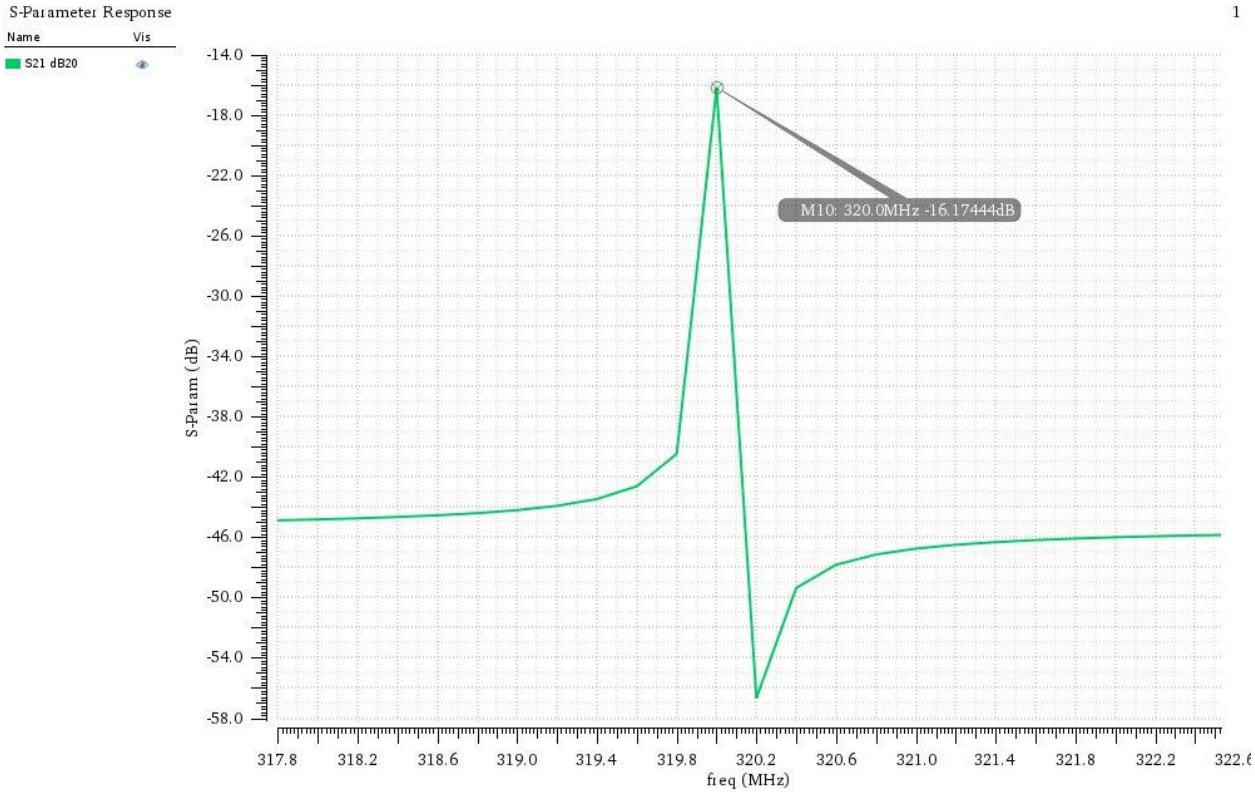

Figure 75- S21 dB for 1 port basic SAW resonator

The peak shows a value of 16.17 dB. This results of course is at a matched load with the resonator impedance.

To measure the phase depth, the phase of S21 is needed. Phase depth is defined as the difference between the maximum and minimum phase of S21. The results is shown in the following figure:

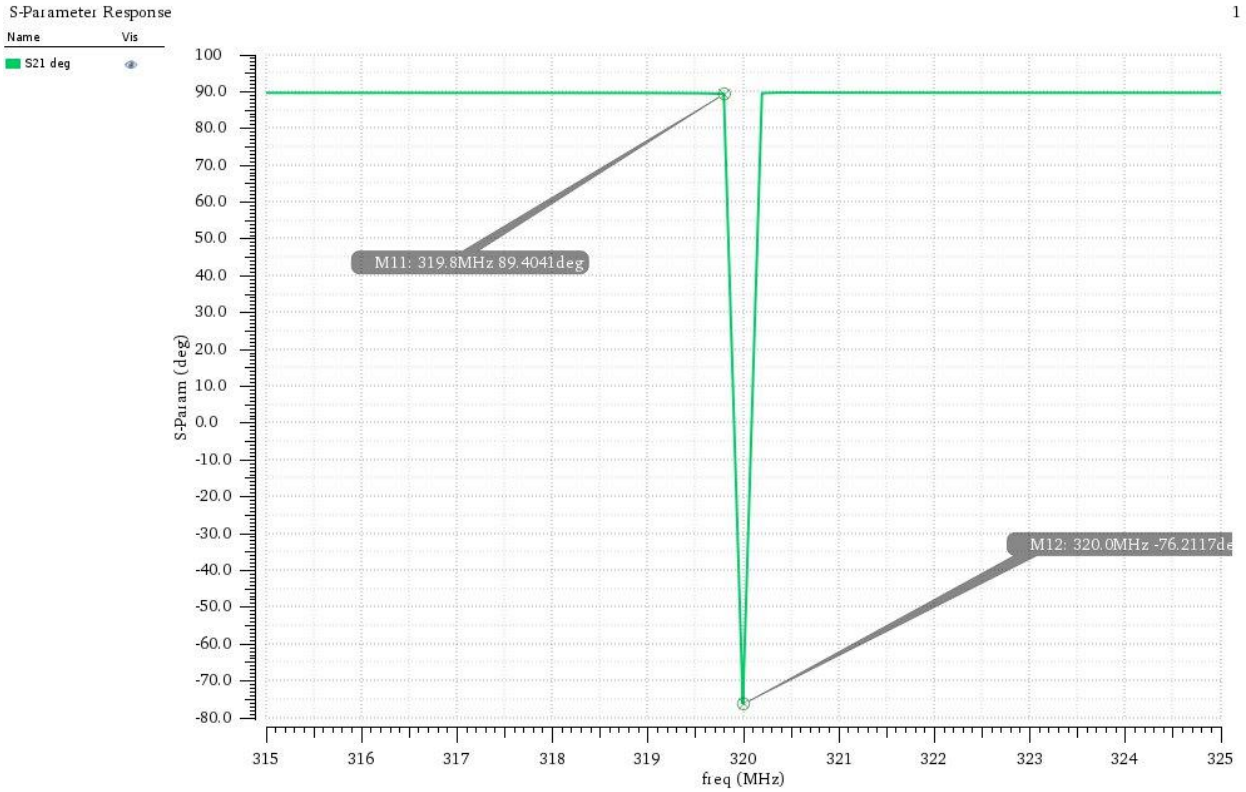

Figure 76- S21 phase for 1 port basic SAW resonator

The value of phase depth is almost 166 degrees.

Quality factor is next calculated. Q factor is calculated from the formula $\frac{f_0}{\delta f}$ where δf is the bandwidth at 3dB (half power). The value of the bandwidth is calculated at half the value of the admittance, which corresponds to -3dB from the maximum dB graph of the admittance vs frequency, where f_0 is the resonant frequency at the maximum admittance.

The simulation graph is shown:

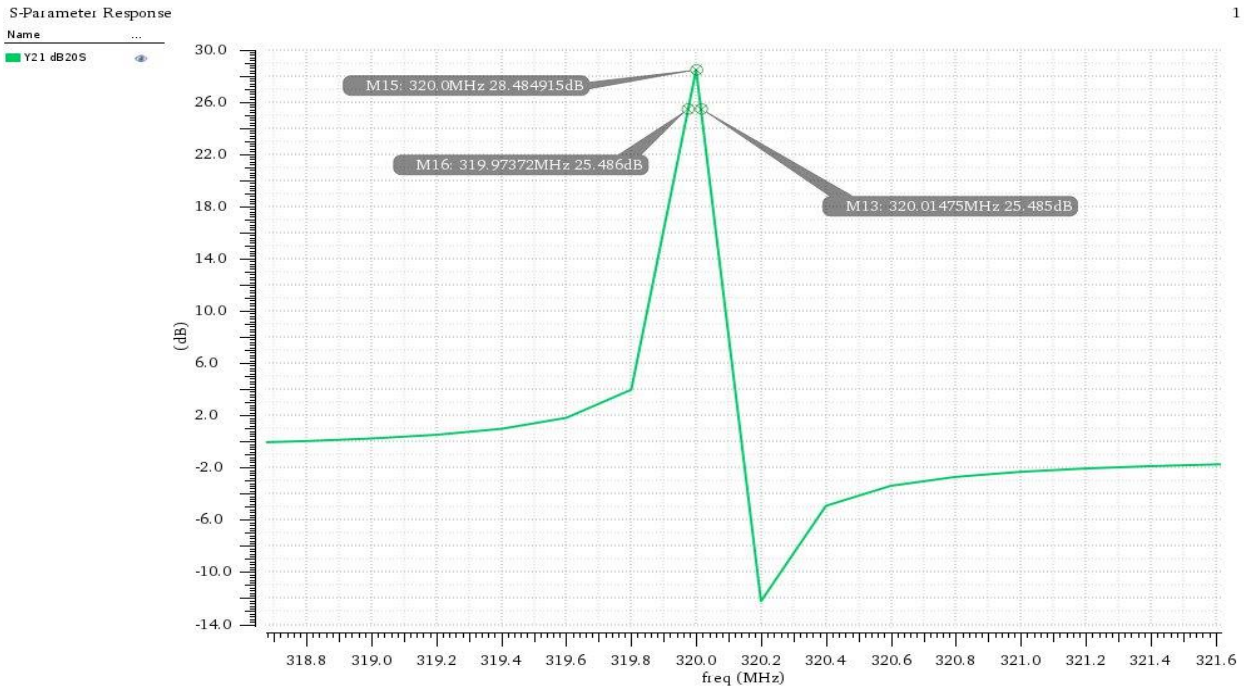

Figure 77- Quality factor with bandwidth at – 3dB for 1 port basic SAW resonator

The quality factor is calculated to be 7799. the same simulation steps are generated for basic design with different number of ports' pairs. Next is a schedule showing a comparison between results for the 7 designs.

Table 8 - comparison between multi ports basic design SAW resonator

No. of IDT pairs	f_r	f_{ar}	IL	Q	Phase Depth
1	319.99	320.14	26.3	7799	165
2	319.99	320.14	24.2	7603	155
3	319.99	320.14	20.3	6562	170
4	319.99	320.14	20.6	5294	173
5	319.99	320.14	19.4	4893	169
6	319.99	320.14	16	3752	170
7	319.99	320.14	11.8	1484	49

Looking at the graph, one can identify the correlation between the Q factor and No. of IDT pairs as shown:

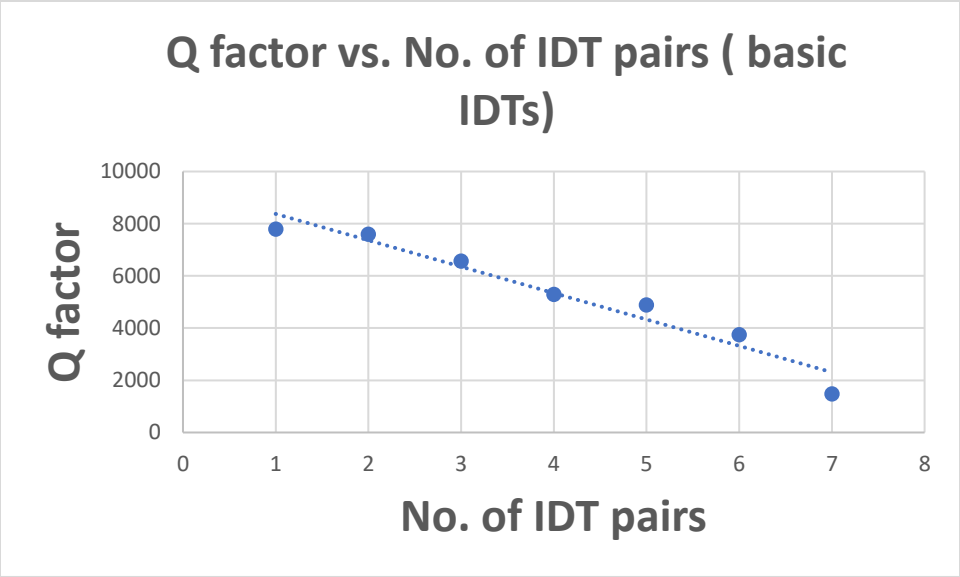

Figure 78 - quality factor vs IDT pairs for basic design SAW resonator

As the number of IDT pairs increases, the quality factor decreases. This is due to the increases of the losses from the IDTs.

For the insertion loss, there is no general trend and they all vary with +- 4 dBs change.

Buried ports

Repeating the same simulations for buried IDT ports design, in the case of one pair of ports, results in the following figures:

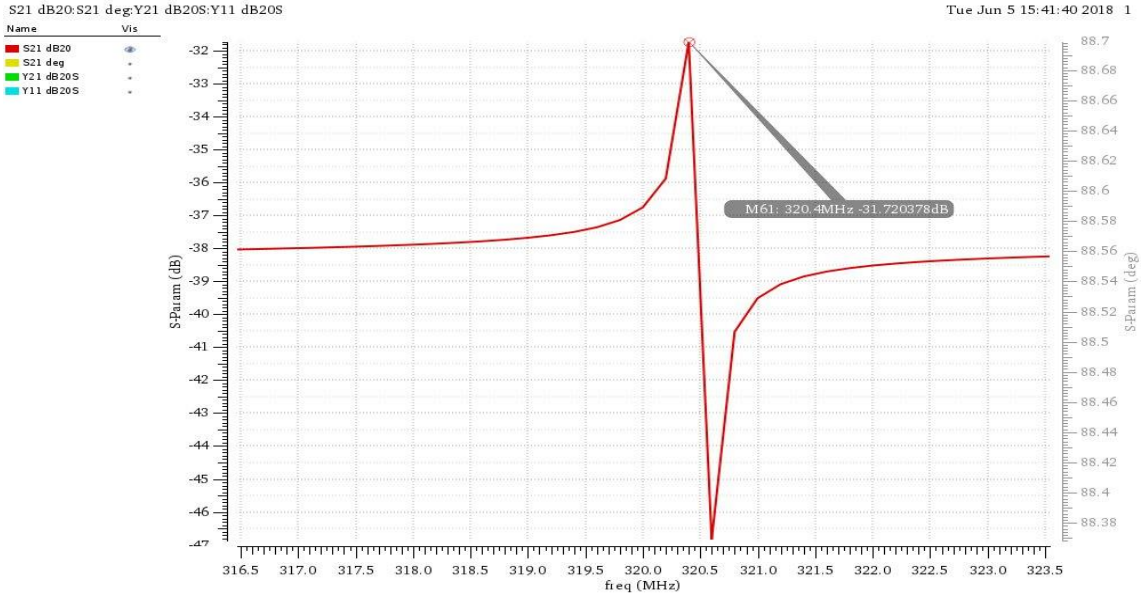

Figure 79- S21 dB for 1 port buried SAW resonator

- 1

  Insertion loss is found to be 31.7 dB.

For the phase depth, the result is as follows:

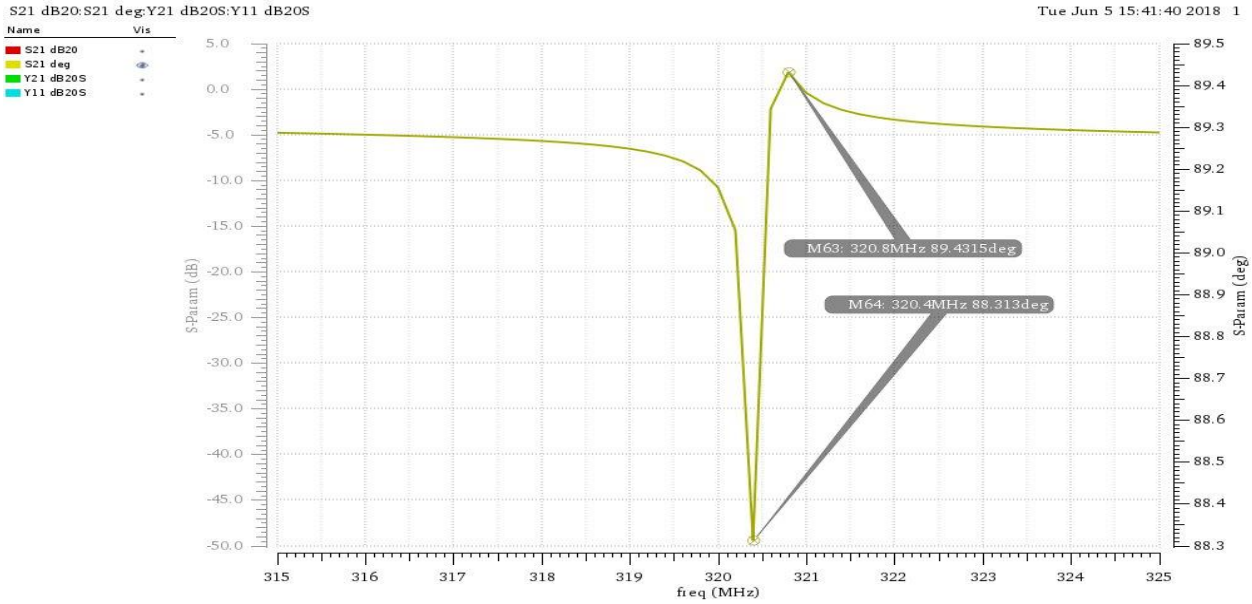

Figure 80- S21 phase for 1 port buried SAW resonator

- Which is about 1.1 degrees.

Regarding the quality factor, the simulation results is:

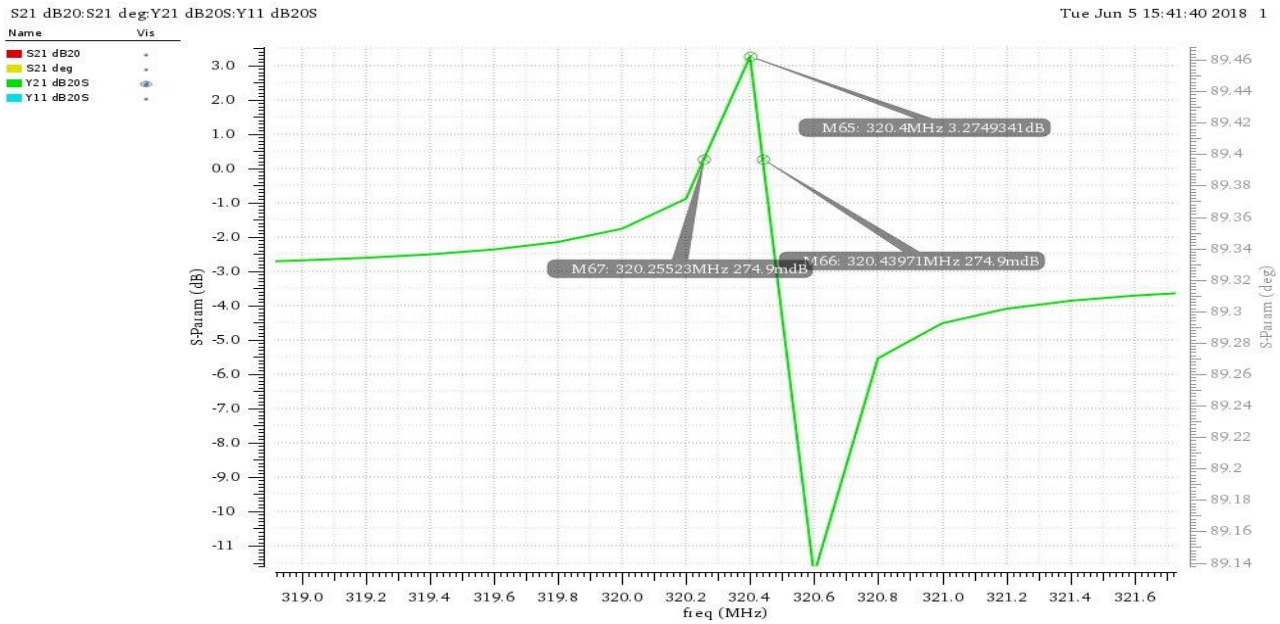

Figure 81 - Quality factor with bandwidth at – 3dB for 1 port buried SAW resonator

- Quality factor is 1736.

Same simulation steps are done to different number of IDT pairs for buried design. And quantitative comparison is done in the following table:

Table 9- comparison between multi ports buried design SAW resonator

No. of IDT pairs	f_r	f_{ar}	IL	Q	Phase depth
1	320.47999	320.58	31.7	1736	1.1
2	320.47999	320.58	33.8	1668	0.9
3	320.47999	320.58	29	1686	1.5
4	320.47999	320.58	30.6	1612	1.2
5	320.47999	320.58	32.8	1551	1
6	320.47999	320.58	35	1273	1.1
7	320.47999	320.58	37.8	1241	1.5

Looking at the table, one could notice the trend between the Q factor and the number of IDT pairs. It also worthy to mention the dramatic change in the phase depth compared to the basic design, Insertion loss, However, is larger, and the quality factor in lower. The trend between quality factor and No. of IDT pairs is shown in the following graph:

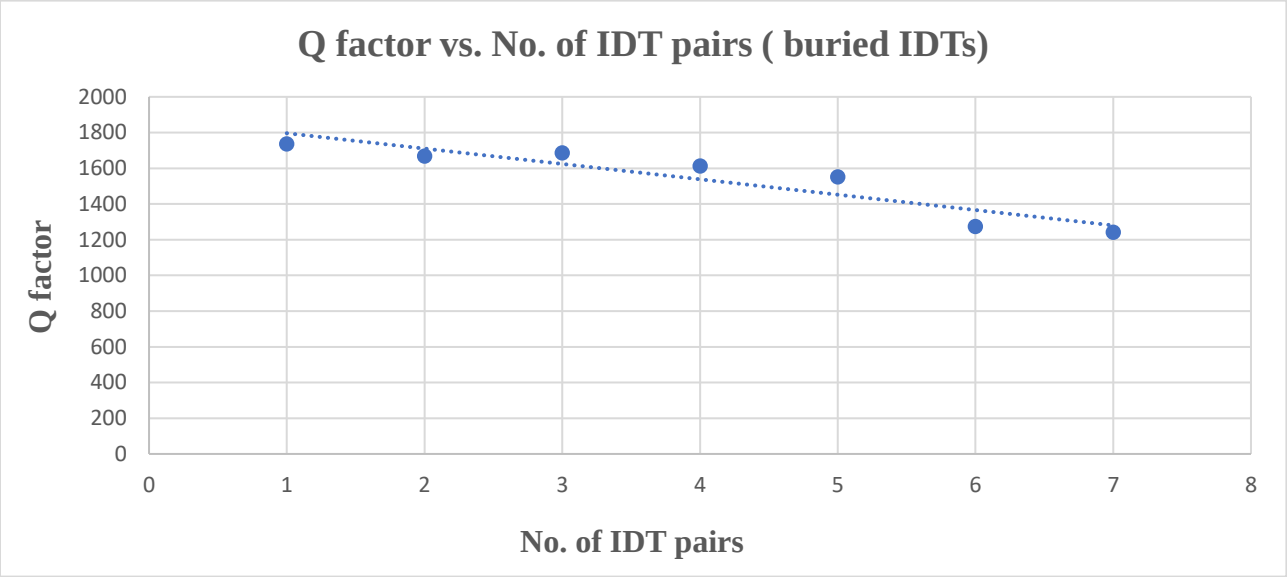

Figure 82 - quality factor vs ID pairs for buried design SAW resonator

Regarding the insertion loss, except for the first two designs, it tends to be increasing slightly with the increase of the No. of ports.

2. Semi buried ports

Simulation results for Semi Buried IDT ports (1 pair) are shown in the following graphs:

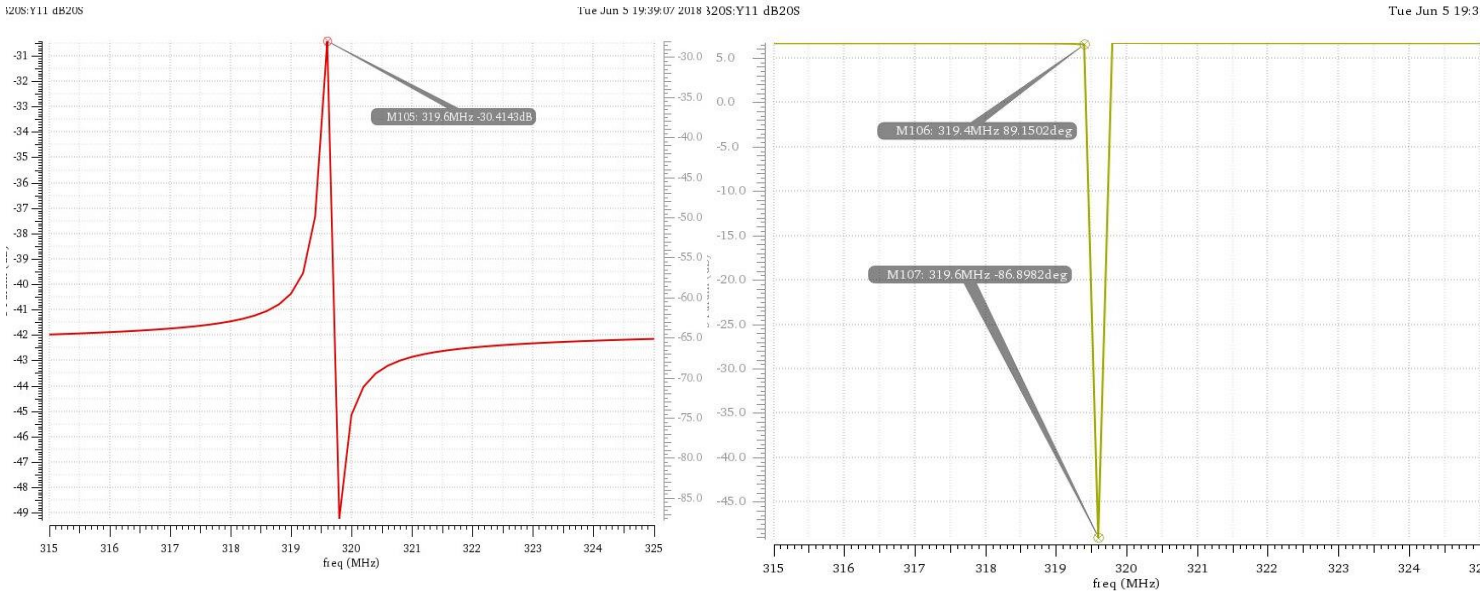

a) b)

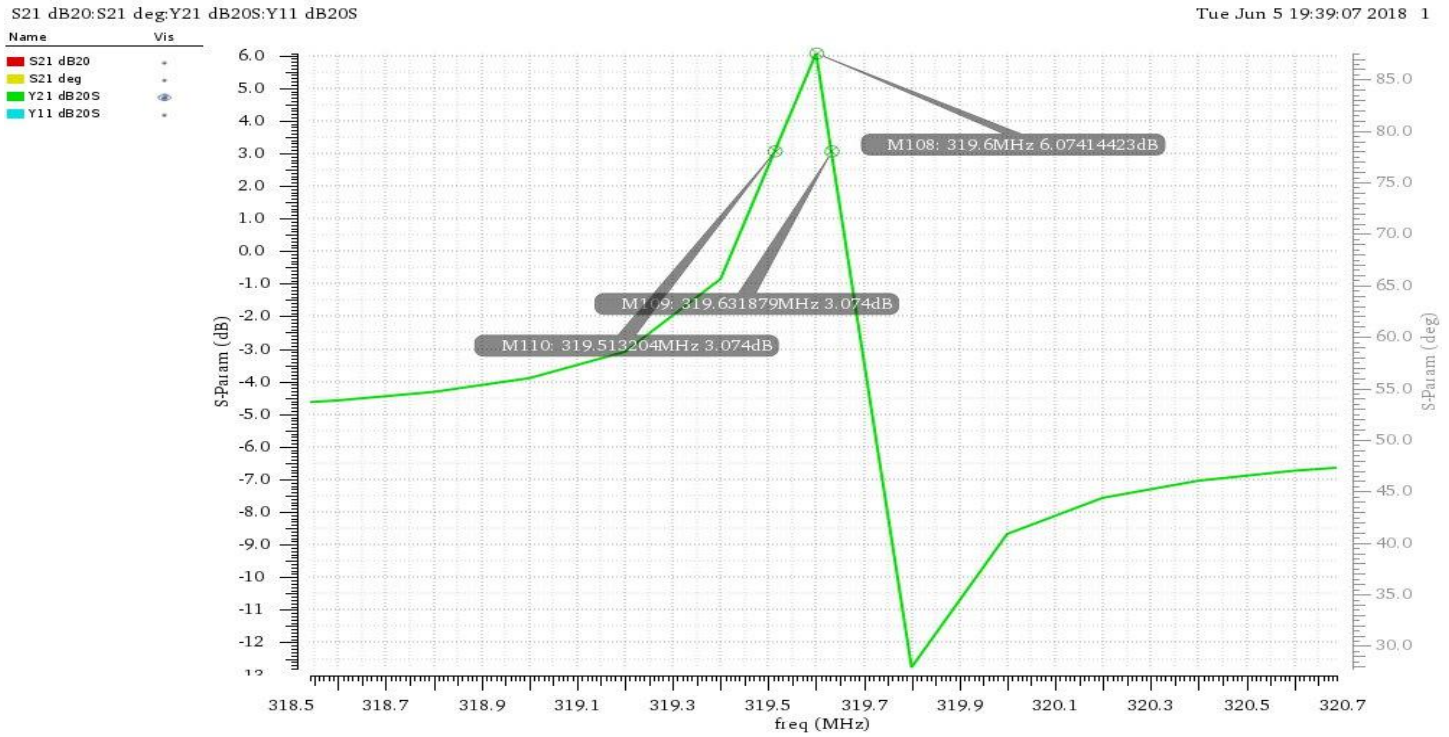

c)

Figure 83- a) s21 dB for 1 port semi buried design, b) s21 phase for 1 port semi buried design

As shown in the graphs: IL = 30.4, Phase depth = 176, and quality factor = 2693.

There is no general trend for Q factor in semi buried designs as they differ slightly from each other. Here the phase depth is large again as the case in the basic designs. And the insertion loss is near the results from the buried designs.

The following table shows a comparison between simulation results for different number of IDT pairs for semi buried structure:

Table 10- comparison between multi ports semi buried design SAW resonator

No. of IDT pairs	Fr	Fa	IL	Q	Phase depth
1	319.565	319.69	30.4	2693	176
2	319.565	319.69	33.4	1588	177
3	319.565	319.69	38.2	1510	178
4	319.565	319.69	39.6	2288	179
5	319.565	319.69	35.4	3355	172
6	319.565	319.69	31.7	2887	177
7	319.565	319.69	23.3	3374	172

Temperature Coefficient of resonant Frequency (TCF)

Frequency shifts can take place due to temperature variations. And as the proposed designs have Aluminum IDTs, thermal expansion can take place that could shift the frequency produced since the frequency produced depends on the spaces between the electrodes. Moreover, the wave propagation is affected by varying the temperature since the elastic, dielectric, and piezoelectric coefficients of the material change, thus altering the wave velocity on the surface of the material. Such alteration of velocity directly affects the frequency produced as well. So basically the effect of temperature on frequency is measured by both the delay line shrinkage and the change of the material properties that changes the wave velocity. [43].

In talking about electronic components or MEMS, these devices are vulnerable to heating and harsh temperature conditions. Accordingly, the effect of such temperature fluctuations on the frequency should be studied in order to put a margin for heating conditions and to further enhance the TCF.

TCF is basically the change of frequency with respect to temperature

$$\frac{1}{f}\frac{df}{dT} = \frac{1}{l}\frac{dl}{dT} - \frac{1}{v}\frac{dv}{dT} \quad (27)$$

Where l is the delay line and v is the surface wave velocity as shown in the figure below as L_c.

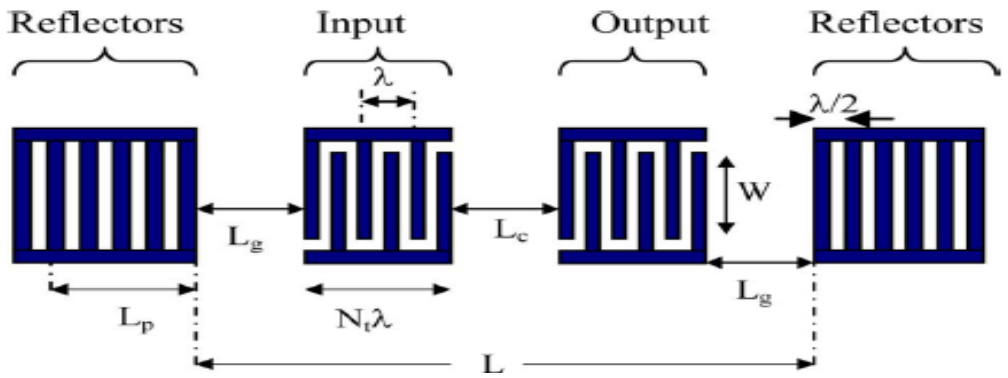

Figure 84 - Plan view of the parameters[17]

Delay line effect on temperature

As thermal expansion takes place of $\frac{\Delta L}{L} = \alpha_L(T - T_0)$ where T is the new temperature and T_0 is the reference temperature, the electrodes expand and L_c or l shrinks, shifting the frequency in $ppm/^0C$. The idea here is to use a material that has low thermal coefficient α_L to control the change of length as much as possible to control the frequency shift. This discussion is about the term $\frac{1}{l}\frac{dl}{dT}$, which is the first term in calculating the TCF that is concerned with the delay line shift[16].

Velocity effect on temperature

The other part of the TCF which is actually the dominant term is $\frac{1}{v}\frac{dv}{dT}$. Although a velocity-temperature relation is found earlier in out literature where $v_s^2 = \left(\frac{\bar{c_{44}}}{\rho}\right)(1 - K^4)$, we looked for another model that has some penetration in the material as it is more realistic in the surface waves propagation and also due to the fact that some of our designs have semi-buried electrodes, which allow wave propagation to few nanometers in the material. In order not to confuse between BAW and SAW, such waves are still considered SAW since they are only few nanometers in the material.

Before simulating the TCF on COMSOL, TCF is calculated theoretically by the velocity models and delay line change in order to have a sense of how TCF is calculated and to make sure that COMSOL calculated all of the effects.

Bleustein-Gulyaev Wave

This type of wave considers piezoelectric symmetry in the planar surface of the piezoelectric material, which is plausible in our case since we only care about one direction of motion from the input IDTs to the output IDTs. Accordingly, there are two solutions to the surface wave which are the Lord Rayleigh surface wave that follows the elliptical path of particles that causes the deformation and the other is a perpendicular component that penetrates in the wave that could be considered as a BAW if there was no piezoelectric wave.

According to this assumption, the wave velocity is calculated to be

$$v = v_t(1 - b^2)^{1/2} \quad (28)$$

Where

$$v_t = \left(\frac{c_{44}(1 + K^2)}{\rho}\right)^{\frac{1}{2}}$$

$$K^2 = \frac{e_{15}^2}{\epsilon_{11}c_{44}}$$

$$b = \frac{K^2}{1 + K^2}$$

So basically the expanded equation is

$$v = \left(\frac{C_{44} + \frac{e_{15}^2}{\epsilon_{11}}}{\rho} \right)^{\frac{1}{2}} \left(1 - \left(\frac{\frac{e_{15}^2}{C_{44}\epsilon_{11}}}{1 + \frac{e_{15}^2}{C_{44}\epsilon_{11}}} \right)^2 \right)^{\frac{1}{2}} \quad (29)$$

After finding the expression of the velocity in terms of the material constants, the next step is to find the relationship between the temperature and the material properties.

AlN is used in all of our designs as the surface material as it has the lowest TCF and can be compensated. According to literature, the only material coefficient matrix that is impacted by temperature is the stiffness matrix. The Bleustein-Gulyaev wave analysis concludes that the important matrix element in calculating the velocity is c_{44}. On the other hand, ϵ_{11} and e_{15} have negligible alterations with temperature, unlike other materials like lithium niobate.

	AlN [15] (6mm)
Stiffness coefficients [10^{11} N/m^2]	
c_{11}^{E}	3.45
c_{12}^{E}	1.25
c_{13}^{E}	1.20
c_{33}^{E}	3.95
c_{44}^{E}	1.18
c_{66}^{E}	1.10
1st order temperature dependence of stiffness coefficients [10^{-6}/K]	
Tc_{11}^{E}	–80
Tc_{12}^{E}	–180
Tc_{13}^{E}	–160
Tc_{33}^{E}	–100
Tc_{44}^{E}	–50

Figure 85- c_ij values and first order dependence in AlN. [44]

First order dependence of $Tc_{44} = -50 * 10^{-6}$ means that $\frac{1}{c_{44}}\frac{dc_{44}}{dT} = -50 * 10^{-6}$. Accordingly, the ordinary differential equation is solved to obtain $c_{44}(T)$ with knowing that from Fig x. that c_{44} at room temperature = $1.18 * 10^{11}$.

After calculating the velocity at different temperatures, the velocity-temperature graph is found with the expected trend of negative slope since the stiffness increases by increasing the temperature, applying resistance to the wave propagation that lowers the speed of the surface wave.

Temperature Coefficient Compensation

TCF values calculated are still not very promising as some applications do not withstand any frequency shift. Therefore, new methods of temperature coefficient compensation are used in order to lower TCF as much as possible. One of these methods is adding a passive oxide layer beneath the substrate in order to reduce the temperature effects. Such method is capable of

reducing the TCF to more than half of its original value. However, simulating this method or solving it analytically is not a clear method yet, so the TCF is measured experimentally in this case. [45]

TCF Simulation

As stated above, the TCF has two main contributing parts, the thermal expansion of the structure dimensions and temperature dependence of the material properties of the piezoelectric material which in turn affects the wave velocity in the material. TCF can be calculated directly from the equation calculations using Excel or it can be simulated on a FEA tool such as COMSOL. In this project, both tools are done but the main results are presented from COMSOL. The calculation of the TCF using COMSOL requires the simulating the thermal expansion and material properties dependence effects simultaneously in order to get accurate results.

Thermal expansion

There are two ways to include the thermal expansion in COMSOL. The first way is to include the expansion coefficients in each dimension in geometry and the new lengths will be:

$$L = L_0 + \alpha \Delta T L_0 \quad (30)$$

where α is the thermal expansion coefficient for each material in the design and L_0 is the original length.

The other way to include the geometry expansion is by using the already default tool in the *Material* under the *Solid Mechanics* node in COMSOL named: *Thermal Expansion*. Here the reference temperature and the new temperature are specified in this window. In addition, the thermal expansion coefficient for the materials are to be added, for the AlN is $4.5 * 10^{-6}$, and for the Al is $23 * 10^{-6}$.

The second effect is the velocity dependence on the temperature. As explained above, the velocity depends on the mechanical properties of piezoelectric, the density, $c44$, ϵ_{11} and e_{15}. So the effect of these properties is explained in the following paragraphs.

Elasticity Matrix, c44

The $c44$ is the tenth element in the elasticity matrix in the material section in COMSOL. The elasticity matrix of a material is 6*6 type. So there are different notations to enter the elasticity matrix in COMSOL. Due to its symmetry and having many zero-elements, the notation can be as the following figure:

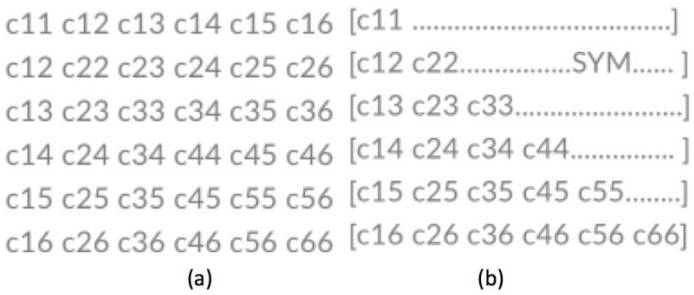

Figure 86- (a) the complete elasticity matrix notation for a material, (b) the shortened matrix.

COMSOL has the symmetric notation and the values can be directly inserted in this window in the material section.

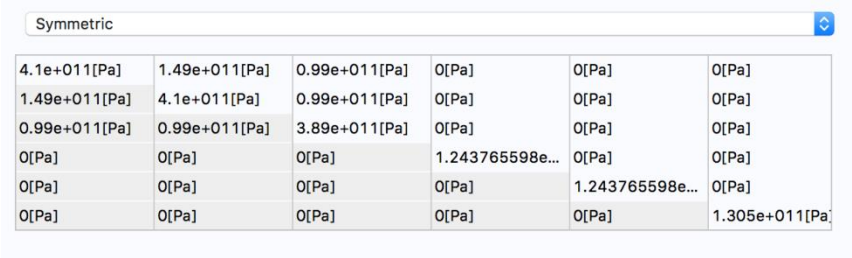

Figure 87- the elasticity matrix notation for a material in COMSOL

From the equations found in the literature, the $c44$ values for each temperature are inserted in this matrix. And the effect is taken into account.

Density

The density of the piezoelectric electric material changes with the temperature. As mentioned above, the wave velocity depends on the density following the equation: $v = \sqrt{\frac{c}{\rho}}$, 4. So if the wavelength of the wave is kept constant (which depends on the IDTs design), the resonance frequency will shift by changing the density. For $LiNO_3$, the density dependence on the temperature follows this equation:

$$\rho = 4644.44 * e^{-0.383*10^{-4}*T} \quad (31)$$

This equation is added in COMSOL as an *analytic function* to describe the density dependence. And the *function* name replaces the value of *density* in the *material* node.

A parametric sweep is done to vary the temperature from room temperature to 70^0C with including the geometry effects and the density following the above equation. The admittance response for all the temperatures are graphed on the same figure to show the effect:

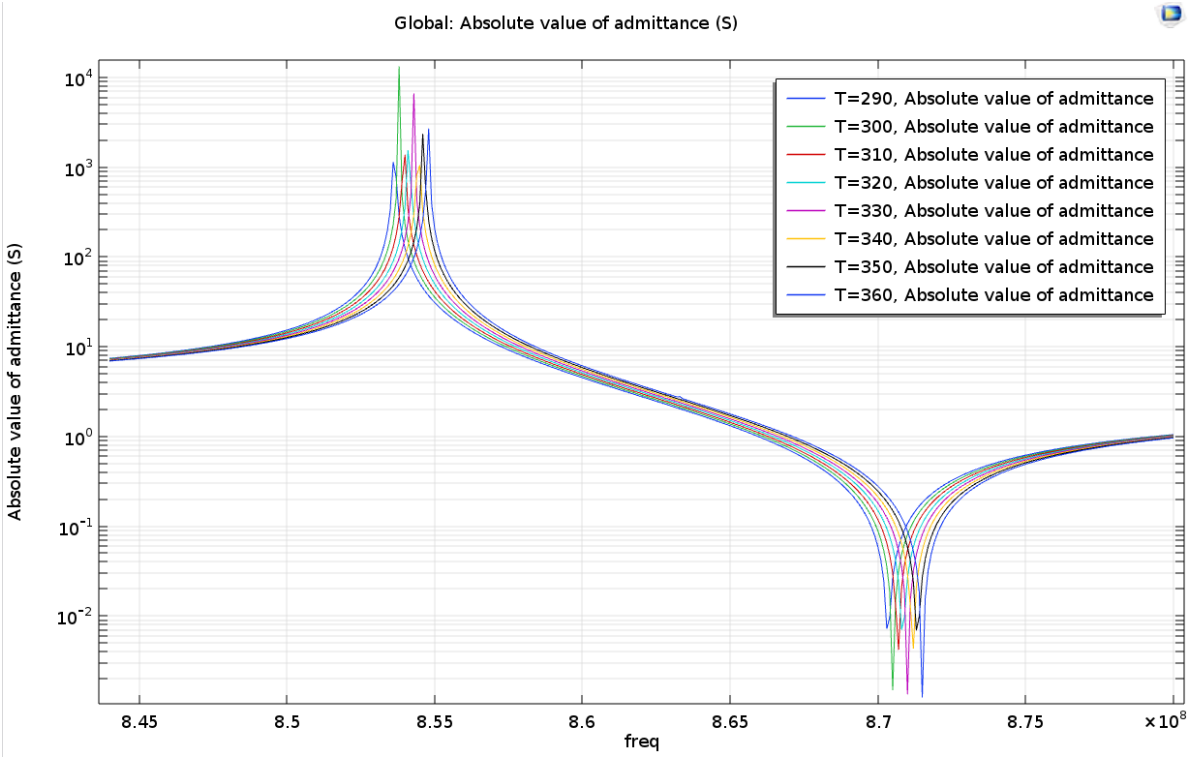

Figure 88- the admittance curve with temperature sweeping, and the effect of geometry and density change with temperature on the resonance frequency shift.

To calculate the TCF, the values of the resonance frequencies at every temperature should be plotted with the temperature (frequency on the $y-axis$ and the temperature on the $x-axis$). The slope is obtained and the TCF value is calculated as:

$$TCF = slope * \frac{10^6}{f_0} \frac{ppm}{^0C} \quad (32)$$

where f_0 is the original frequency at room temperature, and the frequency is plotted in MHz. And all the above parameters (thermal expansion, density, $c44$, ϵ_{11} and e_{15}) should be included.

The following graph shows the results from the *basic* design and using the AlN as a piezoelectric material.

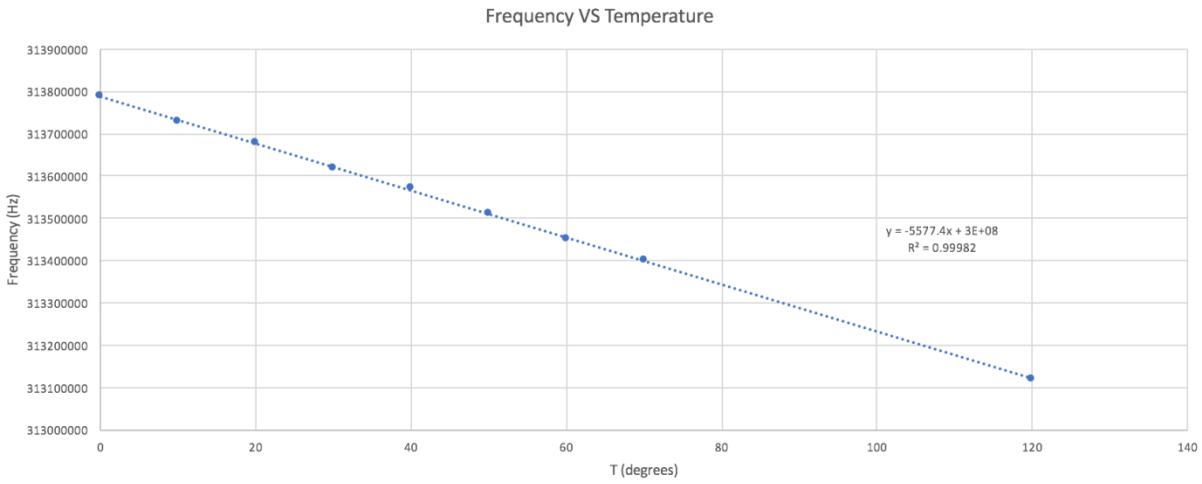

Figure 89- resonance frequency of the basic design at each temperature taking into account the geometry and material parameters

The slope is found to be $-5577.4\frac{Hz}{^0C}$, so the $TCF = -5577 * \frac{10^6}{313700000} = -31\frac{ppm}{^0C}$. This value is obtained from the Excel calculation, it is $-28\frac{ppm}{^0C}$, which is very close to the value obtained from COMSOL.

Two piezoelectric materials are compared as well, AlN and $LiNO_3$. The TCF value is calculated for the basic design. The results are: $TCF_{AlN} = -31\frac{ppm}{^0C}$ and the $TCF_{LiNO_3} = -81\frac{ppm}{^0C}$. It is clear that the value for AlN is better, so all the other designs are implemented using this material.

To calculate the TCF value for other designs using AlN material, the parameter $c44$ doesn't allow variable definition to perform the sweep. So in each design, the corresponding parameters are inserted manually in the material property at each corresponding temperature to plot a figure similar to Fig-89.

Conclusion of Results

TCF Analysis

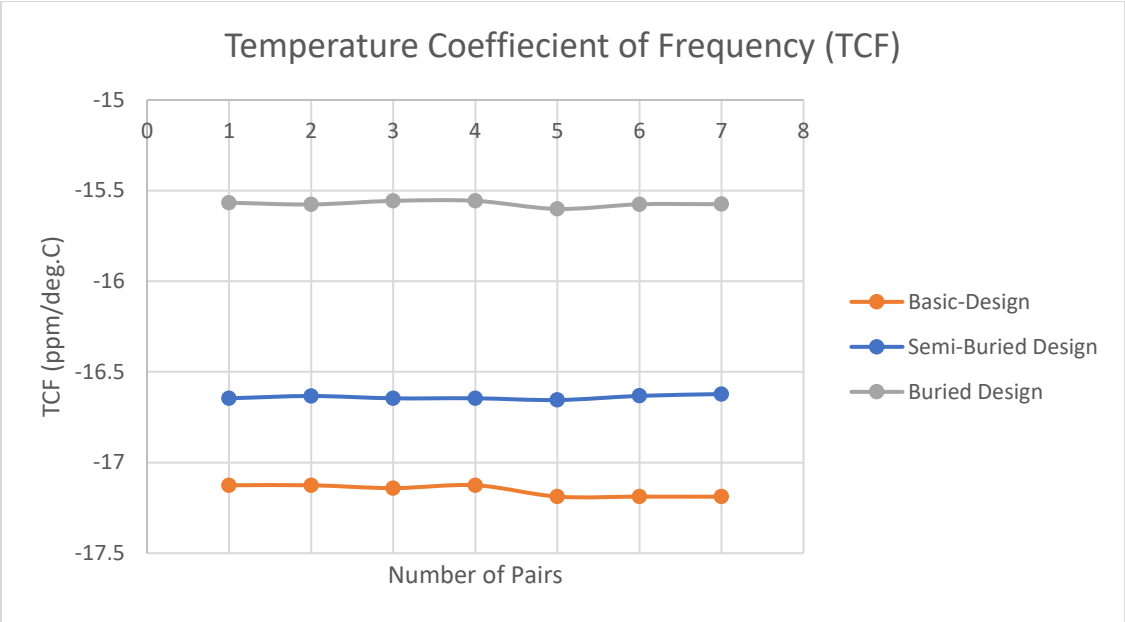

Figure 90-TCF of the three designs

It is obvious that the buried IDTs express the lowest TCF value. The semi-buried IDTs have values of TCF exactly between the above surface IDTs and the buried IDTs. Recall that BAW has lower TCF values when compared to those of SAW, which can be seen here when the IDTs go in depth in the piezoelectric material.

Finalized Table of Comparisons

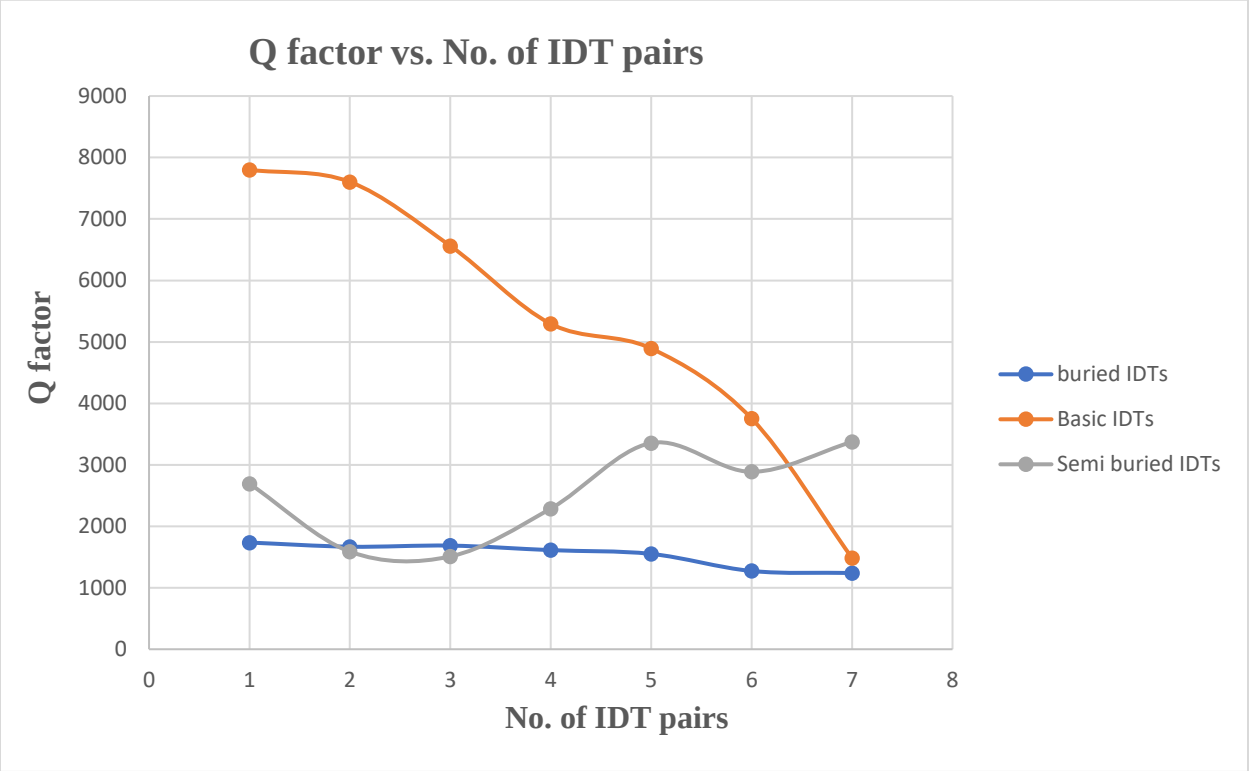

Figure 91-Quality factor of the three designs

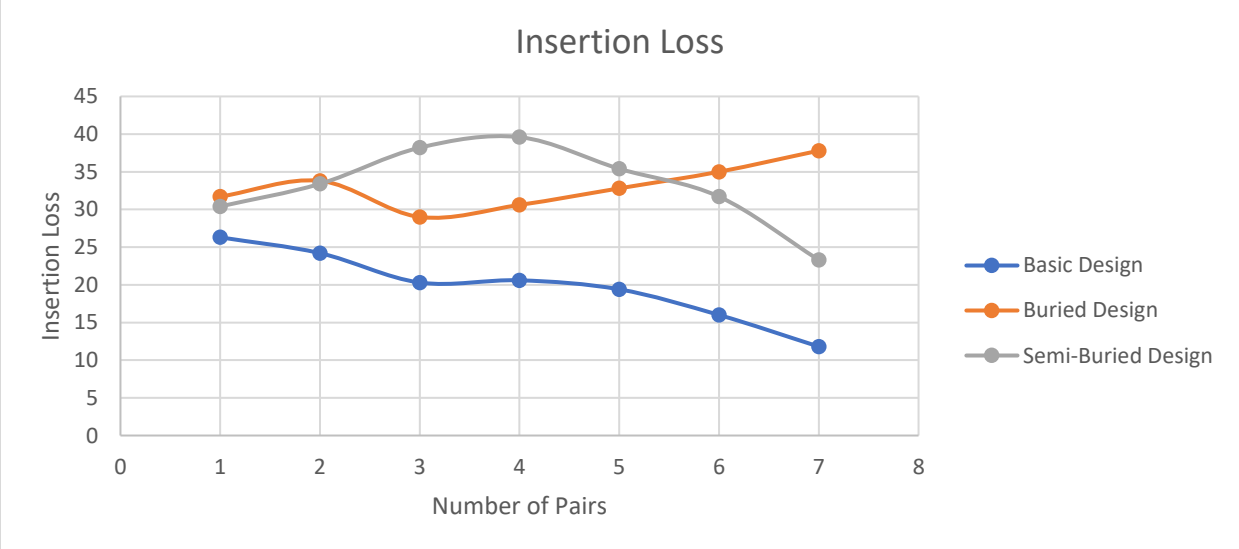

Figure 92- Insertion loss of the three designs

As expected, the quality factor decreases as the number of pairs increases, except in the semi-buried design. Moreover, the insertion loss in the above surface design decreases as the number of pairs increases. The semi-buried and buried designs did not demonstrate a specific trend, but there are design recommendations according to the applications needed.

Table 11- Basin Design

No. of IDT pairs	f_r	f_{ar}	IL	Q	Phase Depth	No. of IDT pairs	TCF
1	319.99	320.14	26.3	7799	165	1	-17.1254281
2	319.99	320.14	24.2	7603	155	2	-17.1254014
3	319.99	320.14	20.3	6562	170	3	-17.141
4	319.99	320.14	20.6	5294	173	4	-17.1253746
5	319.99	320.14	19.4	4893	169	5	-17.1877686
6	319.99	320.14	16	3752	170	6	-17.1880371
7	319.99	320.14	11.8	1484	49	7	-17.1884514

Table 12-Buried Design

No. of IDT pairs	f_r	f_{ar}	IL	Q	Phase depth	No. of IDT pairs	TCF
1	320.47999	320.58	31.7	1736	1.1	1	-15.56652924
2	320.47999	320.58	33.8	1668	0.9	2	-15.57633742
3	320.47999	320.58	29	1686	1.5	3	-15.55652632
4	320.47999	320.58	30.6	1612	1.2	4	-15.5563807
5	320.47999	320.58	32.8	1551	1	5	-15.60106212
6	320.47999	320.58	35	1273	1.1	6	-15.57546307
7	320.47999	320.58	37.8	1241	1.5	7	-15.57492851

Table 13-Semi-Buried Design

No. of IDT pairs	Fr	Fa	IL	Q	Phase depth	No. of IDT pairs	TCF
1	319.565	319.69	30.4	2693	176	1	-16.64564354
2	319.565	319.69	33.4	1588	177	2	-16.63297752
3	319.565	319.69	38.2	1510	178	3	-16.64564354
4	319.565	319.69	39.6	2288	179	4	-16.64548728
5	319.565	319.69	35.4	3355	172	5	-16.65516074
6	319.565	319.69	31.7	2887	177	6	-16.63235296
7	319.565	319.69	23.3	3374	172	7	-16.62210711

Chapter Six

Fabrication & Characterization

Fabrication Masks

Fabricating the SAW MEMS resonators requires defining the masks to be used in the fabrication process. It will not be a so sophisticated process as the proposed multi-ports designs will require only one mask for patterning the IDTs as well as the reflectors.

As the proposed designs are periodic, then the designer is free to choose the number of fingers of the IDTs, taking into the consideration the trade-off that exists between enhancing the functionality of the resonator as the number of fingers is increased and the increase in area which may be critical in some applications.

Using MEMSCAP ^{TM} design rules [46] in drawing the mask for patterning the IDTs and the reflectors which states that the minimum spacing between metal layers is $3\mu m$ while the minimum feature is $3\mu m$, too. Sticking to these design rules and drawing the masks for 2, 4, 6, 8, 10 and 12 ports SAW MEMS resonators was performed using CleWin LAYOUT EDITOR software assuming the most generalized case where the number of fingers for each IDT is two. From Fig-93 to Fig-97 show the masks for the multi-pairs two-ports SAW MEMS resonator.

Figure 93-One Pair two-ports SAW MEMS resonator fabrication mask

Figure 94-Two Pairs two-ports SAW MEMS resonator fabrication mask

Figure 95-Three Pairs two-ports SAW MEMS resonator fabrication mask

Figure 98-Four Pairs two-ports SAW MEMS resonator fabrication mask

Figure 99-Five Pairs two-ports SAW MEMS resonator fabrication mask

Figure 96-Six Pairs two-ports SAW MEMS resonator fabrication mask

Figure 97-Seven Pairs two-ports SAW MEMS resonator fabrication mask

The footprint of the delay-line of each design on the substrate is shown in Table-14.

Table 14-Footprint of the delay-line of multi-ports SAW MEMS resonators

Design	Footprint
1 Pair	$4158\ \mu m^2$
2 Pairs	$5230.44\ \mu m^2$
3 Pairs	$6188.4\ \mu m^2$
4 Pairs	$7179.84\ \mu m^2$
5 Pairs	$8154\ \mu m^2$
6 Pairs	$9126\ \mu m^2$
7 Pairs	$10087.2\ \mu m^2$

It's important to notice that buried, semi-buried, and non-buried delay-lines will have the same footprint as the number of ports and fingers is the same.

Fabrication Steps

Building the conventional SAW MEMS resonator doesn't require many fabrication steps. The fabrication process starts by deposition the piezoelectric material, which is Aluminum Nitride in this case, on a Silicon substrate, it can be deposited by many means, but sputtering is most preferred because it produces highly oriented and dense films, so an RF magnetron sputtering is recommended to be used to deposit the AlN layer. Then to build up the IDTs as well as the reflectors, it's preferred to use ***lift-off*** process as it needs no etching but just developing the photoresist. A summary of the conventional SAW MEMS resonator fabrication steps is shown in steps from A to F.

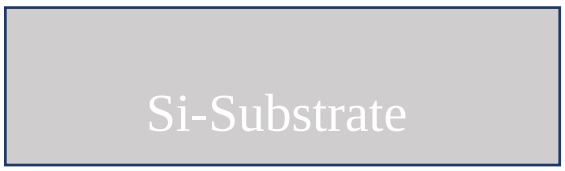

A- Start with Si-Substrate

B- Deposit *AlN* to act as the piezoelectric material

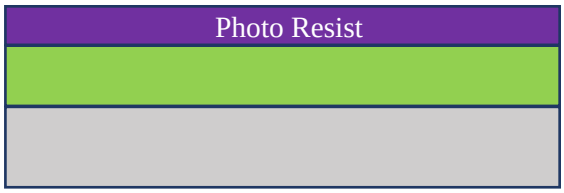

C- Spin-coat photo resist

D- Develop the photo-resist using the mask of the IDTs and reflectors (Leaving their pattern uncovered)

E- Deposit Aluminum

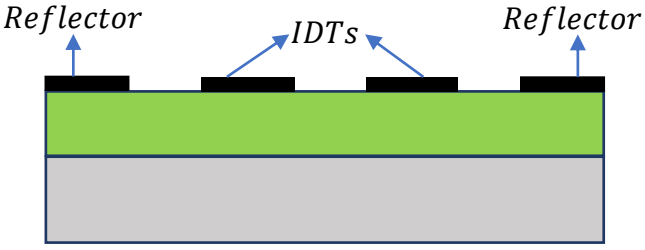

F- Develop the photoresist
(IDTs and Reflectors are built)
Lift-off Technique

The above fabrication steps are for a conventional SAW MEMS resonator with only two ports, any other multi-ports resonator fabrication process will follow the same procedures but with the resonator specific mask.

For the fabrication step for the buried IDTs SAW MEMS resonator, the fabrication steps are described as post-CMOS processing, as the IDTs and the reflectors are built during the CMOS process, after that some processing and piezoelectric deposition is done to obtain the required design. As the CMOS process ends, the chip is encapsulated, and it has a protective layer of SiO_2, so the first step in the CMOS-post processing is to etch the SiO_2 until the IDTs and the reflectors are on the surface, reactive ion etching is the best choice for this step. Then *AlN* layer is deposited and patterned to access the pads of the resonators for probing. A summary of the Buried SAW MEMS resonator fabrication steps is shown in steps from A to D.

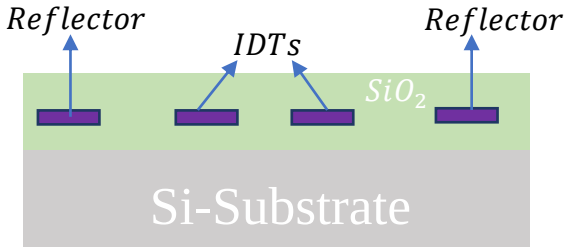

A- The result of the CMOS fabrication process, Perform RIE to the SiO_2 until the IDTs & reflectors are on the surface

B- After performing the RIE to SiO_2

C- Deposit AlN to act as the piezoelectric material (Sputtering preferred)

D- Patterning AlN to provide probing. (Final Structure)

For the semi-buried SAW MEMS resonator, assuming a post-CMOS processing, thus performing the RIE to release the IDTs as well as the reflectors from the SiO_2 layer is the first step to be done. Then spin coating a photo resist and developing it leaving parts covering the IDTs and the reflectors only. After that, the deposition of thin *AlN* layer takes place with only the lower part of the IDTs and reflectors is buried underneath the *AlN* layer whereas the upper part of them is on the *AlN* layer so it is called semi-buried SAW MEMS resonator. Then developing the photo resist to obtain the final desired structure. A summary of the semi-buried SAW MEMS resonator fabrication steps is shown in steps from A to E.

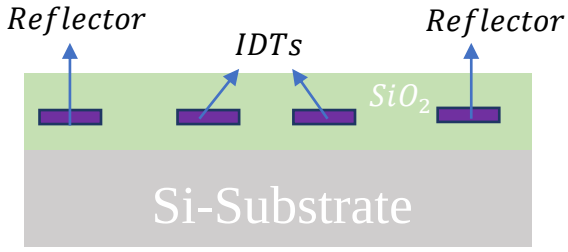

A- The result of the CMOS fabrication process, Perform RIE to the SiO_2 until the IDTs & reflectors are on the surface

B- After performing the RIE to SiO_2

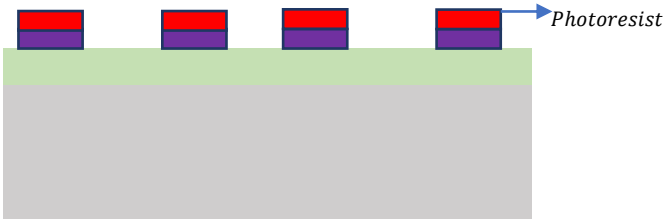

C- After performing spin coating and developing the photoresist.

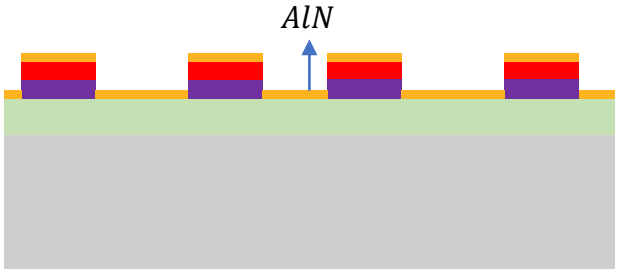

D- After depositing the *AlN* thin layer.

E- After developing the photoresist to obtain the final structure.

MEMS & CMOS Integration

CMOS nowadays is the leading fabrication technology and most researches are concerned to improve the reliability and yield of this fabrication process besides decreasing the features size and the cost of this process [47].

When talking about the integration between MEMS and CMOS integrated circuits there are multiple challenges that faces this process, for example postprocessing process of MEMS, fabrication temperature, interface between both MEMS and CMOS and packaging.

There are three well know integration techniques; hybrid integration, monolithic-integration and heterogenous integration[47].

Hybrid integration

Hybrid integration simply is the integration using connecting wires, MEMS chip and CMOS chip or circuit are fabricated independently, then a process of integration between two chips is held, there are two ways of wire connecting: MultiChip-Module (MCM)-based approach, and commercial wire bonding as shown in Fig-100 [47]

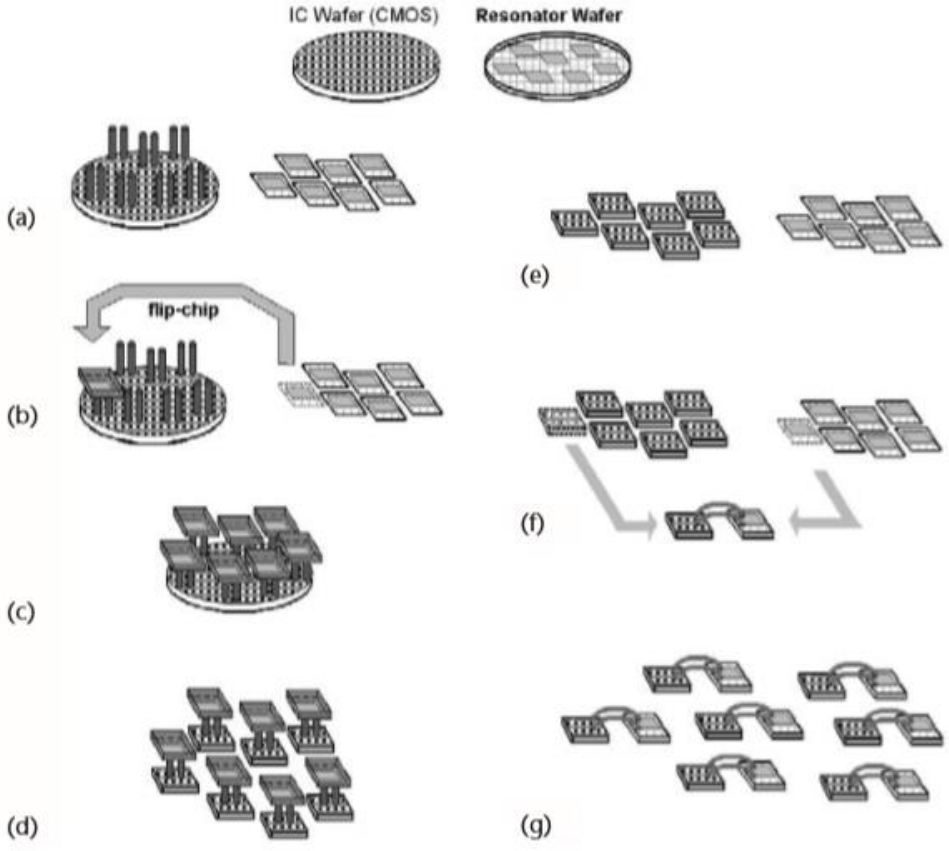

Figure 100 -MCM-based approach (a, b, c, d), and commercial wire bonding (e, f, g) Hybrid integration modes. [47]

As appears above, in the MCM-based integration the resonator chip is diced first then it is flipped and well aligned above the CMOS circuit the wire bonding tacks place and a final dice is made to the whole chip, this is very useful since it reduces the used area, but it takes a lot of work for implementation, dicing and alignment. But for the commercial bonding, the two chips are put beside each other and bonded by wires, this will reduce the area used and the effort for the alignment although it will introduce parasitic resistance and capacitance that must be taken into consideration in the circuit model of the total design.
Hybrid integration is considered the cheapest way to integrate two chips since it only depends on the bonding using wires, but it is done one wire by one wire, so it is very slow and not suitable for mass production.

Mono-lithic Integration

This technique helped avoiding the problems of the hybrid integration, in this technique both CMOS and MEMS circuits are fabricated on the same substrate, same chip. This technique is divided into three techniques depending on the fabrication steps or procedures as follows: pre CMOS, intermediate CMOS and post CMOS [47].
In the Pre CMOS procedure, the MEMS circuit is fabricated first using Micro fabrication techniques, then the CMOS sequence takes place. The MEMS is movable system, so it can not be located under the IC and this will increase the die area. In the intermediate CMOS, the CMOS fabrication process is taking turns with the MEMS microfabrication. And finally, the post CMOS has two different strategies, in the first one the MEMS structure is completely built on the finished CMOS substrate, without any interaction with the CMOS structure. On the other hand, if the MEMS was micromachined on the finished CMOS circuit. In post CMOS, Bulk and surface micromachining are used for the fabrication of these chips [47].
Monolithic integration is very complex and requires specific abilities to choose the materials, temperature and all the surrounding properties of the fabrication process. This concludes that this process needs specific fabrication procedures for all the properties taking into consideration all the limitations for MEMS and CMOS chips [47].

Heterogenous integration

This is a combination of both above, by stacking the substrates above each other as appears in Fig-101 [47]. It overcomes all the restrictions of both the hybrid and mono-lithic integration.

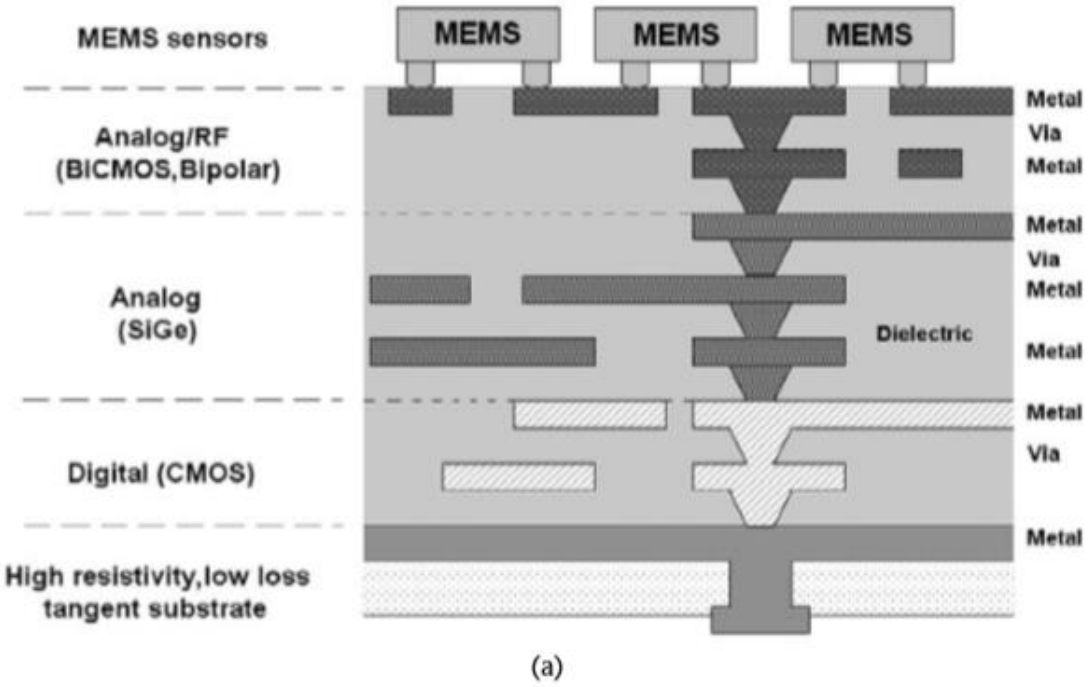

Figure 101-Heterogenous integration [47]

SAW Lab Characterization Techniques

The basic idea of electrical characterization of SAW devices in the lab is to measure the important parameters in the resonator such as "the equivalent circuit parameters, the quality factor, the electromechanical coupling, and the elastic, dielectric, and piezoelectric constants of the resonator, [4]. Network theory and different measurement techniques are the core of this branch. There are different kinds of these characterization techniques: the low/high frequency measurements, open- and short-circuit DC measurements, and scattering parameters measurements.

The electrical characterization depends on passing current or applying voltage on the circuit containing the resonator and other components. So the change in the current passing to the load impendence connected to the frequency dependent impedance of the resonator Z_m is characterized and analyzed. The following figure illustrates the setup configuration, 4.

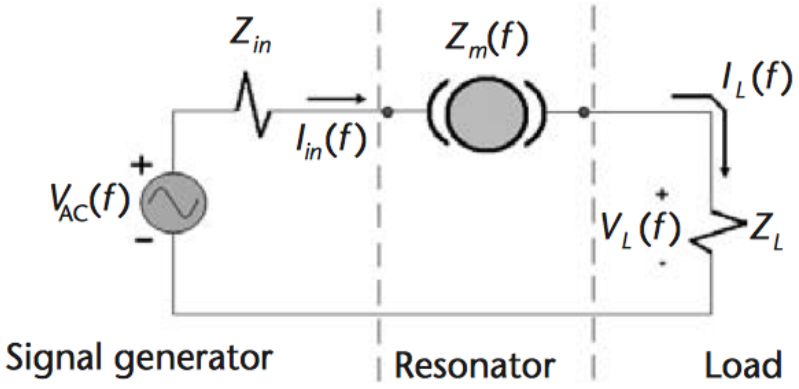

Figure 102-The electrical characterization setup for the resonator[4]

Low & High Frequency Electrical Characterization

There are two kinds of characterization; low and high frequency electrical characterization. Each has their usage and analysis. The low-frequency characterization shows the effect of applying range of frequencies (from 0, DC, to megahertz) on the actuation mechanism, and the resonator design, [4]. It can be used to evaluate the fabrication process. The high-frequency characterization is concerned with the energy flow, in and out of, the transmission lines connected to the resonator. So it is an energetic-based description. It can be used in cases of complex systems with impractical or difficult lumped-circuit representation, [4].

Low-Frequency Characterization and Open-Short DC measurements:

As mentioned above, the low-frequency characterization has a wide band of frequencies which includes the first mode shapes of the MEMS structures. It can be used to extract the material constants. The electrodes and integrity of the MEMS resonator structure are measured by the open-short DC measurements, [4]. The basic idea behind this DC measurement is to check if the different electrodes designed to be non-connected are still not connected after the fabrication process and the electrodes designed to be connected are connected as well. Here a DC probe station, capacitance meter and a semiconductor parameter analyzer are used for this open-short DC measurement, [4]. At the end, the functional device should pass these open/short circuit conditions. In the SAW devices, the two IDTs

should pass the open circuit condition. Also the fingers of an IDT should be connected to each other so the short circuit condition is to be passed, [4].

Scattering-Parameters Representation and Network Theory

One of the most important tools for the device characterization is the scattering parameters description and the analysis using the network theory. So measuring the transmission and reflection provides key data about the electrical response of the MEMS device, [4].

The S-parameters or scattering parameters description is used for the transmission and reflection quantification. It depends on the two-port circuit representation as indicated in the following figure, [4]:

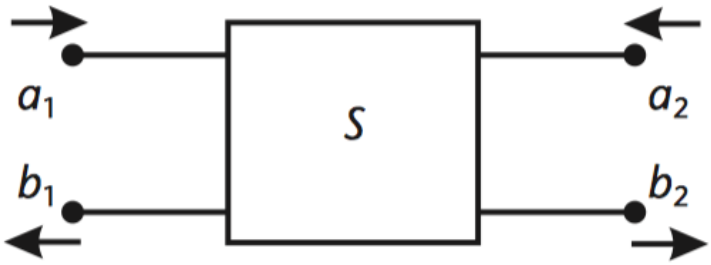

Figure 103-The two-port circuit representation to define the S-parameters, [4]

So the numbers 1, 2 represents the input and the output ports. And there are four quantities the scattering matrix S relates them together. This matrix is:

$$\begin{bmatrix} b_1 \\ b_2 \end{bmatrix} = \begin{bmatrix} S_{11} & S_{12} \\ S_{21} & S_{22} \end{bmatrix} \begin{bmatrix} a_1 \\ a_2 \end{bmatrix} \quad (33)$$

To get the scattering parameters, the independent variables in each port are set to zero and the final parameters are:

$$S_{11} = \left.\frac{b_1}{a_1}\right|_{a_2 = 0} \quad (34)$$

$$S_{12} = \left.\frac{b_1}{a_2}\right|_{a_1 = 0} \quad (35)$$

$$S_{21} = \left.\frac{b_2}{a_1}\right|_{a_2 = 0} \quad (36)$$

$$S_{22} = \left.\frac{b_2}{a_2}\right|_{a_1 = 0} \quad (37)$$

Each of them represents either the transmission or the reflection coefficients at one port when the other port is match loaded,[4].

Using these values, the device impendence (the resonator input impendence, Z_{in} and the source impendence, Z_S) can be calculated using the following equations:

$$S_{11} = \frac{Z_{in}}{(2Z_S + Z_{in})(1 + \lambda L)} \quad (38)$$

$$S_{21} = \frac{2Z_S}{(2Z_s + Z_{in})(1 + \lambda L)} \quad (39)$$

where λ is the propagation constant and the L is the length of the waveguide,[4].

SAW Quality Factor Measurement

For a SAW device, the quality factor is one of the key parameters needed to be well designed and characterized for the precise estimation of the oscillator operation. There are three methods for measuring the quality factor. The first method is called the $S_{21} - S_{11}$ magnitude method, [4]. The two-port scattering parameters are obtained first and the quality factor is calculated using the following equation using the minimum values of the S-parameters measured:

$$Q = \frac{(\frac{\omega_s}{\omega_p})}{1 - \left(\frac{\omega_s}{\omega_p}\right)^2} \sqrt{\frac{(1 - |S_{21Min}|)(1 - |S_{11Min}|)}{|S_{21Min}||S_{11Min}|}} \quad (40)$$

where ω_p and ω_s are the series and parallel resonance frequencies, [4].

Another method to calculate the quality factor depends on the phase response $\emptyset(\omega)$ in the open-loop, [4]. The quality factor depends on the slope of the phase proportionally as:

$$Q = \frac{\omega_s}{2} \left|\frac{\partial \emptyset}{\partial \omega}\right| \quad (41)$$

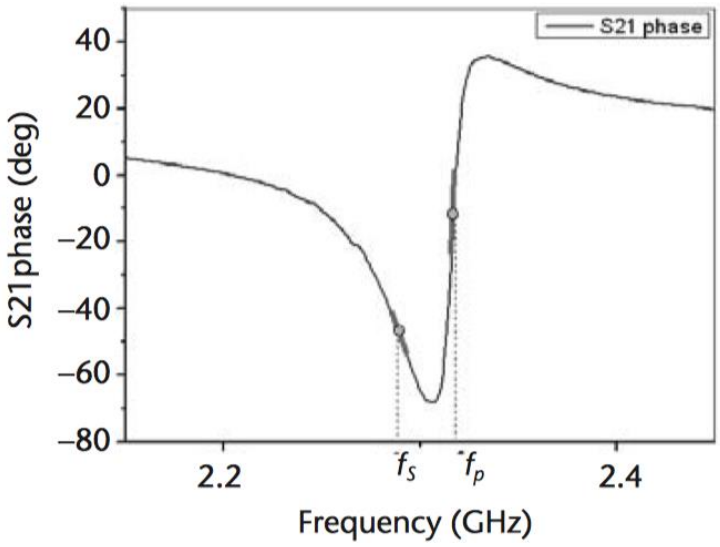

Figure 104-The quality factor calculation based on the phase response in the open-loop[4]

The final method, which is applied in this project, is to use the (-3dB) bandwidth definition, [4]. So the Q is the frequency at resonance divided by the two-sided bandwidth at the -3dB.

$$Q = \frac{f_0}{B} \quad (42)$$

This method will be focused on more in the results section.

Chapter Seven

Applications of SAW Devices

SAW Devices

SAW phenomenon is a key to many applications and there are various electronic devices that are based on using this wave in their operation. Devices range from simple structure such as the delay lines, to a more complex implementation such as the SAW oscillators, filters, and sensors. It is important to know these different devices in addition to the SAW oscillator, being the core of this thesis. The following paragraphs explain these devices.

SAW Delay Lines

The SAW delay line is considered as the simplest and most widely used SAW device. It can be used in signal processing applications that require delays between the input signal and the output signal (ranging from milli/microseconds), [5]. It consists of two interdigitated transducers, one as an input and the other is an output. Both are deposited on a piezoelectric substrate [6]. The input IDT generates the propagating wave and the output IDT receives the wave after some delay, $\tau_g = L/v$, where L is the delay line distance and the v is the SAW velocity, [7].

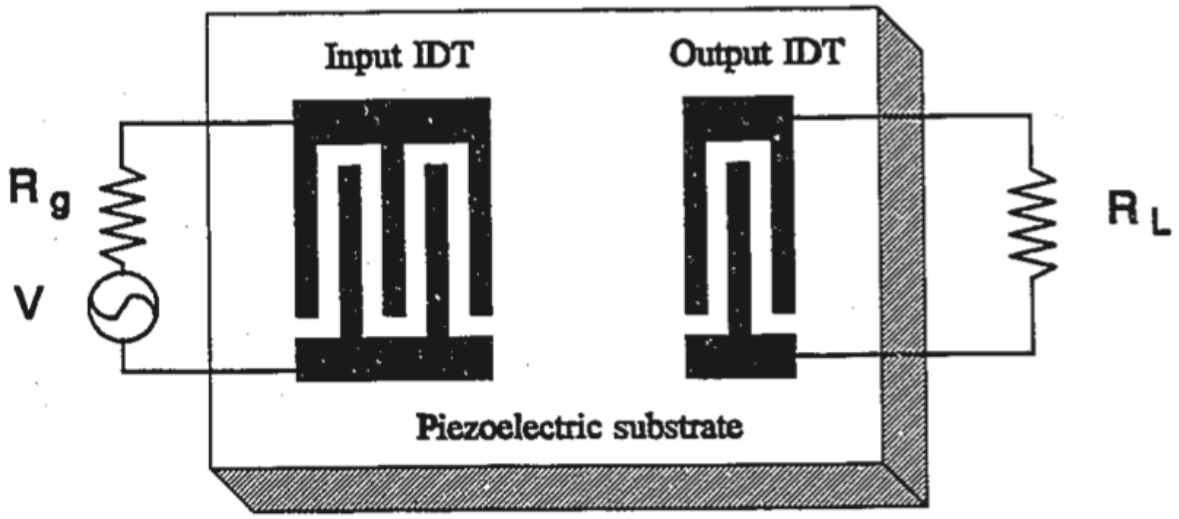

Figure 105-Simple SAW delay line device,[6]

SAW Oscillators:

SAW oscillators witnessed increasing application and market demand for different communications technologies. They are used in the timing circuits for clock recovery and generation. For their high-quality factor, they can operate at frequencies till 3-GHz on ST-quartz substrates, [7]. There are two broad classes of SAW oscillators: firstly, a single mode SAW oscillator using SAW resonator or delay lines and operating at a fixed frequency, and secondly, the multi-frequency oscillators resonating at any one of certain different frequencies using a SAW comb filter. The general condition for oscillation is that the amplifier gain is designed to be greater than the overall insertion losses of the components around the loop, [7].

This project is concerned with first class with is the fixed frequency oscillators, Fig-106. So in this class the delay line should have a narrow band input transducer (the sending IDT) and a broadband output transducer (the receiver IDT). If the time delay in the centers of wave phases propagating is $\tau_g = L/v$, where L is the delay line distance and v is the wave velocity, [7]. Applying the above condition in this

case, the total phase shift around the whole loop is given by, where $\emptyset_a$ is the amplifier phase shift, $\emptyset_c$ is the phase shift around the loop, and P is and integer number, and f_A is the operating frequency [7]:

$$\tau_g 2\pi f_A + \emptyset_a + \emptyset_c = 2\pi P \quad (43)$$

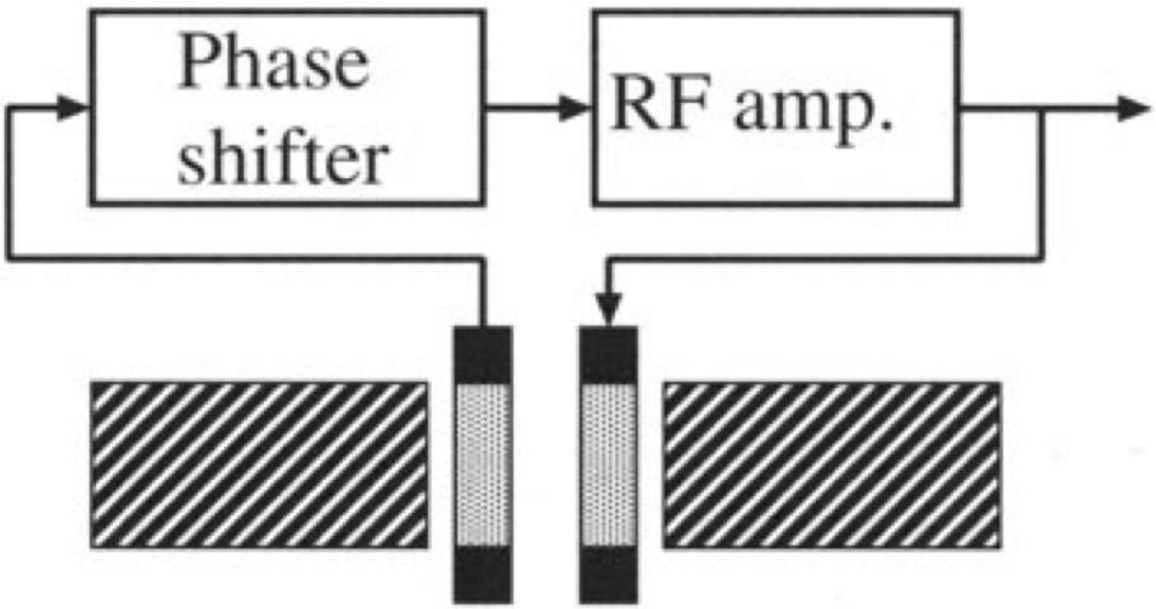

Figure 106 SAW oscillator using the SAW resonator as a feedback element [11]

SAW Sensors:

Any sensor converts between physical quantity to an electronic signal to measure and analyze this physical quantity which can be biological, chemical, temperature, pressure, elasticity change, mass/density changes, viscosity, dielectric, conductivity moisture, contaminants, pH levels, or concentration. SAW sensors are sensitive to most of these quantities perturbations on the surface. So, they are known to be reliable, small in size, cheap, highly sensitive, simple in implementation and versatile in nature (meaning that variety of properties change can induce the monitoring signal), [8].

The basic mechanism in SAW sensors is that the acoustic wave velocity is affected by these quantities change. This velocity change intrinsically happens due to the changes in the resonant frequency, phase angle or the transmission-reflection wave amplitudes. So if the phase velocity is v, so the resonant frequency is $f_r = v/\lambda$. The following equation gives the signal change with respect to the different quantities to be measured, [8]:

$$\frac{\Delta f}{f_0} = \frac{\Delta v}{v_{acoustics}} = \frac{1}{v}\left(\frac{\partial v}{\partial m}\Delta m + \frac{\partial v}{\partial \sigma}\Delta\sigma + \frac{\partial v}{\partial c}\Delta c + \frac{\partial v}{\partial \varepsilon}\Delta\varepsilon + \frac{\partial v}{\partial T}\Delta T + \frac{\partial v}{\partial P}\Delta P + \frac{\partial v}{\partial \rho}\Delta\rho + \cdots\right) \quad (44)$$

where m is the mass loaded on the surface, σ is the conductivity, c is a constant for the mechanical properties, ε is the dielectric constant, ρ is the density.

The sensor sensitivity can be given by the following equation, [8]:

$$S_r = lim\frac{\Delta f}{f\Delta x} = \frac{df}{fdx} \quad (45)$$

which indicates the frequency shift due to the perturbation in any of the factors to be measured.

One example illustrating that is small concentration analyte detection using SAW delay lines [9, 10]. It is used for analyte detection. The structure is based on one input IDT that generates SAW in two directions to hit the output IDT (delay line with one input and one output). The sensing area between the input and output is used to deposit different analyte ligand for sensing as in the following graph:

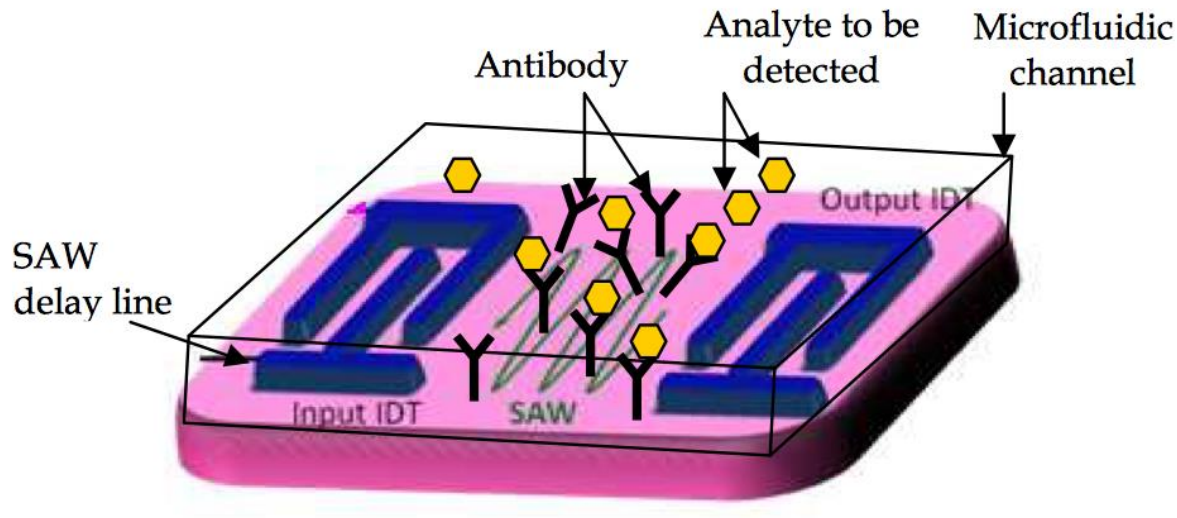

Figure 107-SAW biosensor implementation and analyte detection [10]

When the specific antibody binds to its *key* analyte, the mass loading on the surface changes which leads to change of the viscoelasticity of the layer so the SAW velocity changes leading to the frequency shift, [10].

SAW Port Configurations:

There are different ports configurations a SAW resonator can have. It is based on the number of IDTs and functionality of each one. Resonators can have one, two or multi ports. It is important to know these different configurations before designing a SAW-based device.

One-Port SAW Resonator:

One-port SAW resonator consists of one transducer and two grating reflectors. This one IDT has the role of both generating and receiving the wave. During its operation, the IDT is excited and surface waves get emitted from both directions [7]. The reflectors confine this energy and generate the standing waves at the center frequency [7]. These standing waves can be characterized by either their amplitude or the potential on the piezoelectric surface [7]. It is a two-terminal device that can be used in oscillators. It is to note that the length of the gap between the reflectors and the transducer has a significant effect on the resonance characteristics and the grating separation is to be designed for the resonance to be at the needed operating frequency [7, 11]. The design issue in such configuration is how to make a suitable offset between the

series and parallel resonances [7]. The following figure show the configuration along with the electrical equivalent circuit model mentioned above [11].

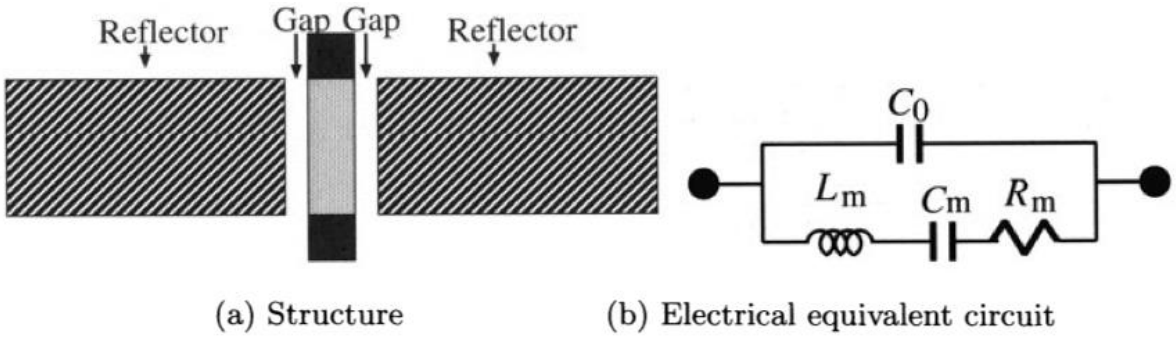

Figure 108-(a) the configuration of one-port SAW resonator, (b) the modeled circuit for the resonator,[11]

This resonator can be also characterized by using Fabry-Perot model. This model depends on replacing the two reflectors with mirrors put at a distance of L from the center of the transducer. So the total resonant cavity has the length of 2L as shown in the following figure [11].

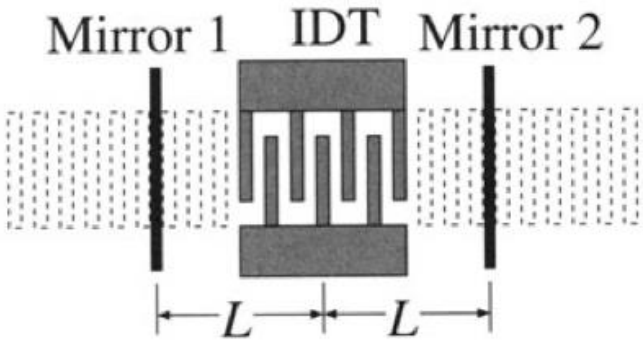

Figure 109-The Fabry-Perot model of the one-port SAW resonator,[11]

The realization of this configuration can be designed similar to the following figure.

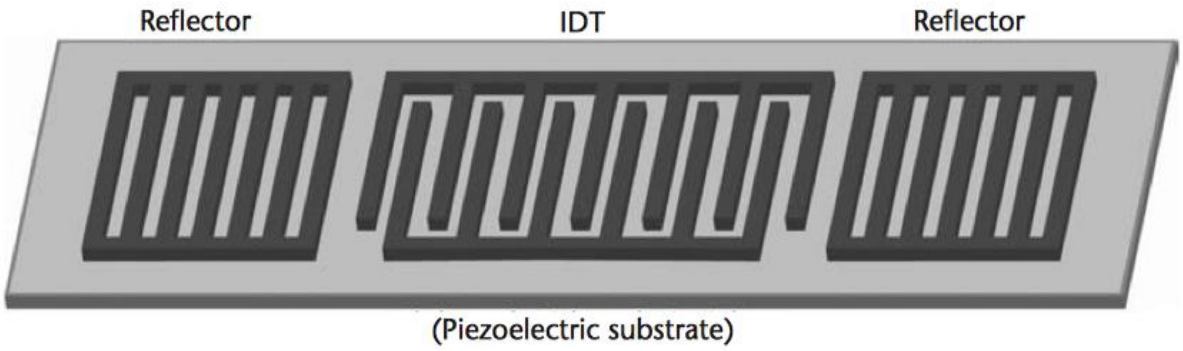

Figure 110-An example of the device realization of the SAW resonator, [4]

Two-Port SAW Resonator:

A two-port SAW resonator consists of two IDTs as transducers and two grating reflectors on both sides of the IDTs. Here one of the IDTs works as an input which generates the wave, and the other IDT works as the output which receive the transmitted wave. The two grating reflectors confine the wave between the IDTs and have the role of generating the standing waves (bounce of the SAW back and forth between the reflectors) in a coherent manner [7]. This kind of configuration is suitable for all the SAW devices especially the bandpass filtering applications because it can be designed to have a large transfer admittance at resonance so a filter with low-loss and narrow passband can be achieved [11]. It is to note that they can be designed for multimode operation at different frequencies [7]. The following figure illustrates the two-port configuration along with its electrical equivalent circuit [11].

And similar to the one-port resonator, the two-port resonator can be characterized by Fabry-Perot model. It replaces the two reflectors with two mirrors at a distance L from the IDT center. The following figure shows the model.

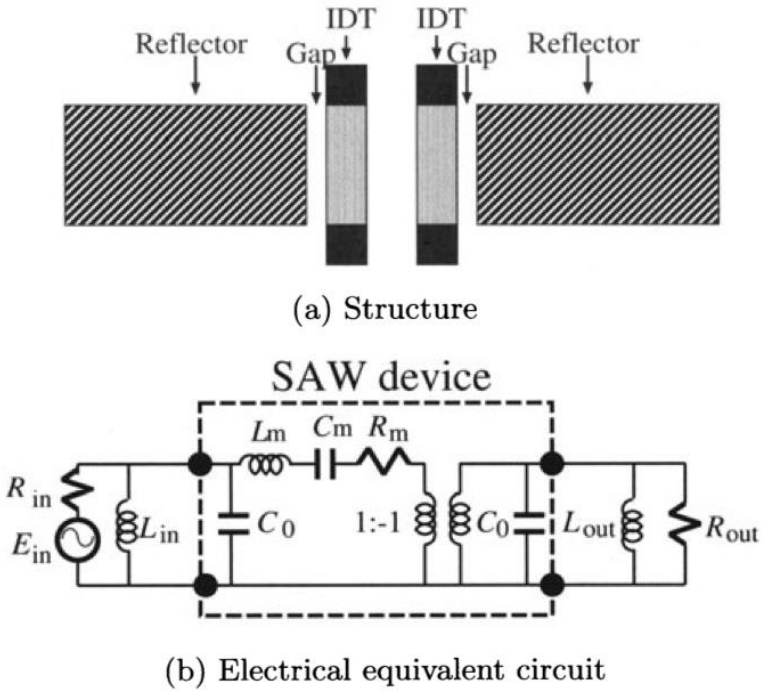

Figure 111-a) the configuration of two-port SAW resonator, (b) the modeled circuit for the resonator, [11]

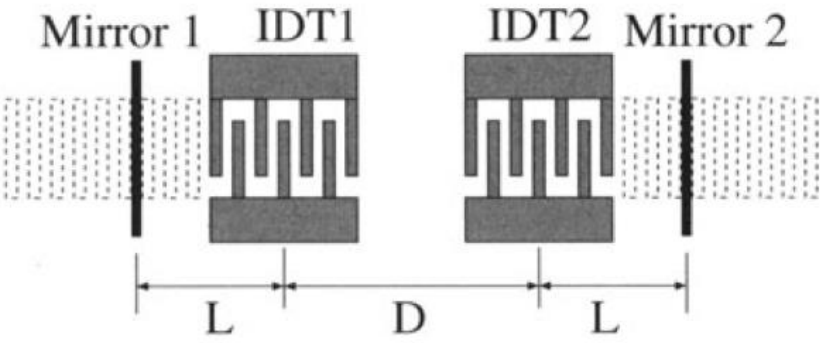

Figure 112-The Fabry-Perot model of the two-port SAW resonator,[11]

The realization of this configuration can be designed similar to the following figure.

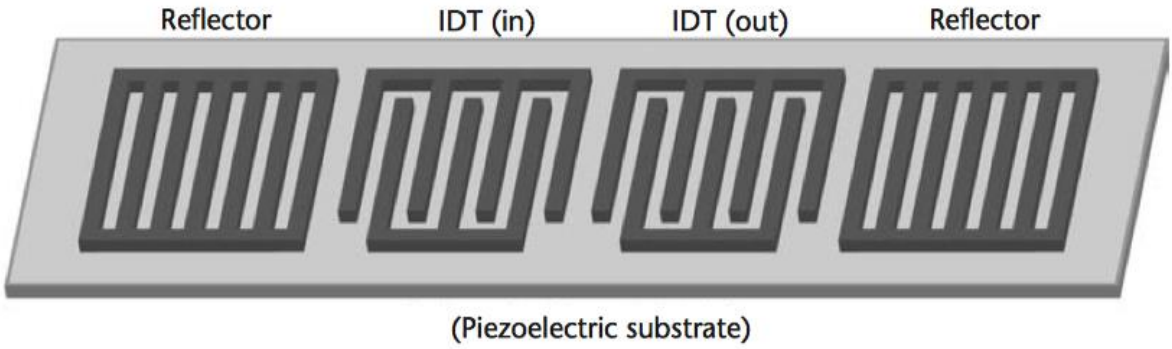

Figure 113-An example of the device realization of the two-port SAW resonator,[4]

Chapter Eight

Conclusions & Recommendations

Multiport SAW resonator designs are simulated to compare their quality factor, insertion loss, phase depth, and TCF. The various designs include above surface, semi-buried, and buried IDTs. The trends for the IDTs above surface have high quality factor at 1 pair of IDTs and starts to decrease as the number of pairs increases. The same trend for insertion loss was found, which shows the trade-off between quality factor and insertions loss. Based upon the application needed, the number of IDTs is used. The semi-buried did not show a remarkable trend regarding the quality factor and insertion loss. However, some design recommendations are present were high or low number of pairs is recommended rather than the number of pairs, which has high insertion loss. The buried transducers do not show much fluctuations in quality factor, but it has an overall similar performance to that of above surface transducers. The insertion loss of 2 pairs of buried IDTs is not recommended as it has high insertion loss. The TCF comparison between above surface, semi-buried, and buried IDTs shows that inserting the IDTs in the surface is much better for TCF.

Picking the number of pairs and the design is dependent on the application needed. For example, high quality factor is obtained from above surface IDTs with low number of IDTs . TCF variations from the three different designs show that the design can be used as a temperature sensor in case the TCF was high or as a clock generator in case the TCF was low. TCF still can be modified by temperature compensation by adding an oxide layer under the piezoelectric material, which is a recommended approach in the future.

References

[1] R. Matthys, *Crystal oscillator circuits*. Malabar (Florida): Krieger, 1992.

[2] J. Karim, A. Nordin and A. Alam, "Pierce Oscillator Circuit Topology for High Motional Resistance CMOS MEMS SAW Resonator", *IEEE-ICSE2012 Proc.*, 2012.

[3] R. Abdolvand, B. Bahreyni, J. Lee and F. Nabki, "Micromachined Resonators: A Review", *Micromachines*, vol. 7, no. 9, p. 160, 2016.

[4] H. Campanella, *Acoustic Wave and Electromechanical Resonators: Concept to Key Applications (Integrated microsystems series)*. Artech House, 2010.

[5] A. Oliner and E. Ash, *Acoustic surface waves*. Berlin: Springer, 1978.

[6] Y. Xu, "Surface acoustic wave longitudinally coupled resonators and waveguide coupled resonators", 1994.

[7] C. Campbell and J. Burgess, "Surface Acoustic Wave Devices and Their Signal Processing Applications", *The Journal of the Acoustical Society of America*, vol. 89, no. 3, pp. 1479-1480, 1991.

[8] Y. Fu, J. Luo, N. Nguyen, A. Walton, A. Flewitt, X. Zu, Y. Li, G. McHale, A. Matthews, E. Iborra, H. Du and W. Milne, "Advances in piezoelectric thin films for acoustic biosensors, acoustofluidics and lab-on-chip applications", *Progress in Materials Science*, vol. 89, pp. 31-91, 2017.

[9] H. Oh, Y. Lee, S. Lee, S. Yang and K. Lee, "Development of Novel LOVE Wave Biosensor for Simultaneous Detection of Multi-Analyte", *Procedia Engineering*, vol. 25, pp. 908-911, 2011.

[10] Acoustic Wave Based MEMS Devices, Development and Applications

[11] K. Hashimoto, *Surface acoustic wave devices in telecommunications*. Berlin [u.a.]: Springer, 2010.

[12] M. Konstantinos, "Development of a multi-analyte acoustic biosensing platform for clinical diagnostics", 2009.

[13] Y. Fu, "Advances in piezoelectric thin films for acoustic biosensors, acoustofluidics and lab-on-chip applications", *Progress in Materials Science*, 2017.

[14] R. White, "Surface elastic waves", *Proceedings of the IEEE*, vol. 58, no. 8, pp. 1238-1276, 1970.

[15] "JISIS: Diamond-based Surface Acoustic Wave Devices: a reverse fabrication design", *Av.it.pt*, 2018. [Online]. Available: http://www.av.it.pt/jisis/saw.html. [Accessed: 07- Jun- 2018].

[16] Andrew J. S., "Surface Acoustic Waves and SAW Materials", *Proceedings of the IEEE*, Vol. 64, no. 5, May 1976

[17] C. Campbell, *Surface Acoustic Wave Devices and Their Signal Processing Applications*. Ontario: Elsevier Science, 2012.

[18] T. Kannan, "Finite Element Analysis of Surface Acoustic Wave Resonators.", Master of Science, Department of Electrical Engineering University of Saskatchewan, 2006.

[19] A. MONTAZERI, "A PERFECTLY MATCHED LAYER (PML) FOR ELECTROACOUSTIC WAVES IN PIEZOELECTRIC MATERIALS USING FDTD.", Master of Applied Science, McMaster University, 2010.

[20] A. Namdeo and H. Nemade, "Extraction of Electrical Equivalent Circuit of One Port SAW Resonator using FEM based Simulation", in *Proceedings of the 2015 COMSOL Conference*, Pune, 2015.

[21] N. Zakaria, A. Nordin, M. Mel, S. Arifuzzaman and I. Voiculescu, "MEMS Biosensor for Potential Cancer Cell Detection", *Volume 12: Micro and Nano Systems, Parts A and B*, 2009.

[22] L. Allies, E. Blampain, H. M'Jahed, G. Prieur and O. Elmazria, "Modelling of wireless SAW temperature sensor and associated antenna", *Instrumentation*, 2014

[23] "Opening a Quartz Crystal Can: Effects Thereof", *The Smell of Molten Projects in the Morning*, 2018. [Online]. Available: https://softsolder.com/2010/05/15/opening-a-quartz-crystal-can-effects-thereof/. [Accessed: 04- Jun- 2018].

[24] ″Quartz Crystals | Quartz Dielectric Resonator | Radio-Electronics.com", *Radio-electronics.com*, 2018. [Online]. Available: http://www.radio-electronics.com/info/data/crystals/quartz-crystals-resonator.php. [Accessed: 04- Jun- 2018].

[25] ”Quartz Crystals | Operation Theory Calculations | Radio-Electronics.com", *Radio-electronics.com*, 2018. [Online]. Available: http://www.radio-electronics.com/info/data/crystals/quartz-crystals-theory-operation.php. [Accessed: 04- Jun- 2018].

[26] ”Quartz Crystal Cuts | AT, SC, BT-Cut, etc | Radio-Electronics.com", *Radio-electronics.com*, 2018. [Online]. Available: http://www.radio-electronics.com/info/data/crystals/quartz-crystal-cuts-at-sc-ct.php. [Accessed: 04- Jun- 2018].
[27] "Quartz Crystal Manufacture | Manufacturing Processes | Radio-Electronics.com", *Radio-electronics.com*, 2018. [Online]. Available: http://www.radio-

electronics.com/info/data/crystals/quartz-crystal-manufacture-manufacturing-process.php. [Accessed: 04- Jun- 2018].

[28] *Geyer-electronic.de*, 2018. [Online]. Available: http://geyer-electronic.de/fileadmin/user_upload/frequenz/service/Comparison_of_Crystal_Oscillator_and_MEMS_Oscillator.pdf. [Accessed: 04- Jun- 2018].

[29] *Www5.epsondevice.com*, 2018. [Online]. Available: https://www5.epsondevice.com/en/information/technical_info/pdf/wp_e20140911_osc.pdf. [Accessed: 05- Jun- 2018].

[30] "SAW Resonators from Golledge | Golledge Electronics", *Golledge.com*, 2018. [Online]. Available: https://www.golledge.com/products/saw-resonators/c-26/c-86?gclid=EAIaIQobChMI-NHj-czz2QIV4b_tCh2LRw9uEAAYASAAEgKH0fD_BwE. [Accessed: 03- Jun- 2018].

[31] "B39122R0959H110 Qualcomm (RF360 - A Qualcomm & TDK Joint Venture) SAW Resonator- Richardson RFPD", *Richardsonrfpd.com*, 2018. [Online]. Available: http://www.richardsonrfpd.com/Pages/Product-Details.aspx?productId=1245672. [Accessed: 03- Jun- 2018].

[32] *Richardsonrfpd.com*, 2018. [Online]. Available: http://www.richardsonrfpd.com/resources/RellDocuments/SYS_31/B39000Z3410A003.pdf. [Accessed: 03- Jun- 2018].

[33] F. Sidek, A. Nordin and M. Zaghloul, "Development of an RF-CMOS Surface Acoustic Wave (SAW) Resonator.", *IEEE*, 2011.

[34] A. Ralib, A. Nordin, A. Alam, U. Hashim and R. Othman, "Piezoelectric thin films for double electrode CMOS MEMS surface acoustic wave (SAW) resonator", *Microsystem Technologies*, vol. 21, no. 9, pp. 1931-1940, 2014.

[35] K. Hashimoto, "Simulation of Surface Acoustic Wave Devices", Japanese *Journal of Applied Physics*, vol. 45, no. 5, pp. 4423-4428, 2000.

[36] A. Md Ralib, A. Nordin, H. Salleh and R. Othman, "Fabrication of aluminium doped zinc oxide piezoelectric thin film on a silicon substrate for piezoelectric MEMS energy harvesters", *Microsystem Technologies*, vol. 18, no. 11, pp. 1761-1769, 2012.

[37] Mohanraj Soundara pandian, Eloi Marigo, Muniandy Shunmugam, Rubiyatulniza Binti Hussain, Charlie Tay Wee Song, Jazril Bin Jamil Din, Chan Buan Fei, Venkatesh Madhaven, Arjun Kumar Kantimahanti, Aamir Farooq Malik and Varun Jeoti, “ Investigation on Surface

Acoustic Wave Propagation for A Nonplanar Piezoelectric Thin Film Device," *IEEE Explore*, November 2015.

[38] SilTerra Malaysia Sdn Bhd, http://www.silterra.com/mems_ppf_saw.html

[39] A. Namdeo and H. Nemade, "of Electrical Equivalent Circuit of One Port SAW Resonator using FEM based Simulation", in *COMSOL Conference*, Pune, 2015.

[40] Hao, W., Liu, J., Liu, M., Liang, Y. and He, S. (2016). Mass Sensitivity Optimization of a Surface Acoustic Wave Sensor Incorporating a Resonator Configuration. *Sensors*, 16(4), p.562.

[41] INVESTIGATION ON SURFACE ACOUSTIC WAVE PROPAGATION FOR A NONPLANAR PIEZOELECTRIC THIN FILM DEVICE. (2015). *IEEE International Ultrasonics Symposium Proceedings*.

[42] P. Varshney, B. Panwar, P. Rathore, S. Ballandras, B. Francois, G. Martin, J. Friedt and T. Retornaz, "Theoretical and experimental analysis of high Q SAW resonator transient response in a wireless sensor interrogation application", *2012 IEEE International Frequency Control Symposium Proceedings*, 2012.

[43] G. Bu, D. Ciplys, M. Shur, L. Schowalter, S. Schujman and R. Gaska, "Temperature coefficient of SAW frequency in single crystal bulk AlN", *Electronics Letters*, vol. 39, no. 9, p. 755, 2003.

[44] Chih-ming Lin, Ting-ta Yen, Yun-ju Lai, V. Felmetsger, M. Hopcroft, J. Kuypers and A. Pisano, "Temperature-compensated aluminum nitride lamb wave resonators", *IEEE Transactions on Ultrasonics, Ferroelectrics and Frequency Control*, vol. 57, no. 3, pp. 524-532, 2010.

[45] M. Pandian, E. Ferrer and W. Tay, "THIN FILM PIEZOELECTRIC DEVICES INTEGRATED ON CMOS", *Symposium on Piezoelectricity, Acoustic waves, and Device Applications*, 2016.

[46] Allen Cowen, Busbee Hardy, Ramaswamy Mahadevan, and Steve Wilcenski *"MUMPs Process Hand Book"* MEMSCAP Inc. available online : http://www.memscap.com/__data/assets/pdf_file/0019/1729/PolyMUMPs-DR-13-0.pdf

[47] H. Campanella, *Acoustic Wave and Electromechanical Resonators: Concept to Key Applications (Integrated microsystems series)*. Artech House, 2010.

Appendix

Cadence Appendix

1. To start transient analysis, choose *launch >> ADE L* as shown in the figure:

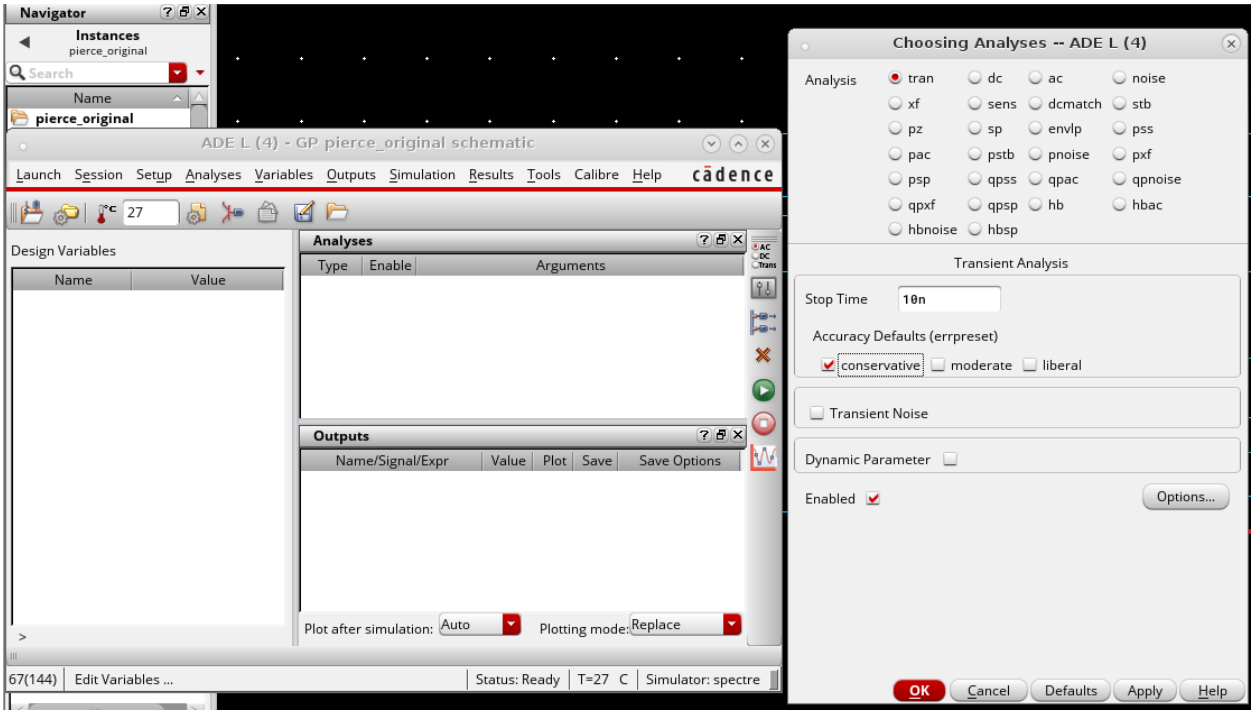

Press on *Choosing the analysis* and choose *tran.* Choose an appropriate stop time and make it *conservative.* To plot the output, choose *setting output* icon:

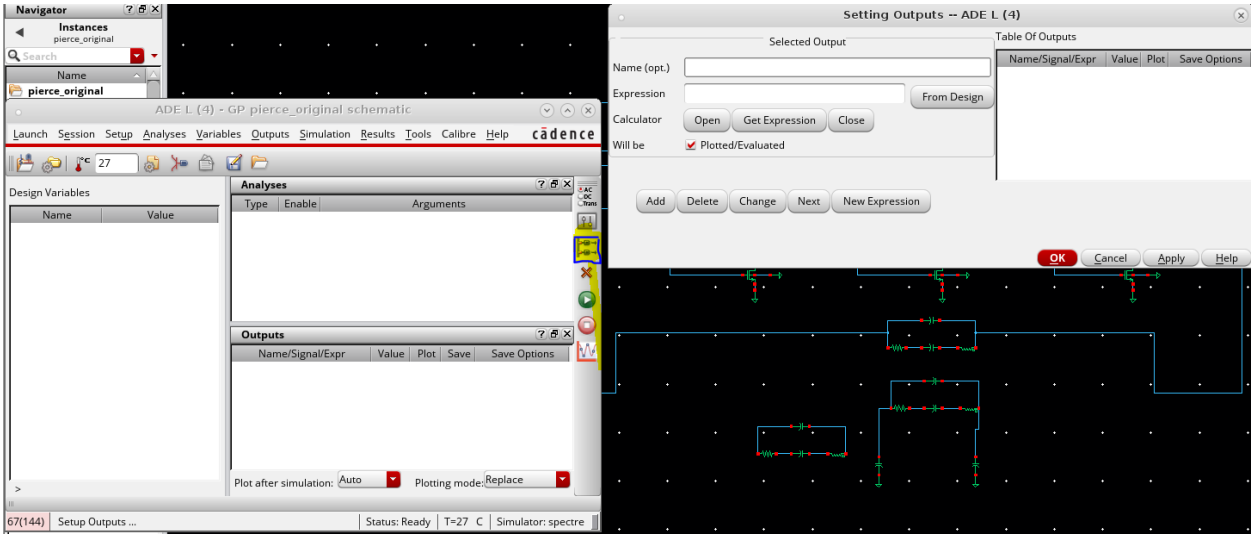

And click on *from design* and choose the negative node of the oscillator (output of the resonator.

2. PSS simulation:
   From *ADE L* choose *PSS* as shown:

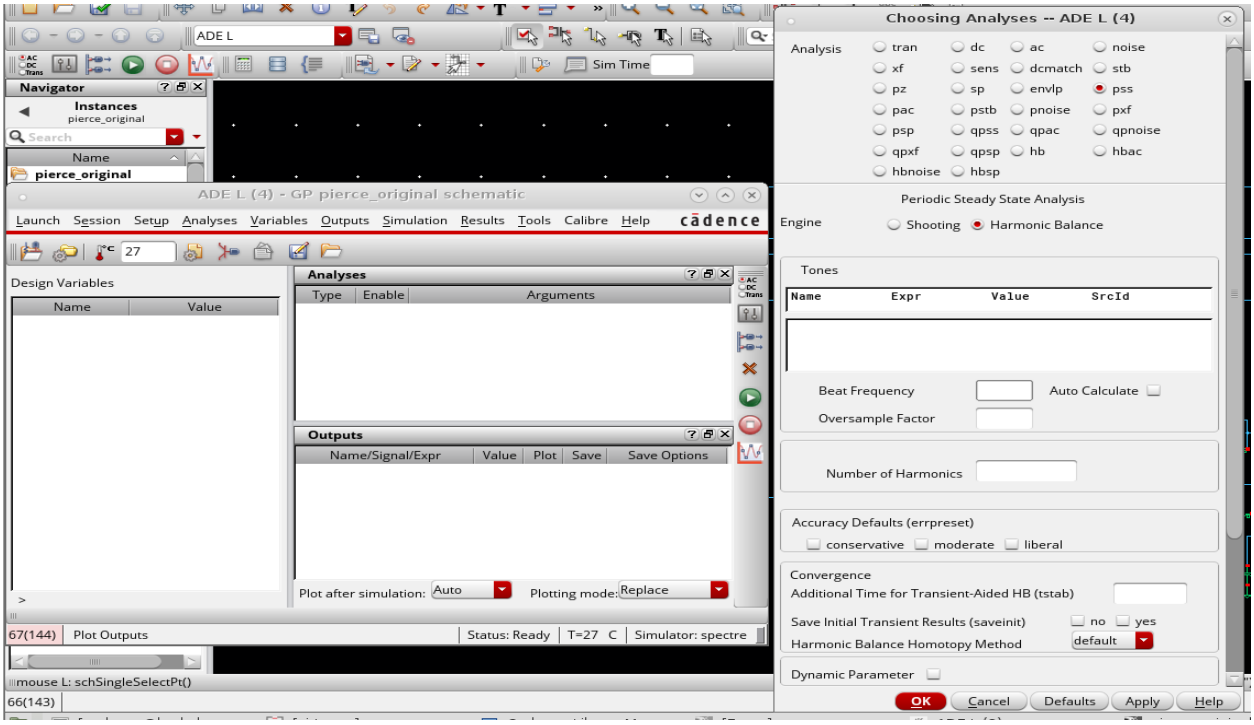

Choose harmonic balance. In the *beat frequency*, put the initial guess of the fundamental resonant frequency.

In *Number of Harmonics*, choose an appropriate value for example, 20 or 50.

In the *accuracy*, choose moderate, and make the *tstab transient aided HB*, a 100 nm.

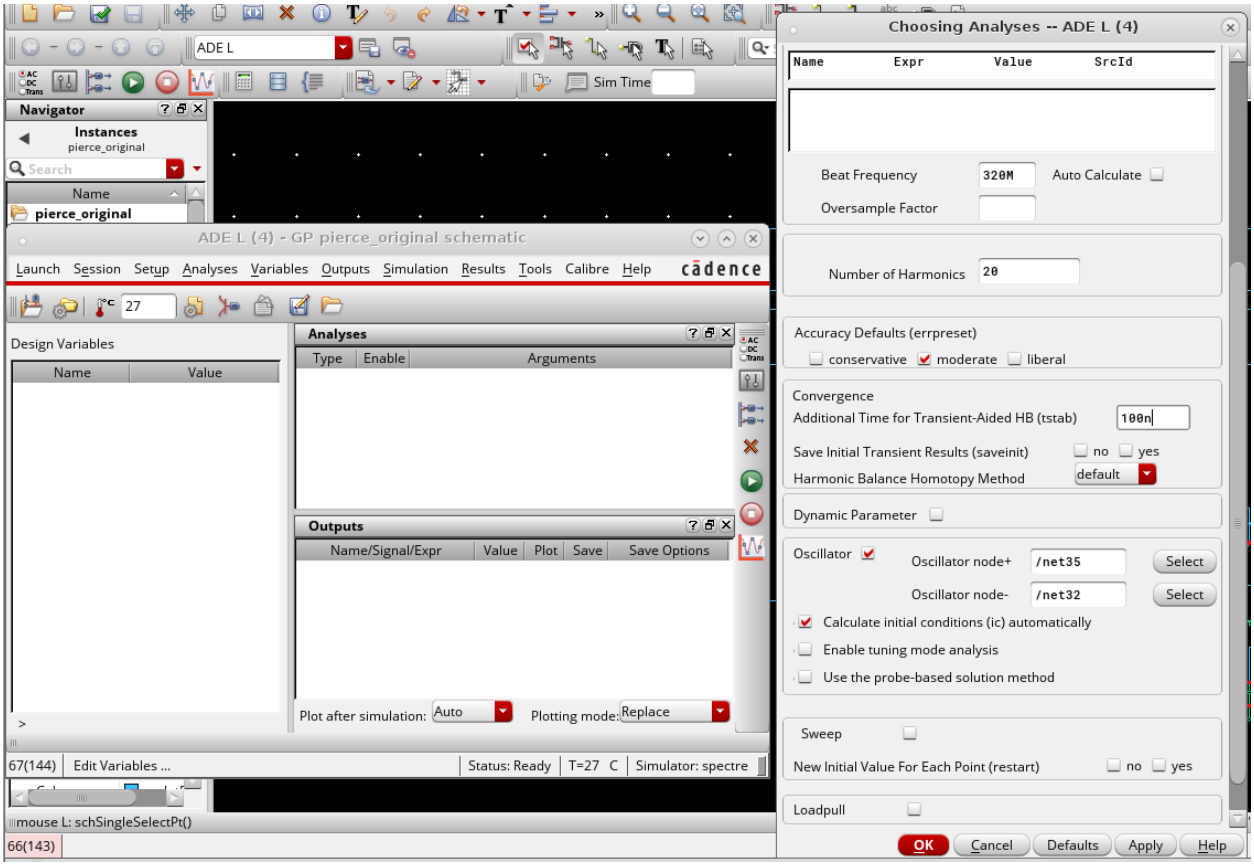

Enable the *oscillator* option and choose the terminals of the resonator as the *node+ & node-*.

3. SP simulation:

First, insert two ports and insert the following parameters:

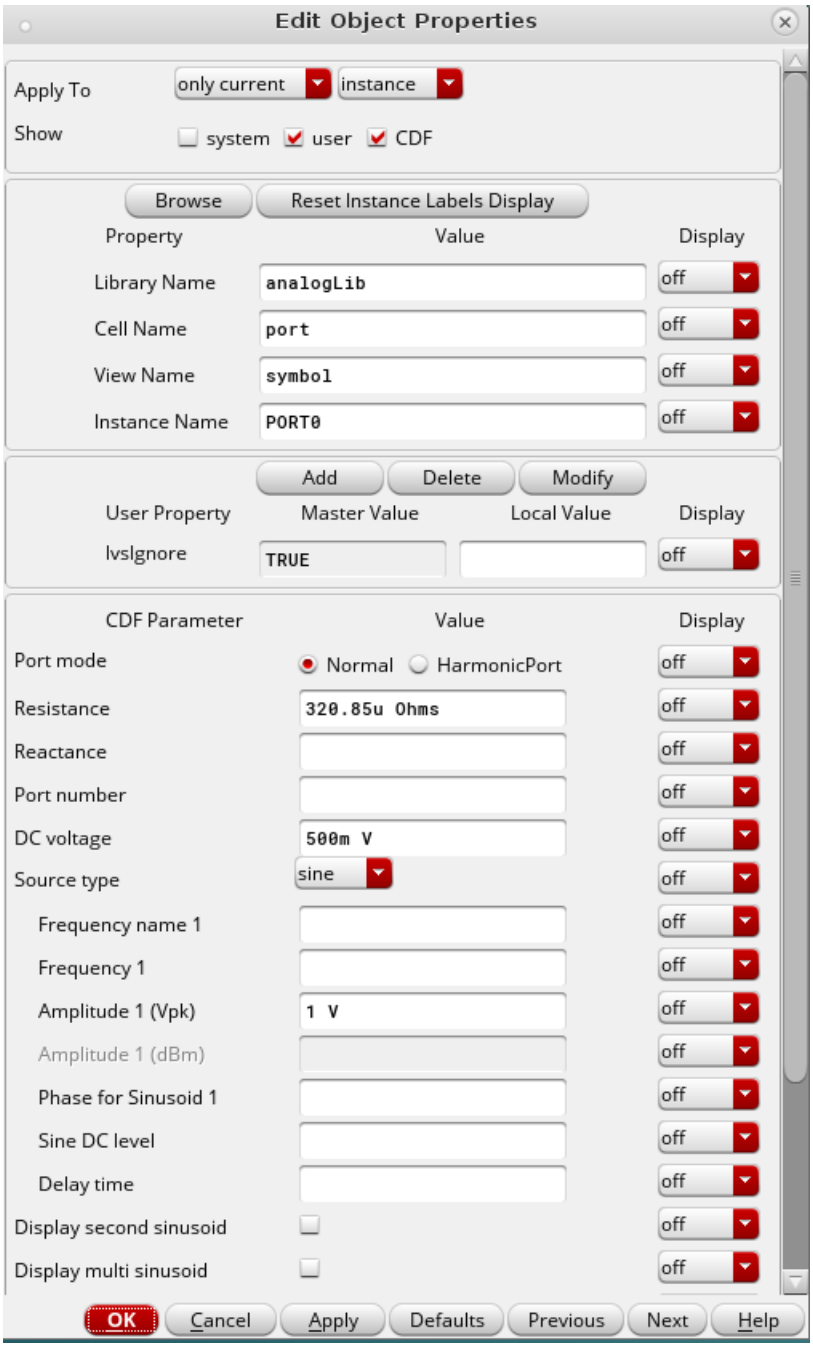

The resistance part is dependent on the real impedance part of the resonator. The parameters in the *SP* simulation is as follows:

From *ADE L*, choose *SP*,

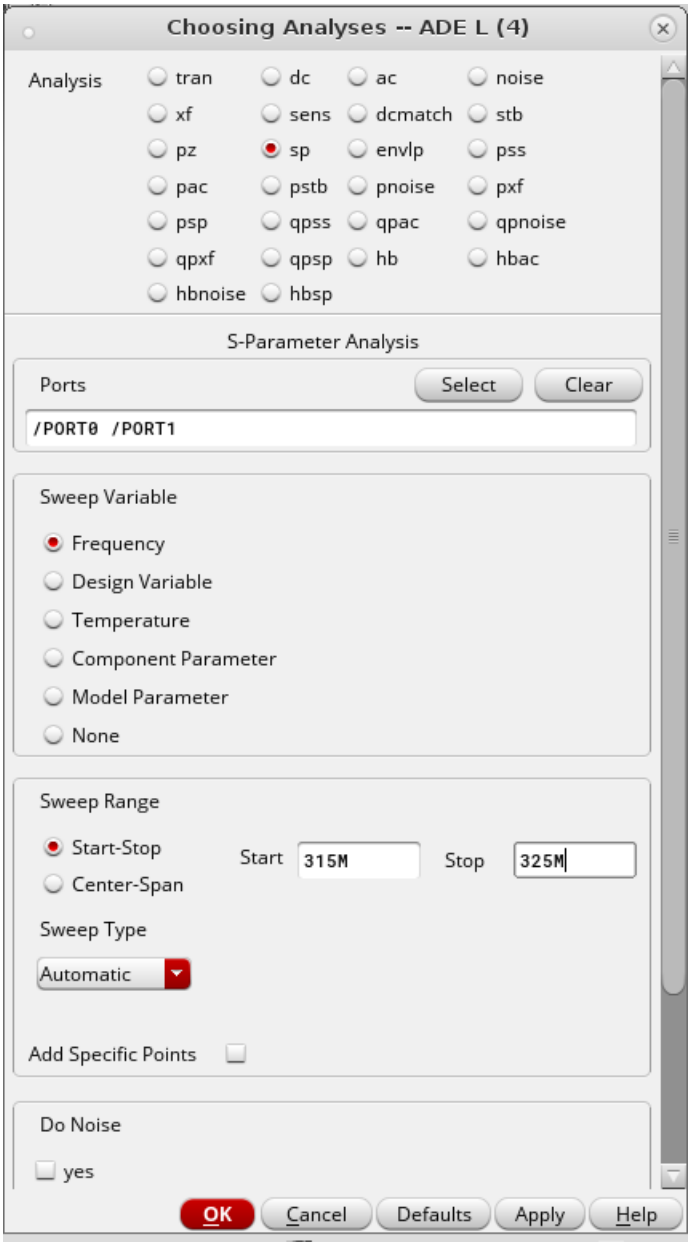

Sweep range is around the resonant frequency.

Click the green button *netlist and run.* To plot the output. Choose *results>>direct plot>>main form* from *ADE L* as follows:

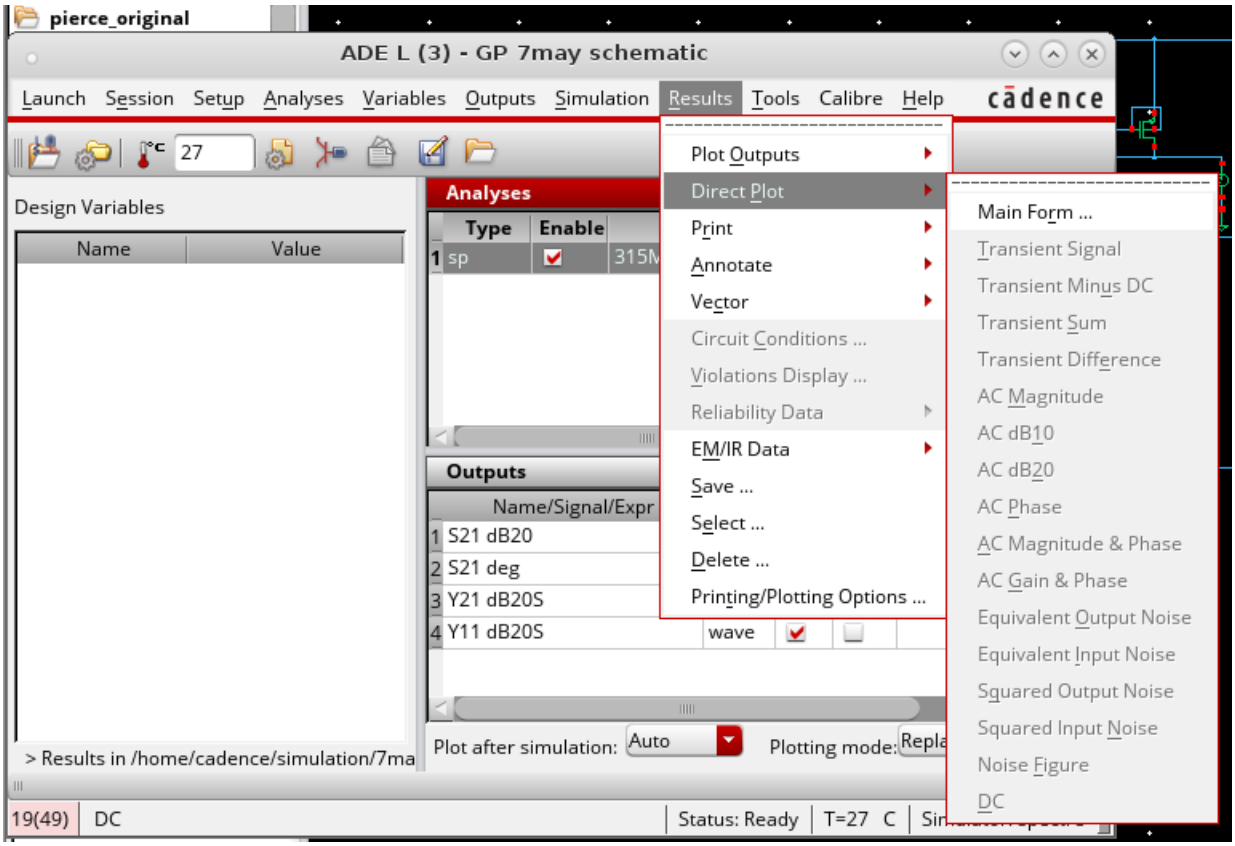

Choose the desired simulation from the following window and click on add to output

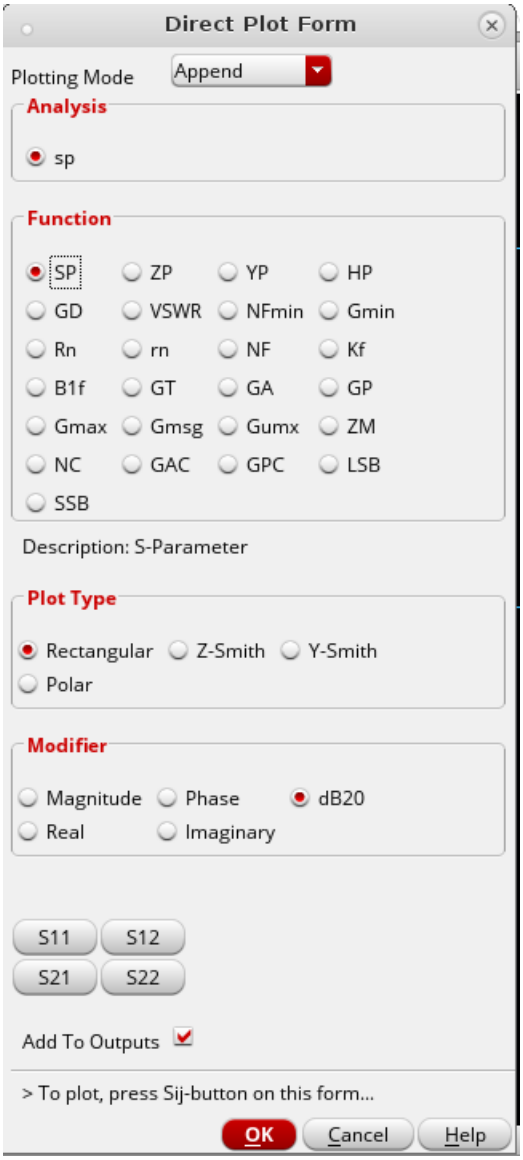

to plot Q factor, choose *Y21 dB20* in and *plot type rectangular*.

At the peak point of the graph, press m and the double click the highlighted point as follows:

Choose *position>> by YMode* and copy the value.

Close the window and press *m* on any point on the graph, double click this highlighted point and choose *position>> by YMode* and subtract 3 dB from the peak point value. Click *apply and ok.*

Repeat the same steps for the other side for the same -3dB and calculate bandwidth and then calculate Q factor from the relation $\frac{f_0}{\delta f}$, $BW = \delta f$.

Challenges and simulation recommendations

- Using the same simulation frequency and time step is essential for the consistency of the results in both COMSOL and cadence, using different time steps is very tricky as it produces greatly different results.
- Finding the BW is very hard specially that the graph from COMSOL is almost a unit step. Polynomial interpolation is needed to evaluate the frequency values at half the admittance values.
- It's also recommended in designing pierce oscillators, to verify the same result with a Verilog A op-amp to make sure that the circuit behavior is as expected before getting into test errors.

- During cadence resonator simulations, its recommended to choose the right nodes around the resonator while graphing the output of the transient response.
- its recommended to match the ports in the SP simulations with the real value of impedance of the resonator, a slight change in the matching load impedance result in a dramatic change in the values of the IL.
- Choosing an appropriate method of initial conditions for oscillator is very important to avoid simulation errors. Assigning initial condition values inside the resonator component itself is the preferred method. Convergence aids is a bit tricky but it's a second option

- Sometimes the peaks at resonance doesn't show up if the range if the simulation is very large, making the range just around the resonance frequency makes the graphs obvious to observe.

- PSS simulation can fail to converge for many reasons. Try to use harmonic balance with an initial guess near the resonant frequency from the results from COMSOL. Increasing the number of harmonics and Transient stop time also helps in converging PSS. Use moderate setting in the simulation results. If PSS still not converging, try to make sure from the transient simulation first that the oscillation is maintained at larger stop times to make sure that the shown oscillation isn't at the initial start of the simulation and then it fades.

- Using AC gain and phase simulation analysis helps to determine whether the oscillator circuits need tuning in the gain by changing the sizing of transistors, or the phase needs to be changed by adding/removing a stage, adding a capacitor.

- PSS simulation is shifted from the resonant frequency sometimes due to capacitance of the large area transistors.

COMSOL Simulation:

First the geometry is built as shown in figure below it composed of four rectangles, when the number of pairs increases the number of rectangles will increase.

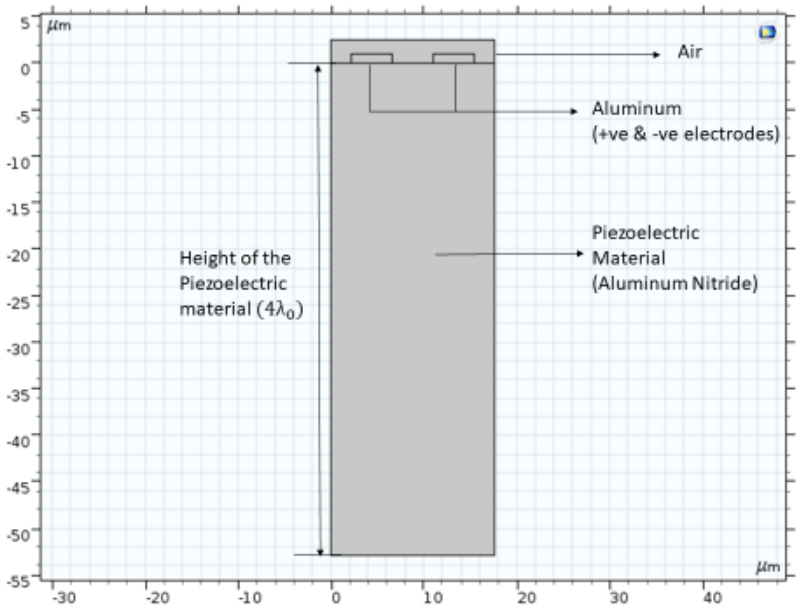

The boundary conditions of the design:

First the physics used are solid mechanics and electrostatics the boundary conditions of the solid mechanics are fixed constraint at the bottom of the piezoelectric material, periodic condition at the two sides of the device to avoid the leakage of the waves from the two sides and piezoelectric material condition to the piezo-material part in the device.

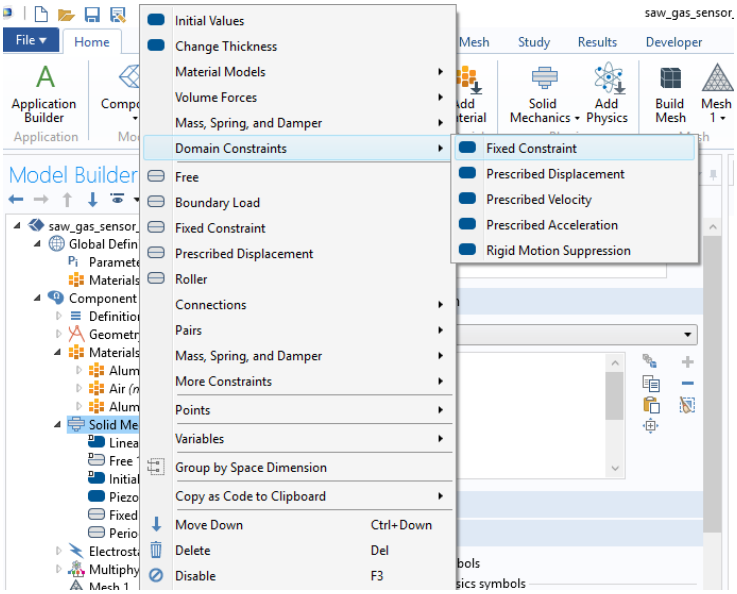

The periodic boundary condition:

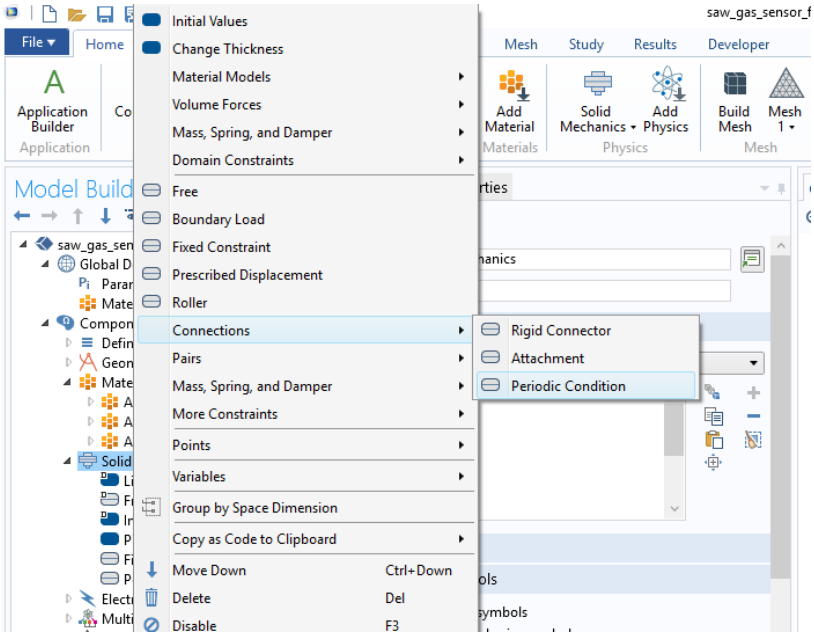

The piezoelectric material chosen for the bottom part of the design which is the piezoelectric material:

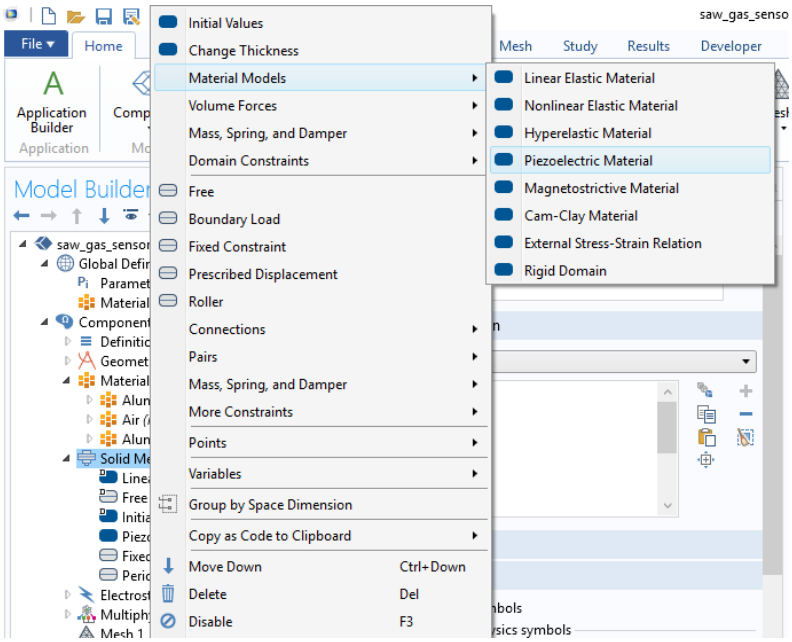

The electrostatic Boundary conditions. Choosing the Charge conservation, piezoelectric material for the piezoelectric material part and the electrode.

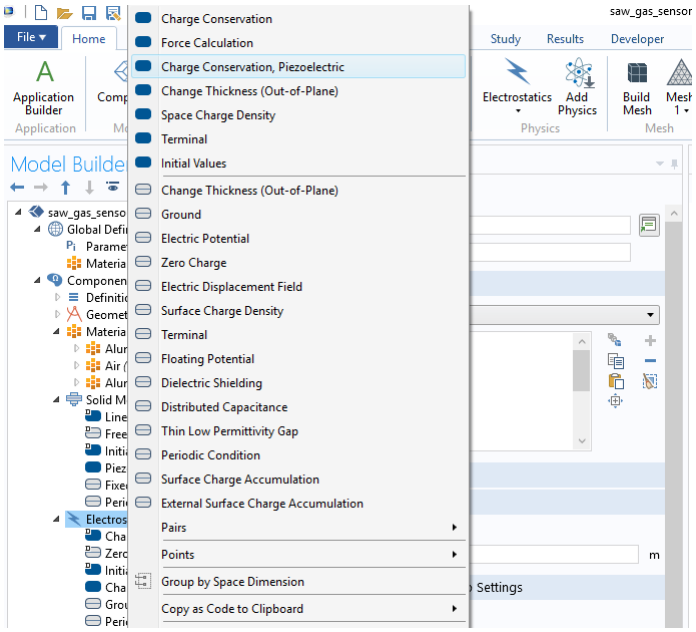

Then choosing the boundary condition charge conservation for the electrodes and air materials.

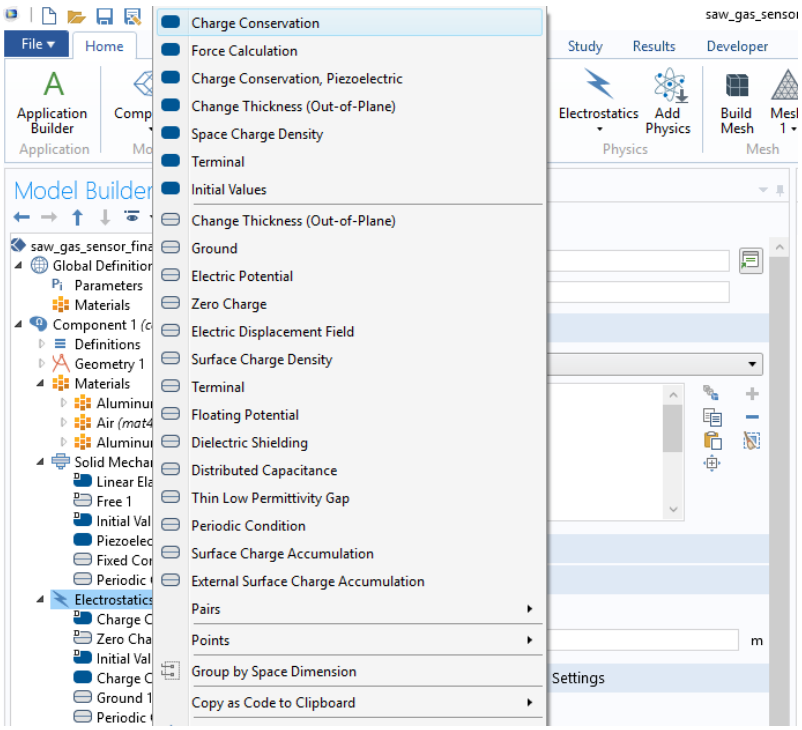

One of the electrode is ground and one is 1 volt. Choosing ground and terminal 1.

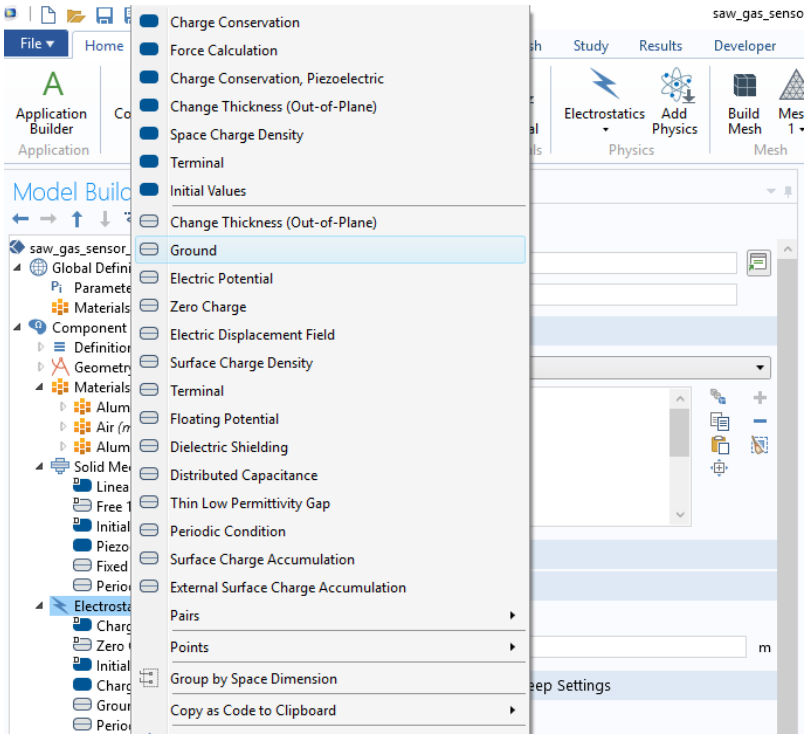

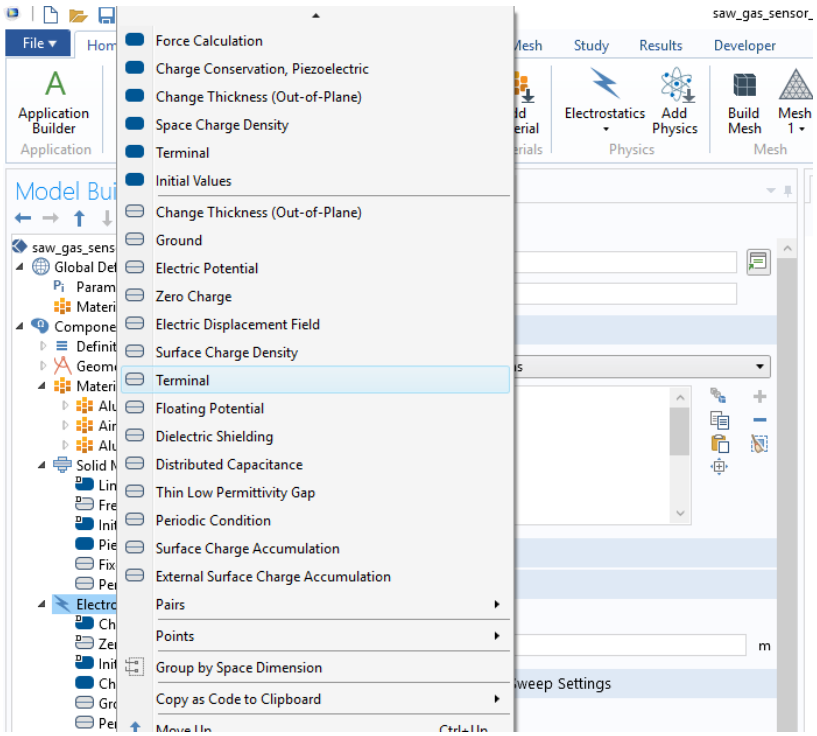

Study one is done to get the Eigen-frequency of the devices which is help in getting the mode shapes. The parametric sweep is as follows.

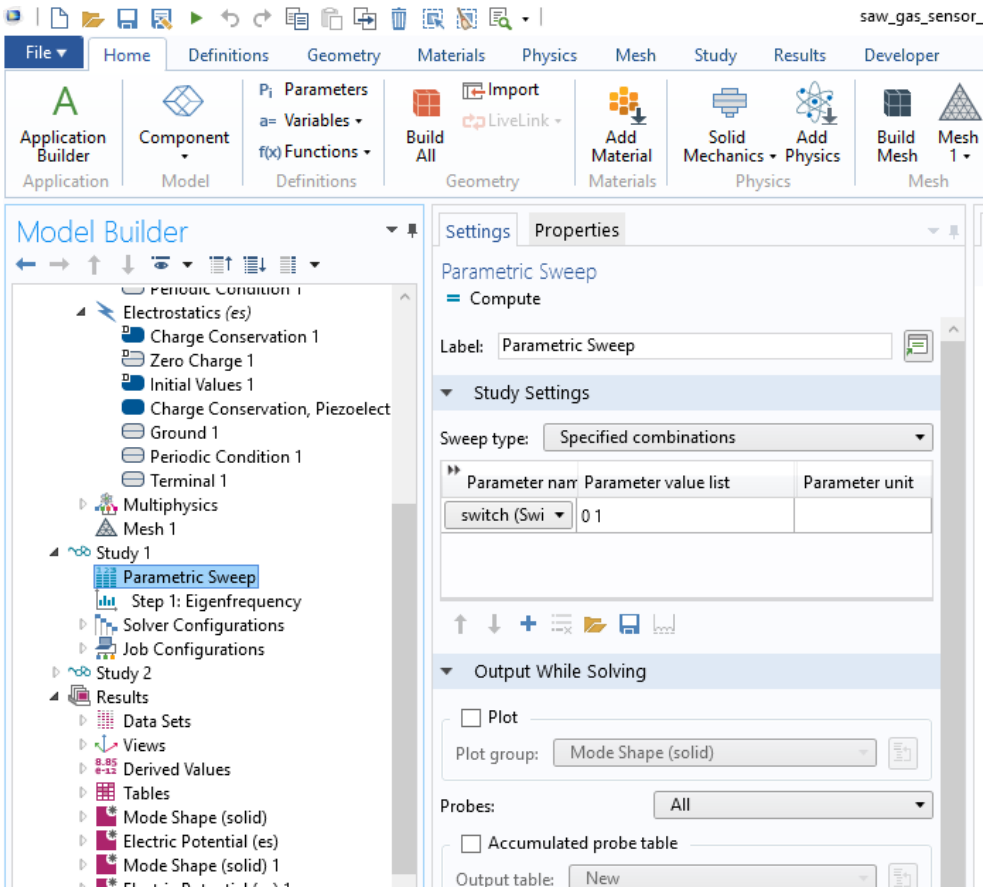

The Eigen-frequency is as follows:

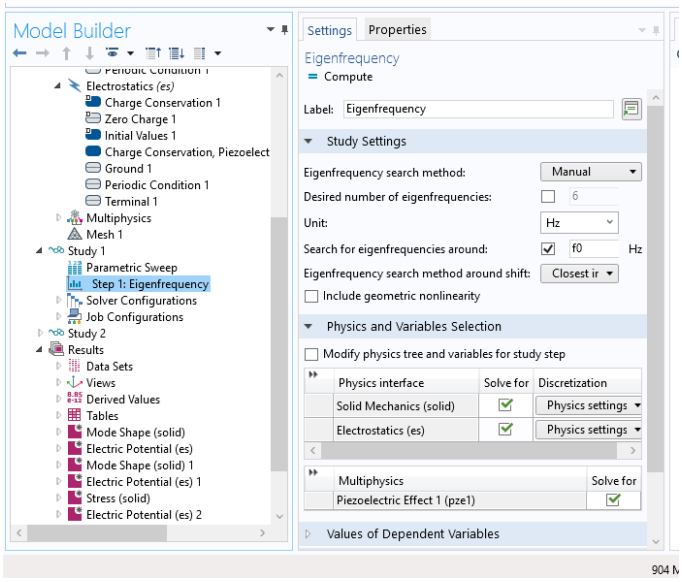

Study two is to get the Frequency domain here is the main part of the project to calculate the admittance and Quality factor. This part of the simulation is time consuming it may take about two days for running one model only.

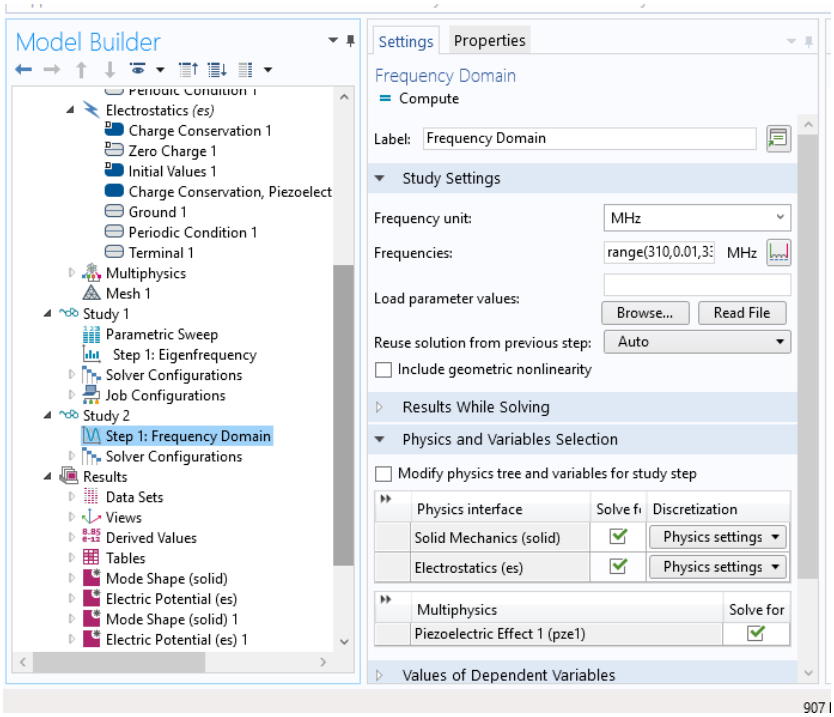

The admittance calculation, choosing 1D plot then choose global after that writing abs(es.Y11) in the part that is shown in figure below.

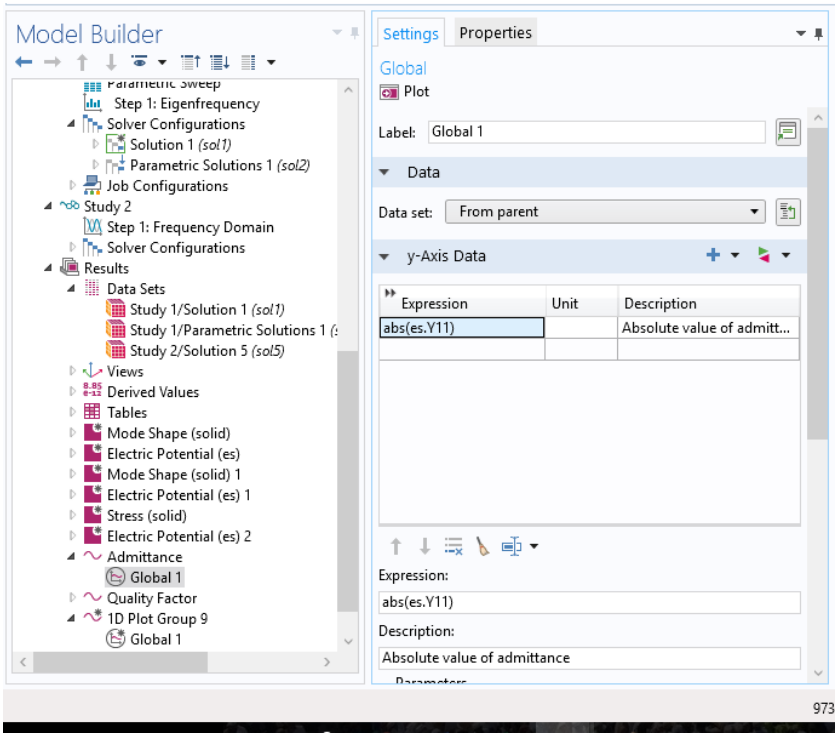

TCF Calculation

1) The values of the different mechanical parameters such as (density, $c44$, ϵ_{11} and e_{15}) are to be obtained for different temperatures in the temperature range of the device operation.
2) The geometry change with temperature should be included, the thermal expansion of the different materials has to be tabulated.
3) Define the *geometry*, *material*, and *physics* nodes.
4) Under the *solid mechanics*, *physics* node, right click on the *Linear Elastic Material*, choose *Thermal Expansion*.

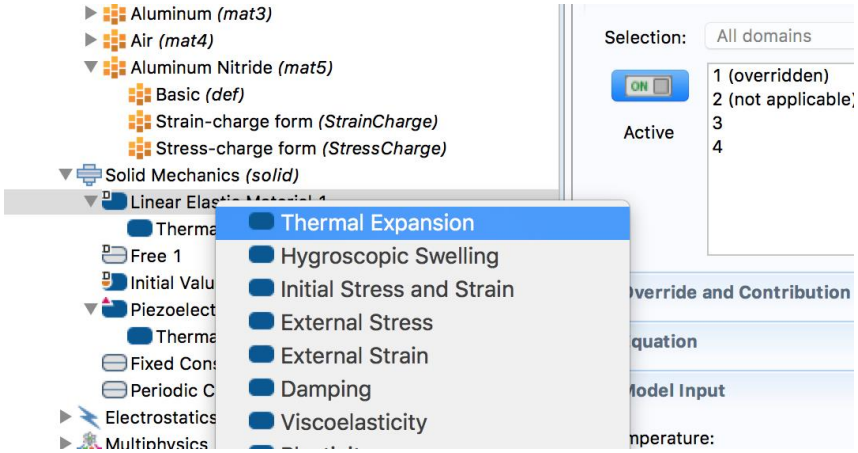

5) In this *window*, specify the reference and the new temperature.

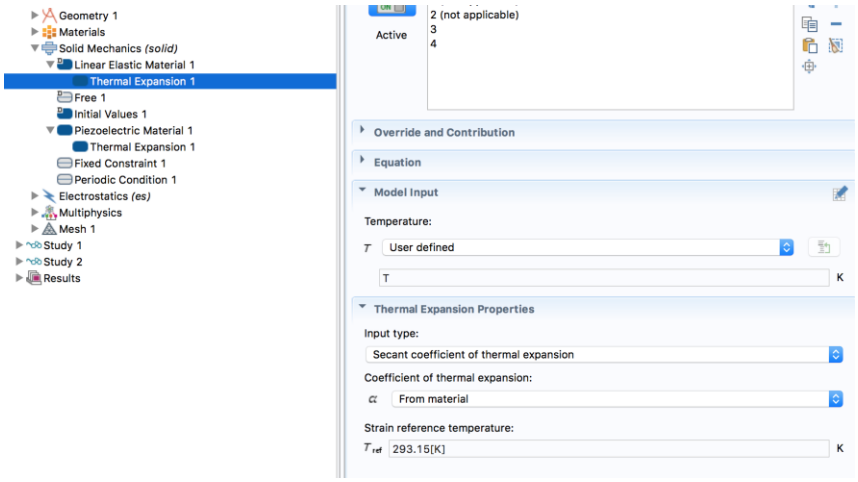

6) Now, COMSOL requires to add the *thermal expansion coefficient* for materials with unknown values of the coefficient in the *material* node.

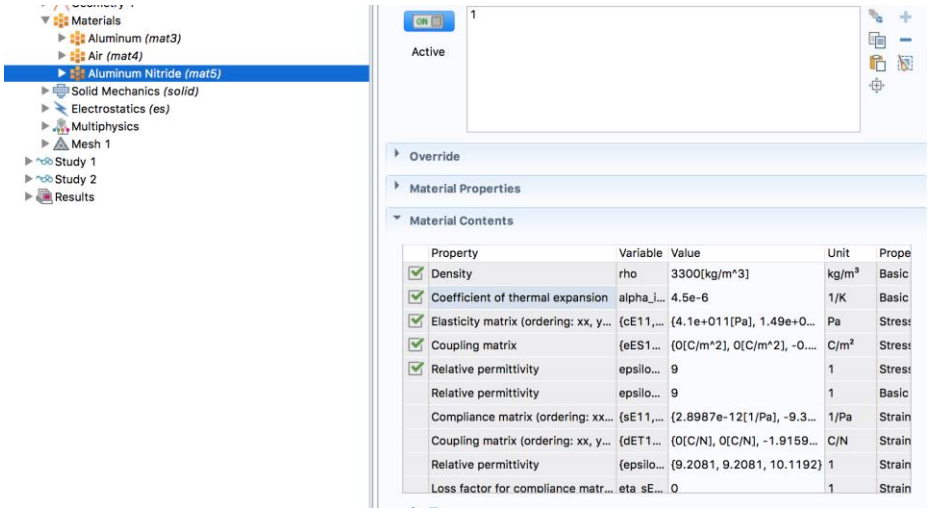

7) Add the *c*44, in the *Elasticity matrix*, it is the tenth element in the matrix, or it can be added by right click on the *Elasticity matrix*, *edit*, and the whole matrix will open, then enter the *c*44 value here.

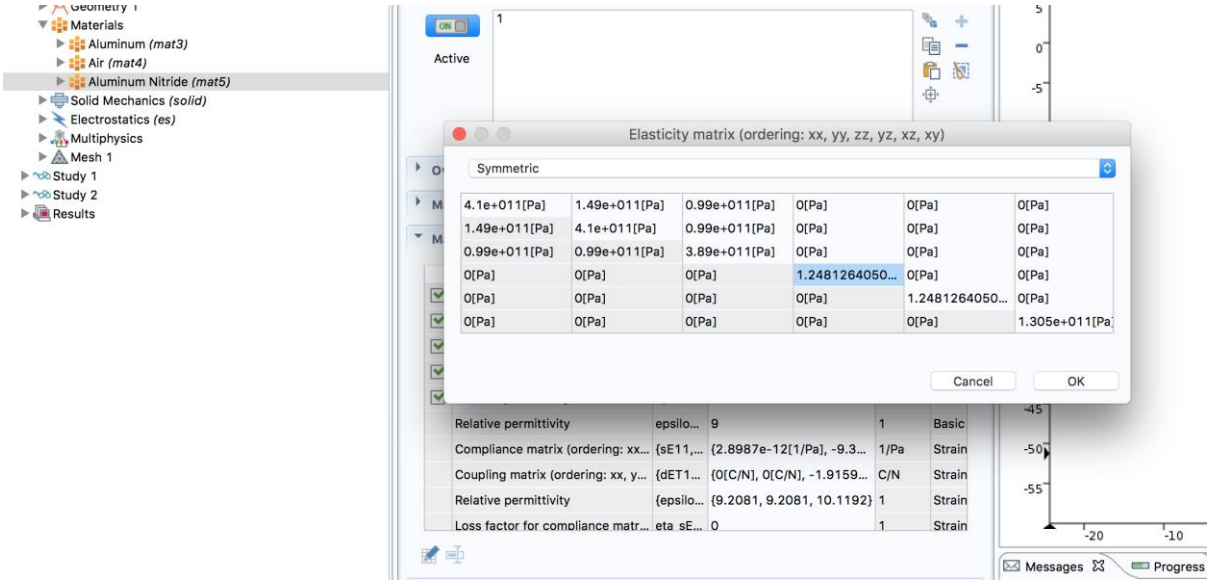

8) For the density, either the value can be added at that temperature or an analytical expression is added.

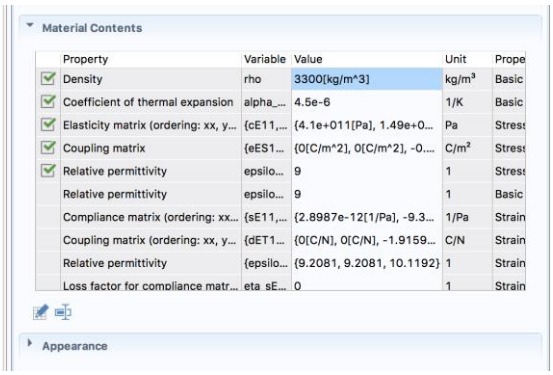

or

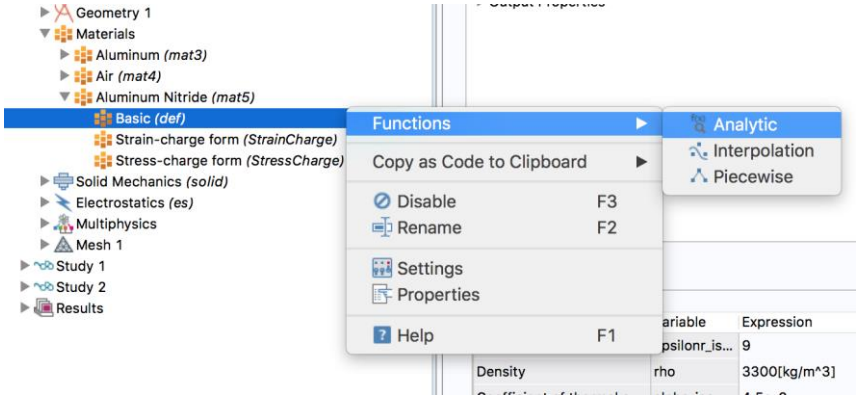

in the function, specify the lower and upper limits of the temperature.

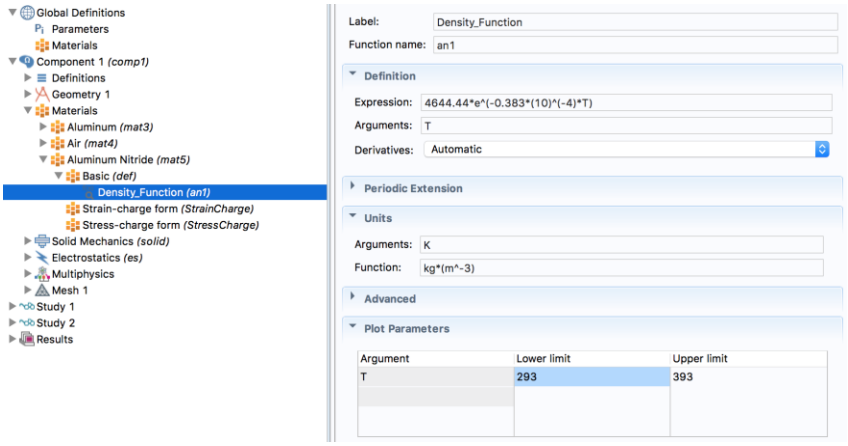

9) Similar to the normal *Frequency Domain* simulation, the frequency sweep is done.

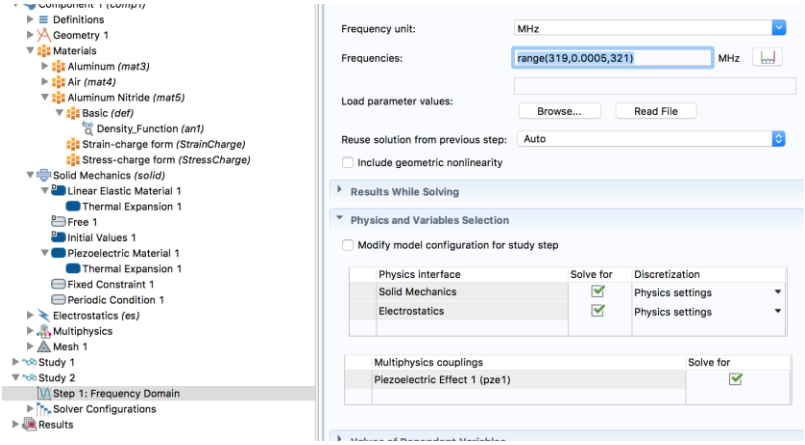

in case there is an equation

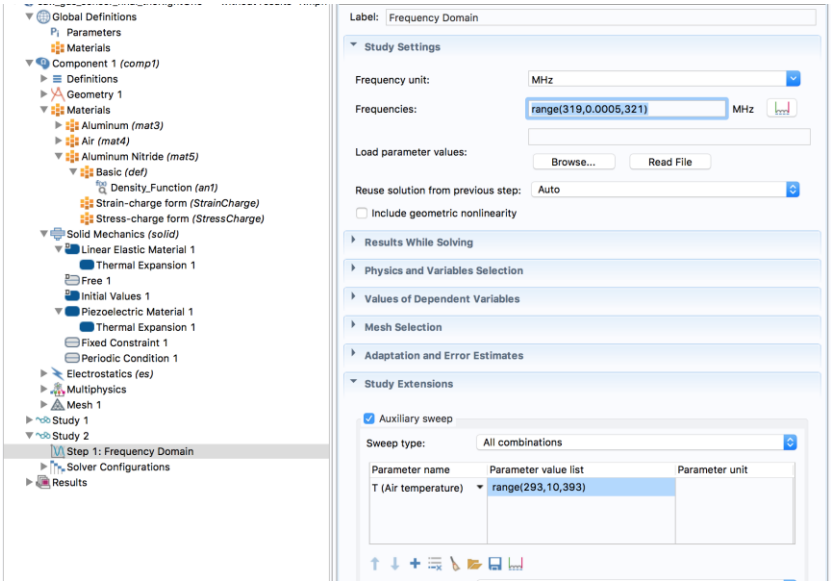

10) Export the admittance graph on a text or an Excel file to find the value of the new resonance frequency.

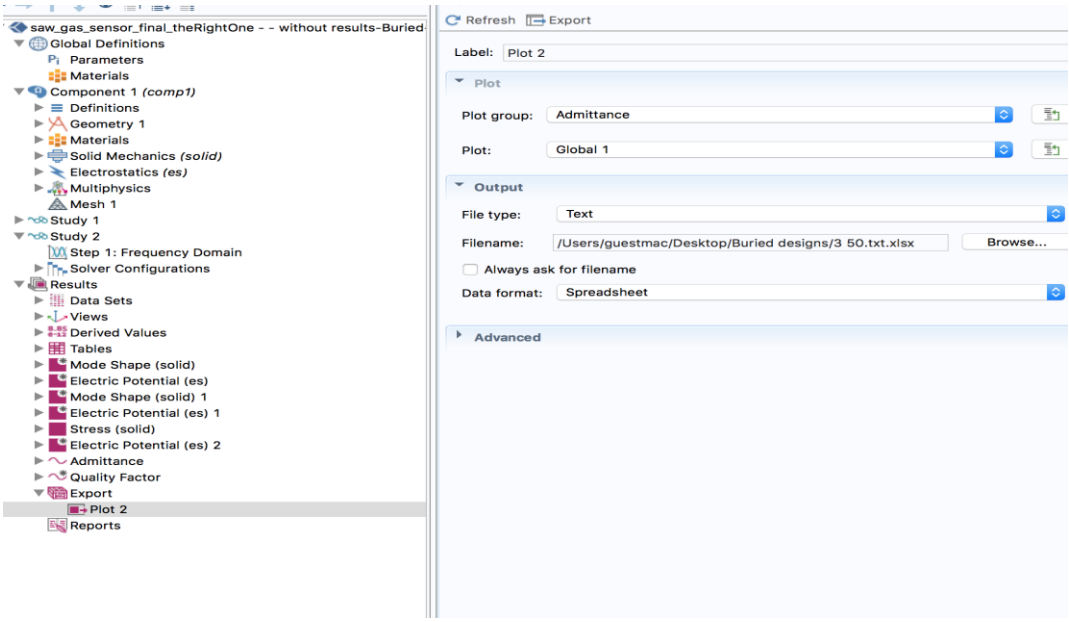

11) Vary the temperature and record the different values of the resonance frequency corresponding to each temperature.
12) Plot the regression line between the resonance frequency and the temperature in Celsius and get the slope.

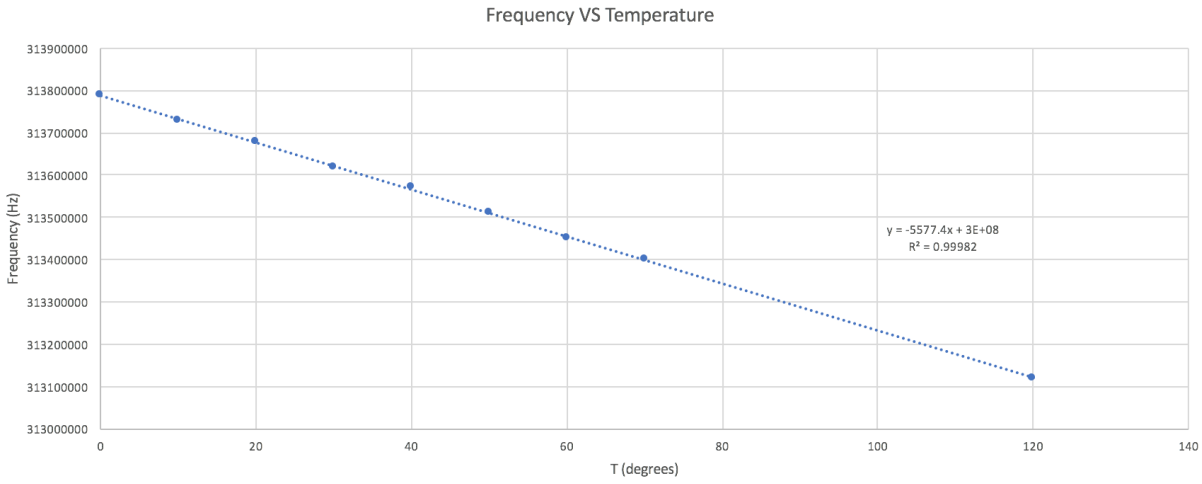

13) The TCF value is calculated from:

$$TCF = slope * \frac{10^6}{f_0} \frac{ppm}{^0C}$$